ORNL/TM-2022/1845-R00
S07040200-TRT10000-R00

Second Target Station (STS) Project

Steerable Optic Design & Testing Report

Van Graves
Doug Bruce
Matt Kyte
Matt Pearson

April 2022

OAK RIDGE NATIONAL LABORATORY
MANAGED BY UT-BATTELLE FOR THE US DEPARTMENT OF ENERGY

S07040200-TRT1000-R00
ORNL/TM-2022/1845

Second Target Station (STS) Project

STEERABLE OPTIC DESIGN & TEST REPORT

V. B. Graves
D. R. Bruce
M. A. Kyte
M. R. Pearson

Date Published:
April 2022

Prepared by
OAK RIDGE NATIONAL LABORATORY
Oak Ridge, TN 37831-6283
managed by
UT-BATTELLE, LLC
for the
US DEPARTMENT OF ENERGY
under contract DE-AC05-00OR2272

CONTENTS

LIST OF FIGURES

EXECUTIVE SUMMARY

Multiple neutron scattering instrument concepts for the Spallation Neutron Source's Second Target Station (STS) incorporate advanced neutron optic designs which incorporate discrete mirrors rather than continuous neutron guides that were the standard for instruments in the First Target Station. These mirrors can be a few to several meters in length and must be stably supported and aligned as a single optic. In addition, due to the length of the STS instruments and the small size of the STS neutron beams, installation and alignment at the micron level of precision will be required, which is beyond the ability of today's survey & alignment technology. Thus, a means of remotely adjusting these mirrors with single digit micron resolution is needed. A Steerable Optic System was designed to provide the precision and resolution required to support and manipulate these large, heavy optics under beamline shielding. This system is based on the original "magnet movers" developed at the Stanford Linear Accelerator (SLAC) in the mid-90's and incorporated at synchrotrons around the world. It uses eccentrically-mounted, motor-driven bearings with high-ratio gear reducers to orient and position objects in five degrees of freedom; it does not inherently manipulate or constrain translations in the beam direction.

A mockup was developed to demonstrate and validate this system for use in neutron optic applications. The mechanical system consisted of an aluminum strongback girder which was supported by five movers, with each mover incorporating a stepper motor and absolute encoder. A motion control system of software and hardware was developed which performed the kinematic equations necessary to simultaneously control each of the movers. In addition, for the purposes of this mockup, digital indicators and Linear Variable Differential Transformers (LVDTs) were incorporated to provide an external means of measuring the position and orientation of the girder.

Multiple series of tests were performed to characterize the Steerable Optic System. Some tests consisted of scans across each degree of freedom separately, while others exercised all degrees of freedom simultaneously. These scans were grouped into low-resolution and high-resolution tests, and the results demonstrated that the system was capable of providing positioning resolution at the single-digit micron level. They also identified that unintended girder motions were occurring, which indicated the girder is not completely rigid. Larger-than-expected movements in the beam direction were observed which may require an external pin or other restraint be employed in a production application. Various thermal tests were also conducted and showed micron-level girder movements due to room temperature changes, which were expected. One unexpected observation was that motor heating during scan motions resulted in heat being conducted into the mover housings, and this also resulted in measurable girder position changes at the micron level.

Much was learned during this mockup testing development, and while there are changes and improvements that can be incorporated into future versions, the capability has been demonstrated and can be successfully deployed for beamline optic applications.

1. INTRODUCTION

Multiple neutron scattering instrument concepts for the Spallation Neutron Source's (SNS) Second Target Station (STS) incorporate advanced neutron optic designs which incorporate discrete mirrors rather than continuous neutron guides that were the standard for instruments in the First Target Station (FTS). In several instances, these discrete optics are nested Kirkpatrick-Baez (KB) mirrors in which vertically- and horizontally-elliptical mirror surfaces are combined into a single optic; generally the beamline incorporates two of these mirrors separated by evacuated flight tubes to provide final neutron focus at the sample. The KB mirrors can be a few to several meters in length and separated by tens of meters of flight tube.

The only experience that the Neutron Scattering Division (NScD) has with these types of focusing mirrors is on the IMAGINE instrument at the High Flux Isotope Reactor (HFIR). In this instrument, the mirror segments are only 70 cm in length. Anecdotal discussions indicated that while aligning these optics, translations > 100 microns and rotations > 0.01° (0.17 mrad) had a measurable effect on the focal image at the sample position. For STS instruments, assuming an instrument length 10X longer than IMAGINE implies translations > 10 μm and rotations > 0.001° (17 μrad) will produce measurable effects at the sample. Thus, KB mirrors on STS instruments will need to be installed and aligned at the micron level. In addition, mirrors of a few meters in length contained within vacuum housings are projected to weigh hundreds of pounds, and off-the-shelf positioning systems capable of aligning to high levels of precision are not designed to support such weights. Finally, installing and aligning neutron optics to micron-level precision is beyond the capabilities of today's Survey, Alignment, and Metrology (SAM) equipment, and even if such precision alignment were possible, subsequent floor deformations would induce even greater misalignment. Thus, a system which can stably support such optics and allow them to be manipulated as a single elliptical mirror at the micron level of precision and adjustability will be required. We refer to such a system as a Steerable Optic, and this report documents the design and testing of a prototype system.

2. DESIGN

A steerable optic system capable of supporting and orienting a strongback girder at the micron level was developed, fabricated, and tested. The mockup is shown in Figure 1. This girder would be capable of supporting a neutron optic of up to 3 m in length. While the overall girder was designed to be prototypic, this mockup version incorporated additional components that would not be part of an actual beamline application. These additional components are the "bridges" that are mounted to each end of the girder in Figure 1, and they include reference surfaces that are contacted by position measuring devices that were used to quantify girder movements. The following subsections describe various design aspects of this mockup.

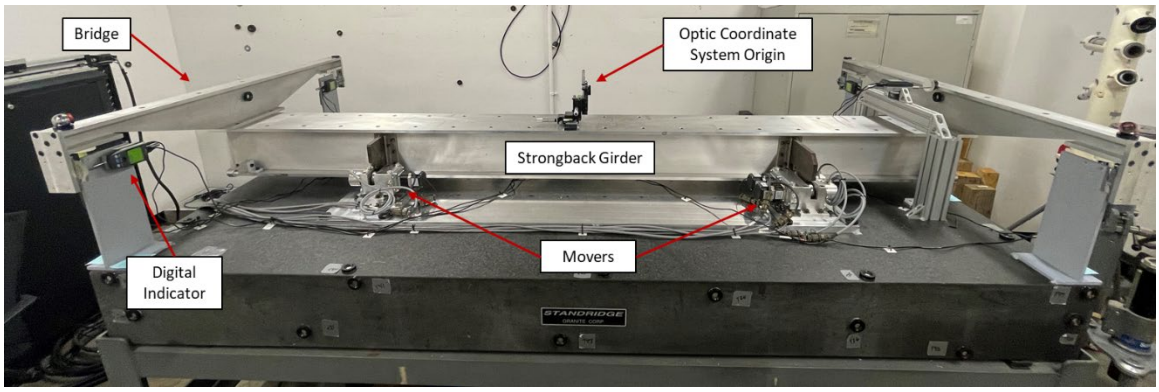

Figure 1. Steerable optic mockup

2.1 BASIS OF DESIGN

While performing research on the problem of how to position long, heavy objects with precision and resolution in the single-micron range, a possible solution presented itself in the form of "magnet movers," which were specifically designed with that scenario in mind [1]. These movers utilize eccentrically mounted bearings on motor-driven shafts to support and position heavy objects. They were originally developed by the Stanford Linear Accelerator (SLAC) staff to mechanically align linac components and magnets for the SLAC Linear Collider (SLC) Final Focus Test Beam (FFTB) [2]. In general, these accelerator components were required to be aligned within 10 microns, and in the case of the FFTB magnets, to tolerances ≤ 1 micron.

The fundamental design of the SLAC magnet movers uses mechanical roller bearings which engage inclined and horizontal flat surfaces on the object the movers are intended to constrain and support. These bearings are mounted eccentrically on shafts rotated by stepper motors, and they incorporate gear reducers with high reduction ratios to support heavy loads and to produce high-resolution motions. Because the FFTB magnets were relatively short in the beam direction, only movements within a single plane were needed, so three bearings were required (movement in the beam direction was not controlled). If STS optics were similarly short in the beam direction, they would be manipulated in a similar fashion. A schematic diagram (Figure 2) shows how the bearings would be arranged relative to short STS optic and its supporting strongback. The three eccentric bearings in the schematic (shown as circles) are arrange such that they engage a vee and a flat which are part of the strongback. As these bearings rotate eccentrically, they can move the optic horizontally, vertically, and in roll. The amount of possible movement is dependent on the geometric relationships between the bearings and the optic and the eccentricity of the bearings.

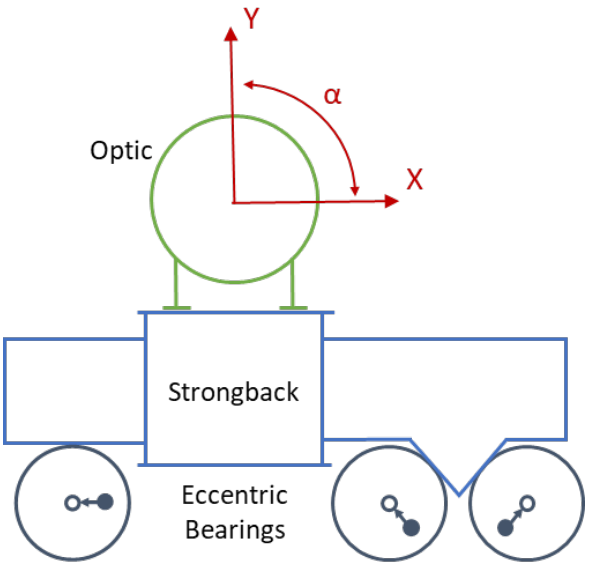

Figure 2. General approach for 3-DOF positioning system

When longer objects require support, as would be the case for STS optics, two additional bearing are required to provide five degree of freedom (5-DOF) support and positioning capability. These two additional bearings engage a second vee in a different plane from the first three bearings. Such a system is shown in Figure 3 and represents the scheme needed for neutron optics. This arrangement of eccentric bearings supports horizontal and vertical translations along with rotations around all three axes; the only motion not supported by these movers is translation along the beam axis.

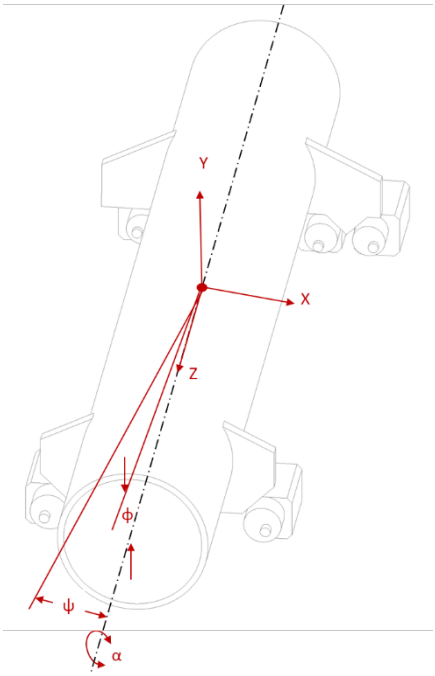

Figure 3. 5-DOF positioning system relevant to STS components

In all applications of a steerable optic system, the motions are made relative to a coordinate system as shown in Figure 3. This coordinate system can be defined by the component geometry that is supported.

In the context of a typical neutron guide, it would generally be convenient to place the reference coordinate system in the middle of the guide; for a KB mirror with two reflective sides and two absorbing sides, a similar convention might be chosen, with the coordinate system in the center of the four-sided optic assembly.

Further investigation revealed that magnet movers are in use in several synchrotrons around the world. Figure 4 shows an example from the Swiss Light Source at the Paul Scherrer Institute in Villigen, Switzerland. This mover system, identified by the green mover blocks, is sized to support the weight of the girder and magnets, a total of several tons. This mover system can provide up to 5 mm of travel of these girders. For our intended application of neutron optics, the design weight will typically be much smaller.

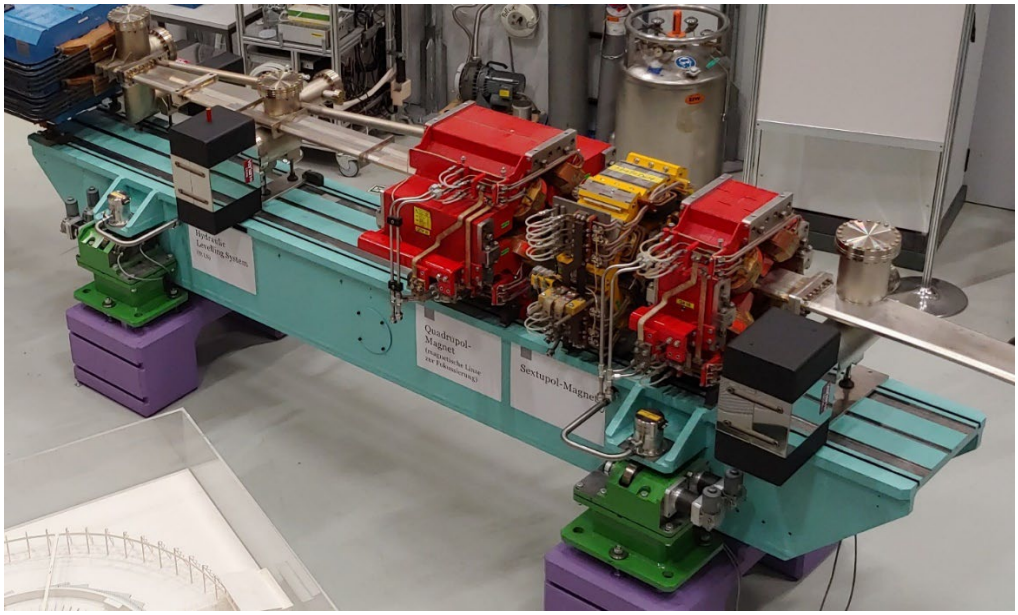

Figure 4. Girder supported by magnet movers at the Swiss Light Source (SLS)

2.2 MECHANICAL DESIGN

The steerable optic mockup was intended to be prototypic in its design to support a neutron beamline optic. Since these optics would be positioned under beamline shielding, minimizing the overall width of the system was a design driver.

Figure 5 shows an overview of the mockup's geometric configuration. In this view, five mover motors can be seen engaging vee or flat brackets protruding from the sides of a box-beam girder, and the optic coordinate system is shown relative to the motors. It is intended that all beamline applications would incorporate the same motor arrangement as shown in the figure, with 2 motors located in a -Z plane relative to the optic coordinate system, and 3 motors in a +Z plane.

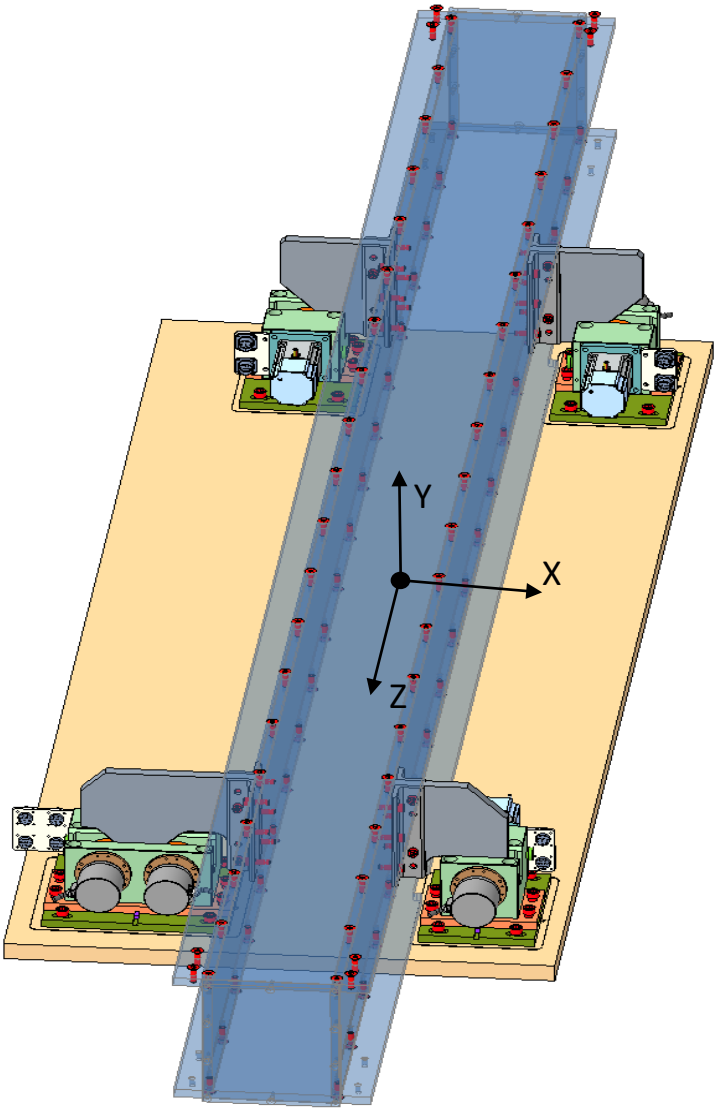

Figure 5. Standard steerable optic mover configuration

As previously mentioned, the original magnet movers were developed at SLAC in the mid-90s. Through published reports and discussions with the original designer, the mechanical design of our steerable optic movers was heavily influenced by the SLAC design. There are two variations of these eccentric-bearing movers, a single-axis (shown in Figure 6) and a double-axis (shown in Figure 7), with two axes in a single housing. Each mover consists of a machined aluminum housing which contains the bearing shaft, bearings, and an integrated gear reducer. Attached to each housing are a stepper motor with integrated brake along with an absolute rotary encoder. Details of these components will be discussed in subsequent sections.

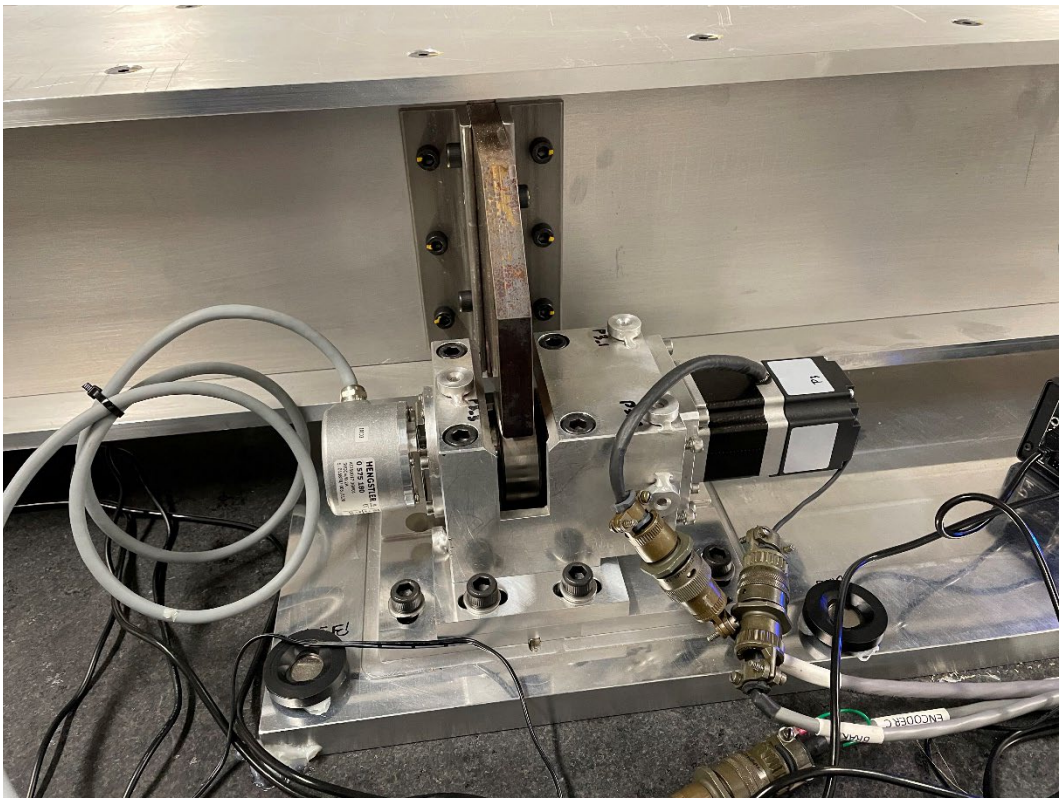

Figure 6. Single-axis mover

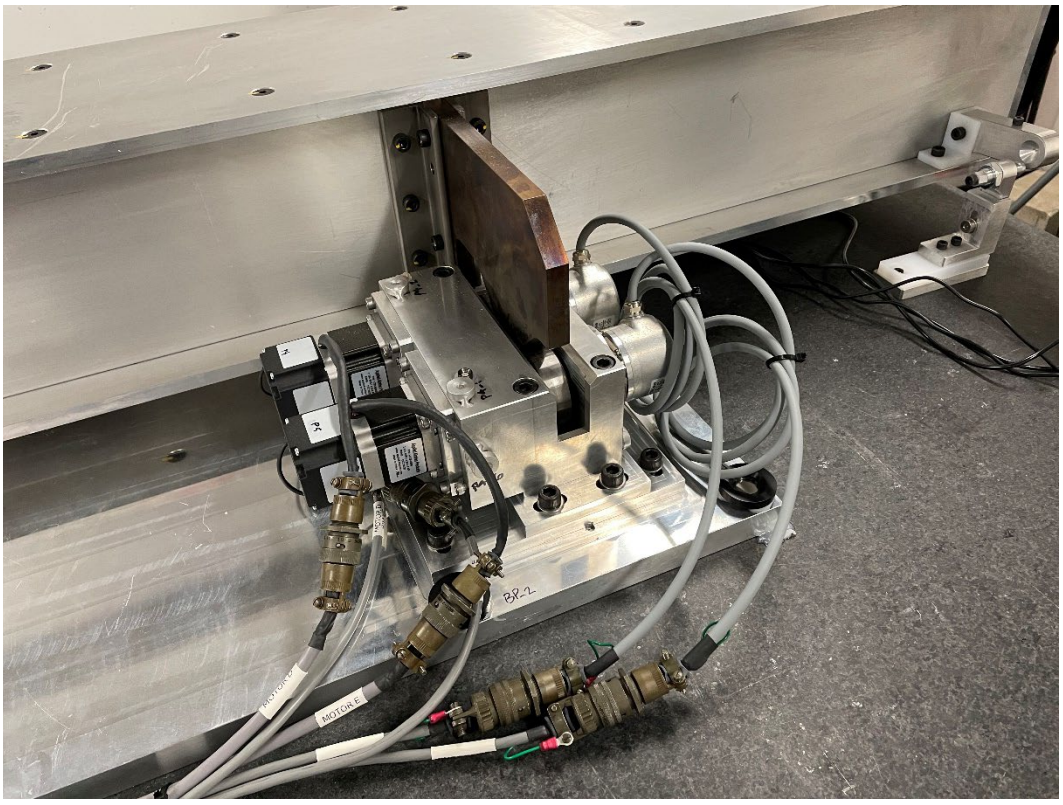

Figure 7. Double-axis mover

2.2.1 Movers

At the heart of the functional operation of the movers is a ball bearing mounted on an eccentric shaft. This shaft is support by two concentric bearings, and this assembly is mounted within a solid housing. Figure 8 shows a vertical section view through a single-axis mover, and the shaft/bearing assembly can be seen. These bearings are designed with a slight interference fit within the housing and on the shaft. The slight eccentricity of the orange bearing (1.5 mm in this design) can also be observed within this figure since the upper step of the shaft differs from the lower step; for the concentric bearings, the upper and lower steps are identical in height.

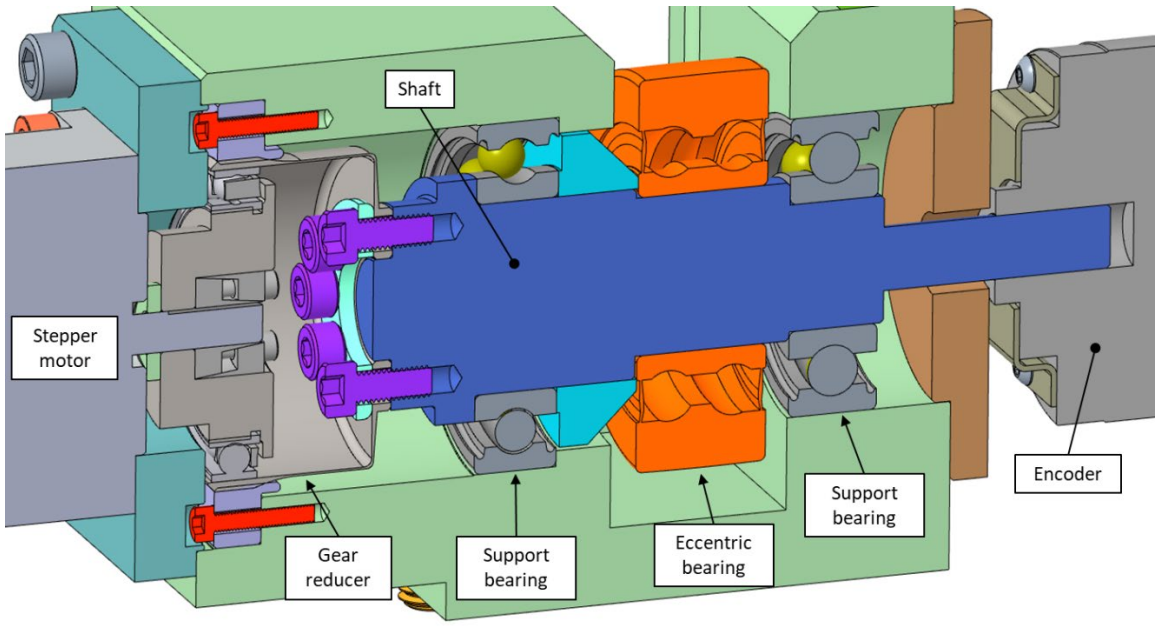

Figure 8. Eccentric bearing on shaft supported by two concentric bearings

The mover shaft design can be seen in Figure 9, with the eccentric section of the shaft identified by the scribe mark. In this design, all the bearings are installed on the shaft from the same end, so each shaft section diameter is designed to match the inner diameter (ID) of the bearing that sits on it. Furthermore, the shaft steps are successively larger in diameter, and the amount of available eccentricity is limited by the difference in IDs of the two support bearings; the eccentric bearing ID is numerically between those of the support bearings, and the maximum amount of available eccentricity occurs when the ID of the eccentric bearing equals the average of the support bearing IDs.

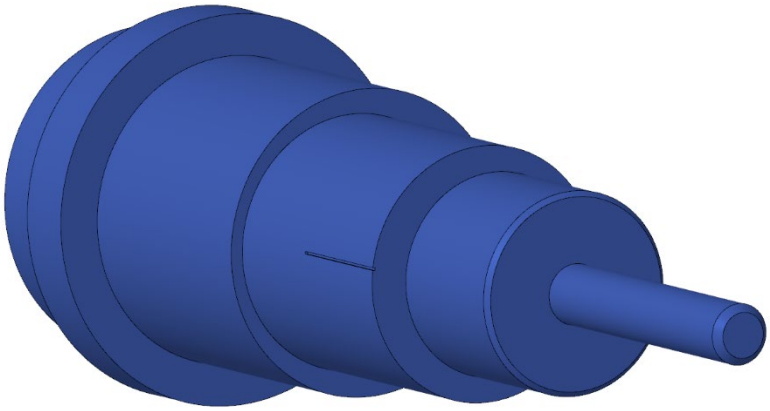

Figure 9. Mover shaft

The shaft input is connected to a high-reduction gear reducer driven by a stepper motor with integrated brake, and the shaft output is connected to a 17-bit absolute rotary encoder.

2.2.2 Gear reducer

One of the design goals for the movers was to minimize their footprint since they would likely be deployed under beamline shielding where space could be tight. Thus, a gear reducer was chosen which could be tightly integrated into the mover housing, an approach also taken by the original SLAC design. The chosen gear reducer, shown in Figure 10, was manufactured by Harmonic Drive and is used for high accuracy and high repeatability applications.

Figure 10. Harmonic Drive gear reducer components (https://www.harmonicdrive.net/technology)

As shown in Figure 11, this reducer incorporates a unique system of components in which a thin-walled cup deforms and changes its circular shape as its gear teeth engage with those of a fixed circular gear that has a different number of teeth than the cup. This deformation causes the cup to slowly precess around the fixed gear as it rotates, which produces the desired speed reduction on the cup and the mover shaft to which the cup is attached. Gear reductions up to 160:1 are available by the manufacturer; a reduction of 120:1 was selected for the mockup mover system, and each full step of a 200-step/revolution stepper motor produces an output of 360/200/120 = 0.015° (262 µrad).

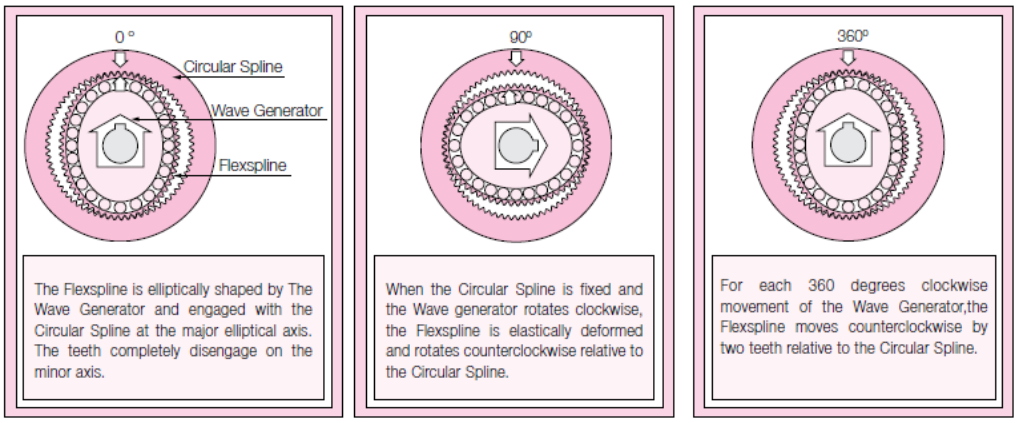

Figure 11. Operation of the Harmonic Drive gear reducer (https://www.harmonicdrive.net/technology)

One characteristic of this gear reducer is that it has no inherent backlash as do most gear-driven systems. This feature is critical to the operation of these movers and allows them to produce highly repeatable angular positions.

These gear reducers can be purchased as separate component parts or as an assembled module. The component set requires less space than the module and thus allows the mover housing to be smaller. The disadvantage of these component sets is they require some very tight machining tolerances in the housing because of their tight concentricity requirements. The mockup housing used the component set to reduce the housing size, but the machine shop producing the housings had some difficulty in meeting the required concentricity tolerances. So future versions of the movers might incorporate the modular gear reducers even though the housings would be larger.

2.2.3 3D Limit Switches

The design of the steerable optic system assumes that a segmented KB mirror is positioned on a support girder, and these mirror segments are supported within vacuum housings. The mirror is steered independently of any upstream or downstream beamline components. If the mirror housings comprise an independent vacuum volume, then any commanded girder motion which is within the range of the movers is a safe move that cannot introduce any external loads on the girder or the optic. However, if it is assumed that the steerable optic is part of a larger vacuum space and is connected to upstream or downstream beamline components via metal bellows, then it is possible that a move within the limits of motion of the movers could exceed the limits of the bellows. Moreover, the lateral motion limit of a typical bellows is independent of the direction of the motion, which results in a circular “safe zone” of allowable lateral displacements. Most systems which allow 2D movements will incorporate separate limit switches for motions in the X and Y directions. Such systems result in a rectangular safe zone of allowable movements; if the X and Y limits are set to match the allowable limit of the bellows, then a bellows displacement along the diagonal of the safe zone could result in damage to the bellows before a limit switch was tripped.

The solution to this issue is to utilize a limit switch scheme which provides a circular safe zone to match that of the bellows. A sphere-in-cone arrangement such as shown in Figure 12 provides such a circular motion zone. In this switch, the sphere and cone are electrically isolated from each other, and if they come into contact, the limit is tripped. To adjust the size of the allowed motion zone, the sphere and cone start in the contacted position. By separating them a known distance through a threaded adjustment screw, an equal gap between the sphere and cone is created, assuming a cone angle of 90°.

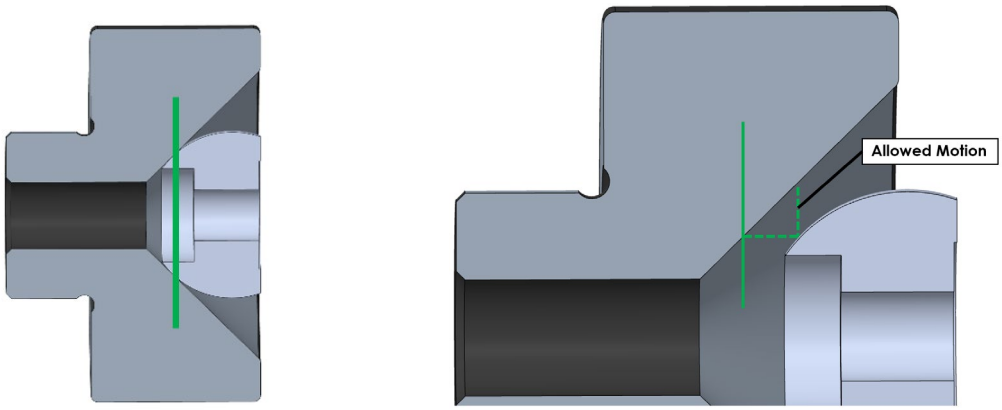

Figure 12. Setting the allowable 3D motion limits

By fixing the sphere and attaching the cone to the movable girder (or vice versa), this custom switch arrangement can be deployed near each end of the girder to provide the necessary protection for bellows or other components as desired. The limit switch designed and developed for this mockup is shown in Figure 13.

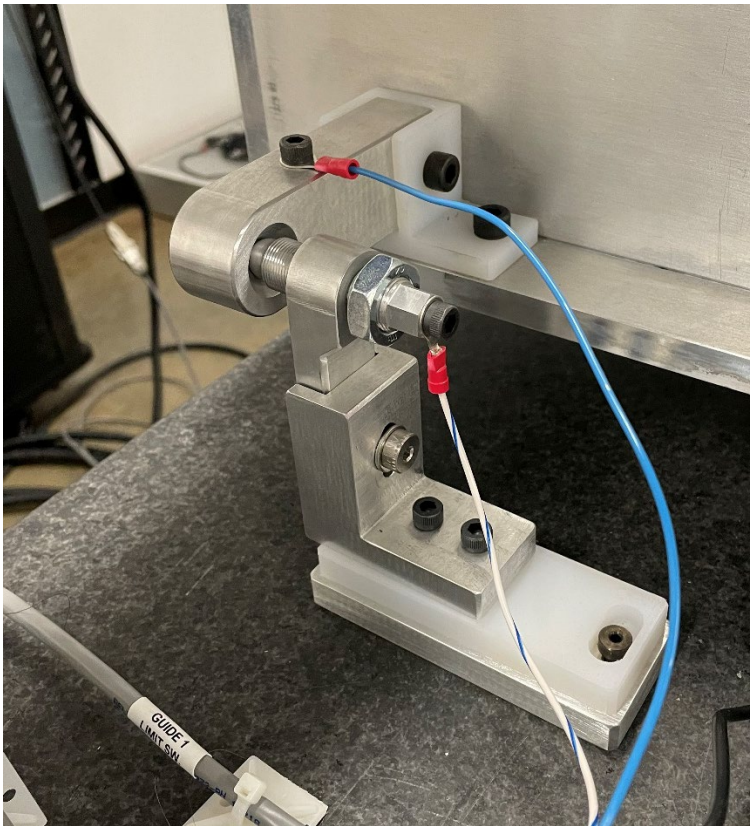

Figure 13. Mockup 3D limit switch

2.3 CONTROL SYSTEM DESIGN

The steerable optics control system provides the controls hardware, controls software, user interface and associated computing and networking. The controls hardware interfaces to the motors in the movers, the

single-turn encoders, the motor brakes and the 3D limit switches. The control system software provides an interface to the controls hardware, as well as an implementation of the kinematic calculations that convert girder degree of freedom (DOF) parameters to and from mover angle positions. Additional hardware and software were provided for the purposes of collecting data, temperature monitoring and position verification.

The control system also included a rack mount Linux server, network switches and a user interface desktop that was remotely accessible. This enabled most of the testing to take place remotely and enabled the project to use the standard SNS control system archiving database, which is useful for diagnostics and evaluating system performance.

2.3.1 Control System Hardware

The controls hardware is described in this section. The hardware chosen for the mockup project was based on the standard control systems in use at the SNS and HFIR facilities.

2.3.1.1 Motion Control and Equipment Protection

The stepper motors in the mover assemblies are the Applied Motion HT23-598B. These are NEMA 23 frame size, with an integrated 24-V brake, and can provide up to 1.116 N·m torque and are rated for 2.12 amp. The absolute single-turn encoders on the mover shaft are the Hengstler AI250017 36M01 model, which use the BiSS-C protocol, and which provide 17-bit resolution in a single turn (0.00275° resolution).

The motion controller used to interface to the motors and the encoders is the Galil DMC 4x00 series 8-axis controller with the D4140 integrated stepper motor amplifiers. These stepper motor amplifiers operate using a fixed micro-stepping resolution of 12,800 steps/rev, which translates into a mover step resolution of 0.000234° (taking the gear reduction into account). The stepper motor 24-V brakes were operated via relays in a separate Moxa ioLogik E1214 unit.

The 3D limit switches were supplied with a 24-V signal from an IDEC PLC. The PLC is responsible for monitoring the state of the switch inputs and implementing interlock logic that controls motor power in the Galil motor controller. It does this by setting the Galil Electronic Lockout (ELO) input. An additional Moxa E1214 was used to monitor the state of the PLC system and to provide a way to remotely reset the 3D limit switch latched interlock.

The motion controller, PLC and ioLogik units were installed in a rack mountable chassis along with power supplies, internal wiring, an industrial ethernet switch and external LED status indicators. The chassis also provides a key switch to enable manual override of the 3D limit switch interlock, which is needed for system recovery after limit switch activation. A photograph of the chassis internals is shown in Figure 14. Inside the chassis the motor power wiring is at the rear of the chassis and several SOLA DC power supplies are on the right side. On the front panel is a mains power switch, limit switch indicator lights, limit switch override key and a motion stop button.

Figure 14: Motion Control & PLC Chassis

The motion control chassis shown in Figure 14 was fabricated by the electrical support group at the SNS, who also provided the cabling and connectors for the motors, encoders and brakes.

2.3.1.2 Controls for Temperature Monitoring

In order to monitor the temperature of the steerable optics system, several PT100 RTD sensors were installed and connected to a Lakeshore 224 temperature monitor. Two sensors were used to monitor the air temperature at both ends of the girder, and several surface mount sensors were attached to the girder, girder wings, mover housing and a motor body. The PT100 sensors were purchased from Omega and are 'Class A' sensors with a rated accuracy of ±0.19 °C at room temperature (20 °C). The SNS sample environment group helped to wire up the PT100 sensors and to configure the temperature controller.

2.3.2 Control System Software

The control system software is based on the EPICS (Experimental Physics & Industrial Control System) toolkit. EPICS is a distributed control system based on a client-server architecture. The software is responsible for hardware device control and monitoring, implementation of the kinematic calculations, high level logic and user interfaces. The user interface software was built using Control System Studio (CS-Studio) software, which is an EPICS client application suite.

Additional EPICS software was also developed to enable data collection and analysis of the mockup during testing. This consisted of software to enable step scanning of the motors and the degree of freedom

(DOF) parameters X, Y, Pitch, Yaw, and Roll. The software was able to record data at each step, which included motor positions, digital indicator positions, temperature sensors and DOF setpoints and calculated readbacks and ranges.

2.3.2.1 Motion Control Software

A screenshot of the main steerable optics user interface is shown in Figure 15. The user interface was designed in a way that makes it suitable for use on an Instrument at the STS. It enables DOF control and readback in the top left part of the screen, detailed and expert control in the bottom left, position history and position table functionality in the top right, and overall status and additional control in the bottom right part of the screen.

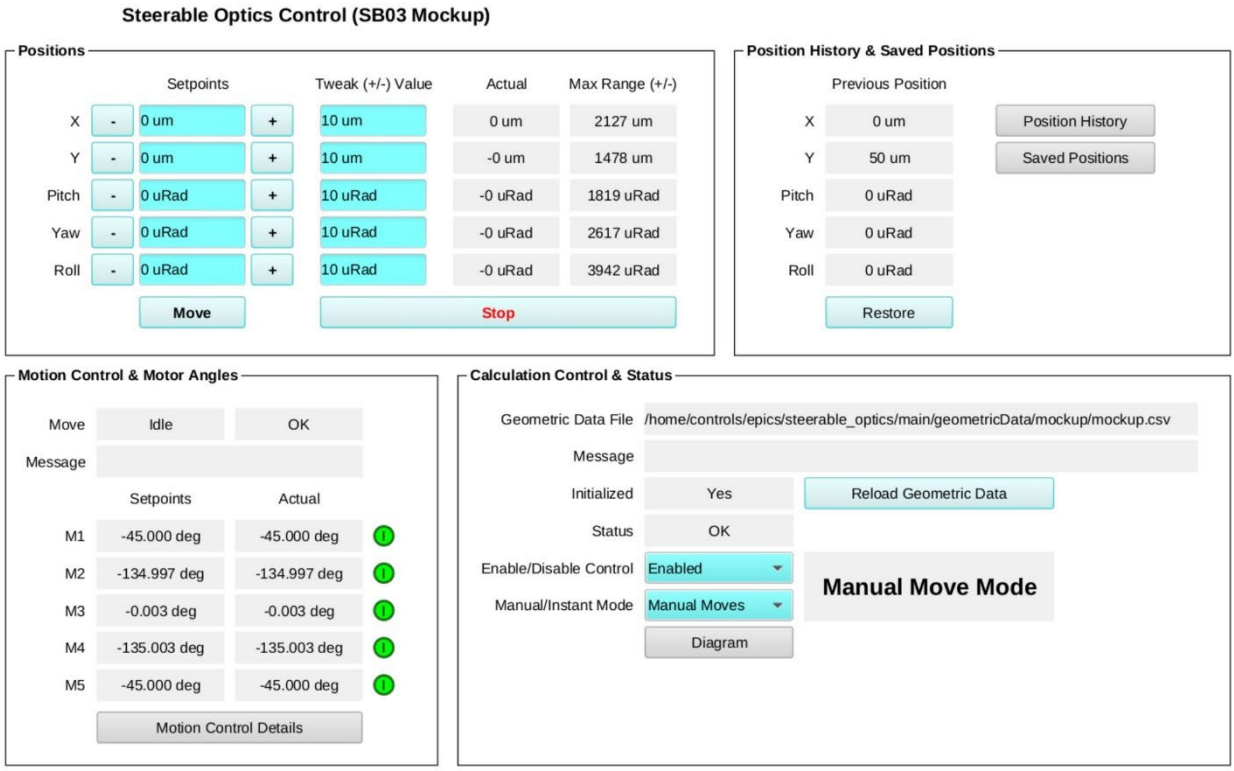

Figure 15. Steerable Optics main user interface based on EPICS and CS-Studio

The 'Motion Controls Details' button provides access to a detailed screen for expert motion control screens, hardware status, motor brake status, limit switch activation status and reset. This screen is shown in Figure 16.

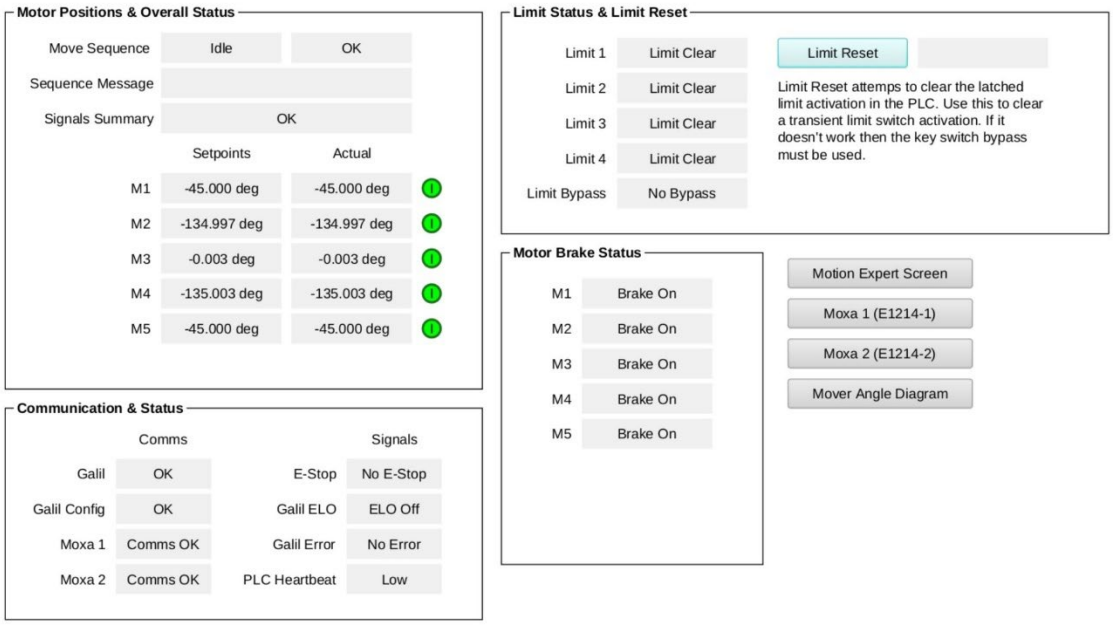

Figure 16. Steerable Optics motion control & status detailed screen

The 'Position History' screen lists a set of the most recent DOF moves along with the time and date of the moves. The 'Saved Positions' screen enables the user to save multiple sets of DOF positions for later use. These screens are very similar in look and feel so only the 'Saved Positions' screen is shown in Figure 17 as an example.

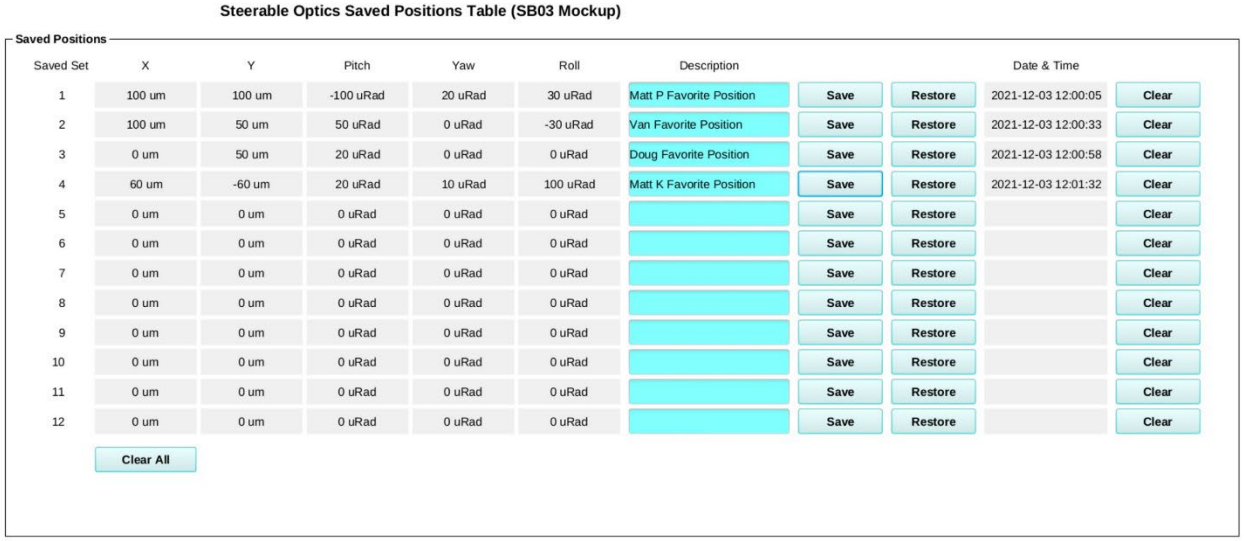

Figure 17. Steerable Optics software saved positions screen

The main purpose of the control system software is to provide motion control and implement the kinematic calculations. The basic motion control is accomplished by the use of a standard EPICS device driver for the Galil motion controller, which was originally developed elsewhere at other EPICS facilities, along with other device drivers & logic developed in-house for this project and for use at the SNS facility. The kinematic equations convert the DOF positions to mover angle positions, calculate the actual DOF

from the mover encoder positions and provide calculations for the available range of each DOF based on the current configuration. The kinematic calculations are described in more detail in the following section.

2.3.2.2 Kinematic Calculations

The kinematic calculations are derived and described in detail in a paper from the Paul Scherrer Institute [3]. The kinematics are configured with a table of input parameters which define the coordinate system origin (i.e. axes of rotation), the location of the motors relative to the origin, the radii of the eccentric mover bearings, the measured eccentricity of the movers and the initial starting angles. The specific table used for the mockup is shown in Table 1.

Table 1. Geometric data input parameters for the mockup system

Parameter Description	**Symbol**					
Girder mover number	*i*	1	2	3	4	5
Midpoint of motor axis	m_x(mm)	-199.959	199.941	199.958	-194.972	-283.872
	m_y(mm)	-346.497	-346.493	-346.357	-346.480	-346.490
	m_z(mm)	-812.881	-812.805	812.791	812.865	812.903
Radius of motor axis	*e*	1.5044	1.5137	1.4784	1.5092	1.5137
Radius of excentric disk	*r*	31	31	31	31	31
Excenter ideal angle	ϕ_o	-45	-135	0	-135	-45
Contact surface of ideal angle	ψ_o	45	135	90	135	45
Constants	*c*	1	-1	0	-1	1
	s	1	1	$\sqrt{2}$	1	1
	p	-1	1	-1	1	-1

In Table 1, the position of each mover is defined by m_x, m_y and m_z. These values were established by the Survey & Alignment group using a Leica laser tracker. See Figure 3 and section 2.2 for the description of the coordinate system and the rotation conventions. The nominal eccentricity of the movers, *e*, is 1.5mm; however, the actual values were determined by measurement using a Mitutoyo dial indicator at various points on the mover bearing and fitting a sine function to the resulting data points. Measurement of the eccentricity proved to be an important step, as it was found that relying on the nominal values gave worse results when comparing demanded DOF positions to measured positions.

The table data is input into the control system using a Comma Separated Value (CSV) text file. The file can be modified and loaded at runtime which facilitates changing the origin of the coordinate system while the software is running. This could be useful if the user needs to demand motions that affect only one end of the girder, which could be accomplished by redefining the m_z values so that the origin is directly above either one of the sets of movers at the ends of the girder.

The formula for calculating the mover angle positions ϕ_i, using Table 1 and a set of desired DOF parameters, is equation 24 in reference [3], and is:

$$\phi_i = \psi_{oi} + \sigma + p_i \left[arccos\left(\frac{c_i(u - \sigma m_{yi} + \eta m_{zi}) + s_i(v + \sigma m_{xi} - \chi m_{zi}}{\sqrt{2} e_i} \right) - \pi \right] - \pi$$

where $i = 1 \ldots 5$, and:

u is translation in X
v is translation in Y
χ is rotation about the X axis (Pitch)
η is rotation about the Y axis (Yaw)

σ is rotation about the Z axis (Roll)

The above equation needs to be computed five times for each move of any set of DOFs. However, before executing a move it is also necessary to check if the desired DOF positions are obtainable. This can be done by checking if the arccos argument is between -1 and +1, since for any angle ∅, $|\cos(\emptyset)| \leq 1$. It can therefore be useful to indicate to the user what the obtainable range is for each of the DOF parameters based on the current girder position. This can be done by solving the above equation for u, v, χ, η or σ, when the result of the arccos term is either 1 or -1. As an example, the maximum range of u when the arccos term is 1 is given by:

$$u = \sigma m_{yi} - \eta m_{zi} + \frac{\sqrt{2}e_i - s_i(v + \sigma m_{xi} - \chi m_{zi})}{c_i}$$

A similar expression can be derived when the arccos term is -1, and the smallest of the two values of *u* is then the current available range for that particular DOF. The available ranges can be calculated on a continuous basis as the steerable optics system is moved around. The maximum possible range of any DOF is available when the girder is at nominal zero position, but as it is moved away from nominal zero, the ranges of all, or some, of the DOFs will start to reduce in magnitude. We can see that the above expression for *u* reduces to:

$$u = \frac{\sqrt{2}e_i}{c_i}$$

when *v*, χ, η and σ are at zero, so that the maximum possible range of X translation is purely defined by the eccentricity of the cams. Similar expressions can be derived for the range and maximum range of *v*, χ, η and σ. In the case of the mockup system the maximum possible DOF ranges are given in Table 2.

Table 2. Maximum ranges of each degree of freedom for the mockup

Degree of Freedom	Symbol	Maximum Range
X Translation	*u*	2.128 mm
Y Translation	*v*	1.478 mm
Pitch (rotation about X)	χ	1.819 mrad
Yaw (rotation about Y)	η	2.617 mrad
Roll (rotation about Z)	σ	3.942 mrad

The formula for the inverse kinematics, which enable calculation of the DOF parameters from the current positions of the 5 movers, is equation 27 in reference [3] and involves a product of an inverse 5x5 matrix and a 5-element vector:

$$\boldsymbol{T} = M^{-1} \cdot \boldsymbol{q}$$

where $\boldsymbol{T} = (u, v, \chi, \eta, \sigma)$ is a vector containing the 5 DOF parameters.

The vector $\boldsymbol{q}$ is defined as:

$$q_i = \sqrt{2}e_i \cos(\phi_i - \psi_{oi}) \qquad i = 1 \ldots 5$$

Each row of *M* is defined as:

$$\boldsymbol{M}_i = (c_i, s_i, -m_{zi}s_i, m_{zi}c_i, p_i) \qquad i = 1 \ldots 5$$

with

$$p_i = m_{xi}s_i - m_{yi}c_i - \sqrt{2}e_i \sin(\phi_i - \psi_{oi}) \qquad i = 1 \ldots 5$$

The results of the inverse kinematics tell the user the DOF positions the girder is in based on the encoder readback positions from the movers. This information, along with the current calculated range of each DOF, show the user how far they are able to steer the girder in each direction of each DOF.

The kinematics, inverse kinematics, and range calculations were implemented using the C language. The matrix and vector algebra is accomplished using GNU Scientific Library (GSL), making use of the linear algebra package and the technique of matrix LU decomposition.

In the context of EPICS software, the kinematics, inverse kinematics and ranges are calculated in an EPICS database, via a subroutine record, whenever there is a new DOF setpoint demand position or whenever the mover encoder positions change. This can be up to ten times each second, depending on how fast the software is polling the motor controller for information. The calculations were timed and found to take less than 100 µs on an Intel i7-8700 3.2GHz CPU. This means that we can easily monitor the DOF positions as they are in motion, and we can update the DOF range parameters at the same time. If the mover is disturbed or manually moved, causing a change in the encoder position, then we can detect this and the DOF information is updated accordingly.

The kinematic calculations and associated EPICS database logic, including the standard CS-Studio screens, are hosted and maintained in ORNL GitLab in the STS Integrated Control Systems group at ‘STS Project/STS ICS/Common/Steerable Optics’.

2.3.2.3 Temperature Monitoring Software

The software for the Lakeshore 224 temperature monitor was previously developed for use at the SNS and so it was installed and configured with minimal effort for this project. The controller has an ethernet interface and it is a simple matter of periodically (every second) sending an ASCII format command to read all the temperature values. A new user interface screen was developed for this project and this is shown in Figure 18.

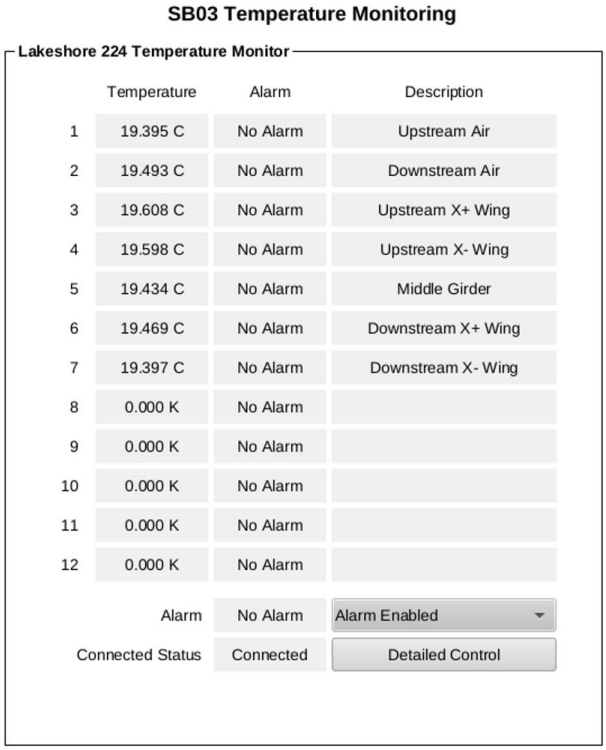

Figure 18. User interface screen for the Lakeshore 224 temperature monitor

2.3.2.4 High-Level Software

The control system software used for this project was built in a way very similar to a standard SNS Instrument and includes useful high-level utilities such as continuous data archiving of select information, a method to run automated sequential commands and data capture, and remote access capabilities. The software used to run automated sequential commands is called the Scan Server, which is used extensively on existing SNS Instruments.

Additional project-specific software was developed to aid in constructing automated sets of commands (known as 'scans') and to provide a way to capture data points at specific timestamps, either periodically or on demand. This software is written in Python and provides an easy way to construct and submit a scan of any of the DOF parameters, which means moving a DOF between two points in sequential steps and recording data along the way with configurable delays. For example, it is possible to translate the girder in the X direction between –1000 μm and +1000 μm in steps of +10 μm, waiting 10 s after each move, and recording a set of data points after each delay, with just a few button clicks and data entry fields. This is shown in Figure 19.

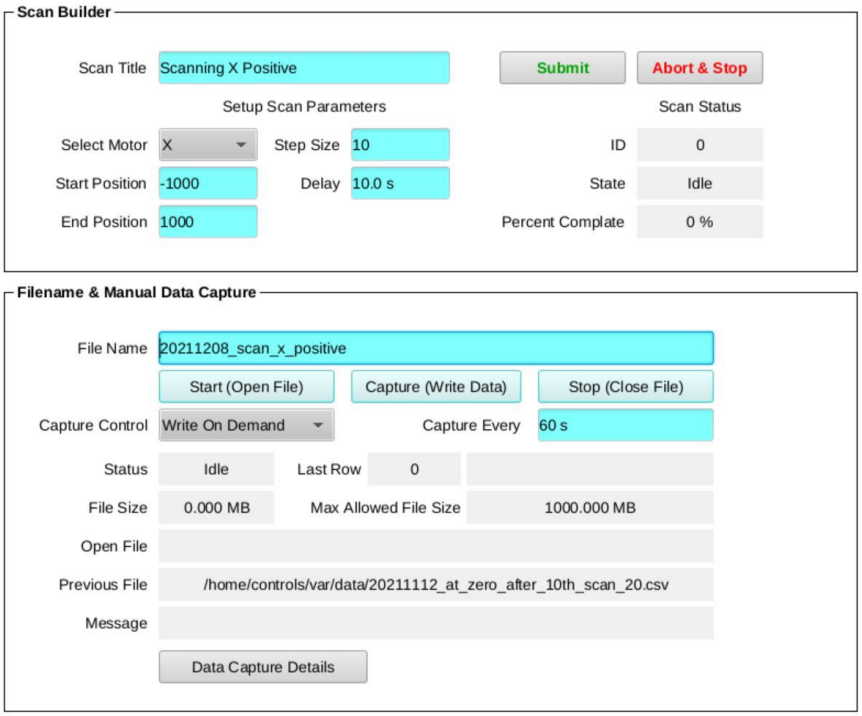

Figure 19. Scan builder & data capture screen

The 'scan builder' user interface constructs and submits the scan to the Scan Server. The Scan Server then executes the commands and controls data collection. In the bottom part of Figure 19 one can see the data collection control panel, which allows the user to specify the data file name, manually perform data capture, setup periodic data capture and see the status of any current file being written to. The list of parameters that were captured as part of a scan were:

- Date and time
- DOF setpoint positions
- Calculated DOF positions
- Current range of each DOF
- Mover angle setpoints
- Mover angle encoder readbacks
- External position sensors
- Temperature sensors

For each scan that moves the girder to N different positions and captures data, a file is produced that contains N rows of comma separated value (CSV) data containing the above information. Each row in the file corresponds to a different date and time, which means a different point in the scan. The data from these CSV files were used to evaluate the performance of the mockup and to generate the plots presented in this report.

2.4 POSITION VERIFICATION SYSTEM DESIGN

To confirm that the mover system was functioning properly, an independent motion-verification system had to be devised to measure the resulting girder motions. Several criteria for the motion-verification system were identified:

- Able to resolve sub-micron translations and sub-micron rotations, alone and in combination, in all six degrees of freedom. The mover system produces intentional motions in only five degrees of freedom, but Bowden et al [2] described unintended motion in the last degree of freedom, Z translation, so measurement along that axis was needed, too.

- Able to resolve these motions over the full range of translations and rotations expected to be produced by the mover system.

- Minimize vulnerability to thermal expansion effects.

- Minimize cost.

Various measurement systems were considered, including laser trackers, other interferometer-based systems, and physical distance measurement systems like Linear Variable Differential Transformers (LVDTs). Laser trackers and other large-volume metrology instruments were available on site, but none were precise enough. The other interferometer systems identified were expensive. In the end, two relatively inexpensive types of linear displacement systems were chosen for the two main phases of the test plan: Mitutoyo digital indicators and Micro-Epsilon LVDTs. The former were to be used for the initial full-range tests, and the latter in the high-precision tests over smaller ranges.

The 3D datum from which all girder motions are computed is the granite surface plate on which the mover system rests. Accordingly, the motion-verification system was mounted to the granite surface plate too. This arrangement avoided any possible differential motion between the mover system and the verification system that might have occurred with an off-the-granite mounting scheme. Similarly, the monuments of the survey control network were all attached to the granite. Granite is not invulnerable to thermal expansion effects, but we relied on the thermal mass of the table and the short timespans for the mover tests to help minimize such effects in the verification system.

When the girder is subjected to any combination of three translations and three rotations, a set of six well-placed linear indicators in contact with it will measure a unique set of linear displacements that can be used to compute those six motion parameters. A total of six linear sensors would be enough to determine the six parameters describing the position and orientation of the test girder, with no redundancy. However, since eight channels were available without purchasing further controllers, we decided to use a total of eight linear sensors. The redundancy in the number of sensors allowed the motion equations to be solved by least squares, providing a slight improvement in the precision of certain motion parameters, and allowing for some degree of deformation detection. The mathematical model assumes that girder and bridges (see below) together constitute a rigid body. Violations of the rigidity assumption (thermal expansion or girder twisting) were detectable as larger residuals in the solution.

The sensors were mounted in locations intended to optimize the precision of the computed girder motion parameters (see locations in Figure 1):

- The precision of the pitch parameter was optimized by placing sensors as far as possible from the X axis.
- The precision of the yaw parameter was optimized by placing sensors as far as possible from the Y axis.
- The precision of the roll parameter was optimized by placing sensors as far as possible from the Z axis.

The logical outcome of the combined optimizations for pitch and roll is to mount sensors vertically at the extreme corners of the granite. However, the test girder does not extend to the corners, so "bridges" reaching the corners of the table were attached at each end of the girder. These bridges served to transmit the girder motions to more optimal positions for precise measurement. Vertical sensors at three of the corners would have sufficed for computing pitch, roll, and Y translation, but the relatively small lateral extent of the granite limited the precision with which roll could be computed. To improve the precision of roll measurements one of the redundant sensors was mounted vertically at the fourth corner of the table. But even with this geometric advantage, the roll angle is still the most weakly determined parameter among the three angular degrees of freedom.

Taking advantage of the mounting fixtures required at the corners for the first four sensors, additional sensors were positioned at three of the corners, parallel to the X axis, to measure yaw and X translation. Only two sensors are actually required to measure these two parameters, but the remaining redundant sensor was added to this group, positioned opposite of one of the others to detect thermal expansion in the bridge.

The eighth sensor was positioned parallel to the Z axis to detect unintended motion in the Z direction, as described by Bowden et al [2].

To provide the flattest possible contact surfaces for sensor probe tips, we chose to attach mirrors to the girder bridges, recognizing that the probe tips would be sliding across them. We did not want surface roughness or other non-planarity to be interpreted by the verification system as motion.

Rather than trying to precisely align the sensor axes to be parallel to the coordinate axes, we chose to measure their installed positions precisely. Similarly, the mirror contact planes were precisely measured instead of being precisely aligned. This saved time and effort and negated the need for providing precise adjustment mechanisms. It is often true in metrology that objects can be measured more precisely, and more quickly, than they can be aligned. The mathematical model handles these measured sensor and mirror orientations rigorously in the conversion of these linear displacements into the six parameters of girder motion. So:

- Sensors don't need to be precisely perpendicular to mirrors.
- Sensors and mirrors don't need to be precisely parallel to coordinate system axes.
- The changing indicator/mirror contact points are dealt with rigorously.
- Multiple simultaneous rotations and translations can be resolved rigorously.

However, there are some assumptions in the mathematical model:

- Assume that lateral displacement of indicator stem within its housing has negligible effect.
- Assume that the girder is perfectly rigid and shows no thermal scaling (until shown otherwise by large residuals).
- Assume that the spherical probe tip isn't significantly gouging into mirror surface.
- Assume that the spherical probe tip is not significantly mis-centered on axis of the indicator.

3. MOCKUP TESTING

3.1 PREPARATIONS

Several tasks were required to be completed before the system was ready for testing. Some of these pertained to the movers themselves and their initial angular orientation, while others pertained to the setup and configuration of the external survey network.

3.1.1 Mover assembly

A description of the movers was provided in Section 2.2.1, with a cross-section CAD image of an assembled single-axis mover shown in Figure 8. The components shown in that figure were supplied by multiple vendors, and a machine shop provided the mover housing, shaft, and other machined parts. The machine shop assembled the bearings and shaft into the housings, which required some custom fixtures designed by ORNL. The gear reducer, motor, and encoder were procured separately by ORNL, so the final assembly of these components was completed on site. Figure 20 shows the assembly of the gear reducers into the housing.

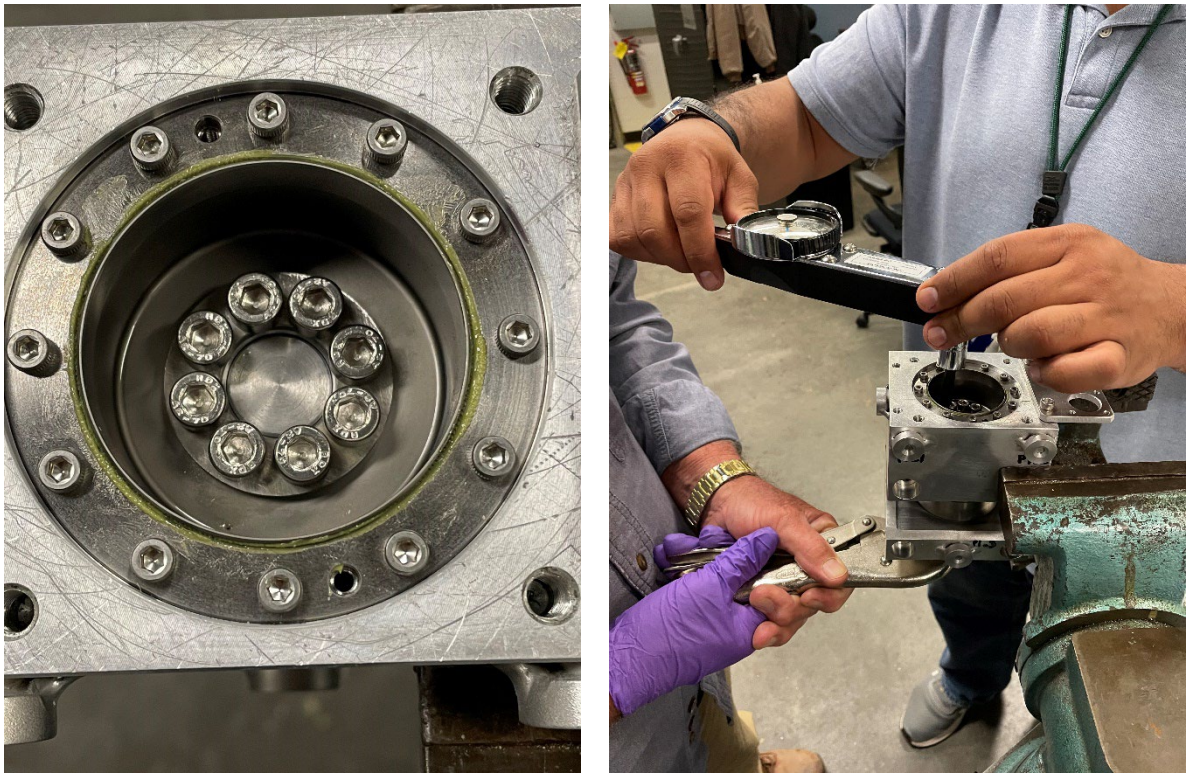

Figure 20. Assembly of the integrated Harmonic Drive gear reducer components

Figure 21 shows the assembly of the stepper motor with integrated brake and the absolute encoder onto the housing. The photos show the assembly of one of the three single-axis movers; the double-axis mover incorporates all the components of two single-axis movers into a wider housing, but the installation processes were the same.

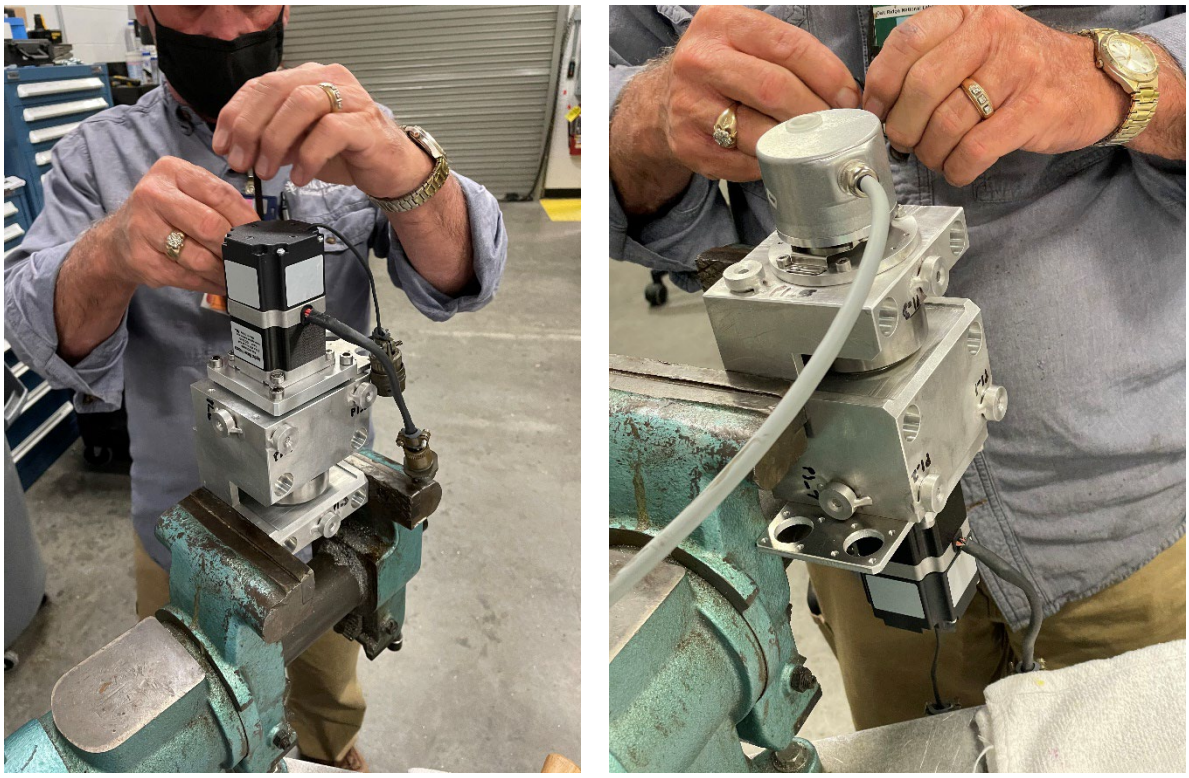

Figure 21. Assembly of the motor/brake (left) and encoder (right)

The final completed mover assemblies can be seen in Figure 6 and Figure 7.

3.1.2 Determination of eccentricity and TDC

After the movers have been assembled and installed, it is necessary to configure the control system so that the motors and encoders are moving in the correct directions. For movers 1 & 2, the positive direction should be counterclockwise, as seen from the motor side, and for movers 3, 4 & 5, the positive direction should be clockwise, as seen from the motor side. This means that, when rotating positive, the top part of the movers should all be rotating towards the negative X direction. To accomplish this, it is first necessary to ensure the motor is moving in the same direction as the encoder, which needs to be done by setting the motor direction on the motion controller. The encoder direction cannot be changed in the case of absolute encoders. Then, if the mover direction is not already correct, the sign of both the motor and encoder software scaling factors would need to be changed.

It is then necessary to determine the encoder position of the top dead center (TDC) of the eccentric cam, which is necessary for aligning the cam to the correct starting angles ϕ_o as listed in Table 1. This was done by mounting one of the Mitutoyo digital indicators in a vertical position, pressing against the mover cam, and using the motion control system to step through a series of angles and recording the indicator position at each step. This setup is shown in Figure 22.

Figure 22. Measurement of mover eccentricity and TDC

The vertical displacement of the cam is simple harmonic motion and can be represented as a sine profile, with the peak height obtained with the cam at 90° (relative to the starting angle ϕ_o). The following sine function was used to fit the digital indicator data as a function of encoder angle:

$$y = a\sin(b - c) + k$$

where:

y = measured vertical displacement
a = amplitude (cam eccentricity)
b = measured encoder angle
c = phase offset
k = vertical offset to account for the arbitrary zero position of the indicator

The phase offset is used to compute the encoder position corresponding to the 90° position, and the amplitude a of the function is the cam eccentricity. The nominal eccentricity is 1.5 mm; however, it is necessary to measure the actual eccentricity of each cam to obtain the best results. It was found that using the nominal eccentricity values significantly increased the positioning errors for larger DOF magnitudes, as shown later. The measured eccentricity values are listed in Table 1.

Once the encoder positions are established for the 90° position of each mover, it is then necessary to rotate the mover to the starting angles ϕ_o. However, this cannot be done before first calibrating the single turn absolute encoders so that the starting angles are 180° away from the 'zero' position of the encoder. This is necessary to avoid encoder position 'roll over' during normal operation, which would cause the encoder positions to suddenly transition from 359.999° to 0.0°, or from 0.0° to 359.999° depending on the

direction of motion. This can be accomplished by first rotating to 180° opposite to the starting angle ϕ_o and pressing the hardware position reset button on the encoder. The exact procedure varies slightly between each of the movers, depending on the relative distance from the TDC and the starting angle and the direction of rotation. As an example, the procedure for mover 1 is:

1. Find the 90° position (TDC)
2. Move relative +45° to orient the mover 180° opposite to the starting angle -45°.
3. Zero the encoder by pressing the reset button
4. Zero the motor position in the motion controller
5. Set the motor offset value in the motion control software to either:
    a. +135° if the control system is using a negative encoder scaling factor
    b. -225° if the control system is using a positive encoder scaling factor
6. Move to the starting angle -45°.

This procedure ensures that the starting angles are 180° away from the encoder zero position, such that the zero position would never be encountered during normal operation because the maximum commanded angle for any mover is ±90° relative to its starting angle.

3.1.3 Survey control network, coordinate system

To construct a stable coordinate system for the steerable optic mockup, spherically mounted retroreflector (SMR) monuments were epoxied to the granite surface plate prior to installation of the assembly. A total of 43 monuments were arranged at various locations around the top and side planes of the surface plate. The monuments were measured from 16 stations using a Leica AT960 laser tracker. A set of ideal composite points were constructed from the measurements using the Unified Spatial Metrology Network (USMN) tool in Spatial Analyzer software. The resulting network of monuments, all referenced to the coordinate system of the mover system, permitted the use of a laser tracker from any position around the table for mapping and alignment tasks.

The coordinate system shown in Figure 23 uses the standard SNS beamline definition, X+ Beam Left, Y+ Vertical (parallel to the local gravity vector), and Z+ Horizontal (parallel to the beam trajectory). The planes of the surface plate were also measured during the mapping of the monuments to construct a local coordinate frame. The tabletop origin was constructed at the intersection of the X+/- Bisector Plane, Z+/- Bisector Plane, and the top surface plane. The Nominal Guide Center frame origin was then constructed at 444.89 millimeters Y+ based on the nominal drawing geometry. This origin point represents the center of a hypothetical neutron optic mounted on top of the girder.

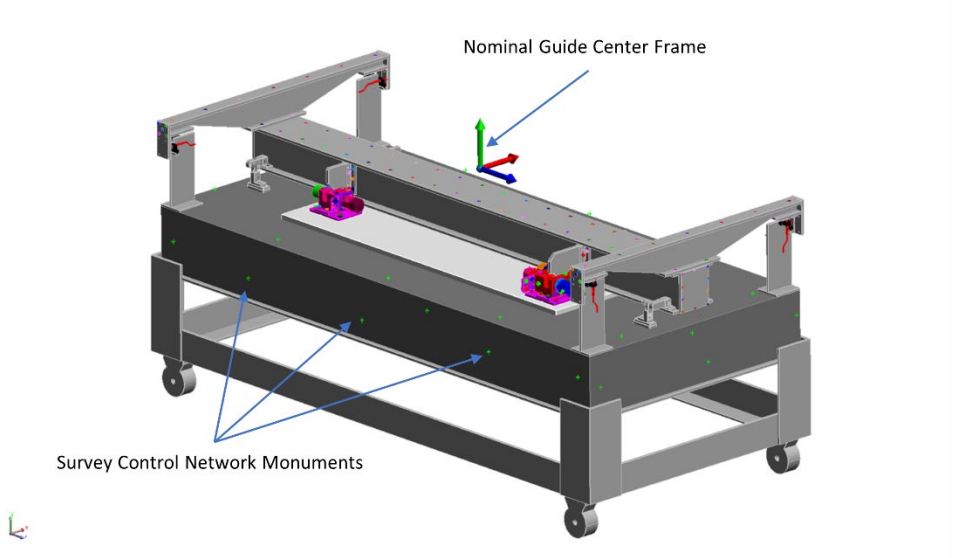

Figure 23. Survey control network coordinate system

3.1.4 Mover fiducialization and alignment

The mover assemblies were mapped using a Faro Edge portable coordinate measuring machine (PCMM). The mover assemblies were measured while partially complete, without the motors and encoders installed, to allow access to the bearing shaft (at the encoder interface) and motor/gear reducer bore. The surface plate plane was measured to establish the Y axis, datum A of the mover housing, and then the 55.0-millimeter diameter bearing mounting bore and the bearing shaft were measured to establish the Z axis. The origin was constructed at the intersection of the Z axis and the midplane of the cam/vee interface of the housing. The fiducial nests mounted on the faces of the housing were then mapped with respect to the individual assembly's coordinate frame using a 0.5" probe tip.

As shown in Figure 24, coordinate frames were constructed in the metrology software package Spatial Analyzer at the ideal locations for each of the mover assemblies based on the nominal dimensions of the assembly print. The measured features and fiducial locations were imported for the mover assemblies to define the ideal locations for each mover. The foundation base plate was located on the granite surface plate with the completed mover assemblies and adapter/base plates roughly aligned (Figure 25). Final alignment of each mover assembly was achieved using a Leica AT960 laser tracker based on the ideal fiducial locations from the preceding fiducialization process. Adjustments along X and Z axis were accomplished by sliding the mover base plates and adapter plates along the 6-mm key stock alignment features. Adjustments in Y, Rx (Pitch), and Rz (Roll) required the addition of shim stock between the mover housing and mounting plates.

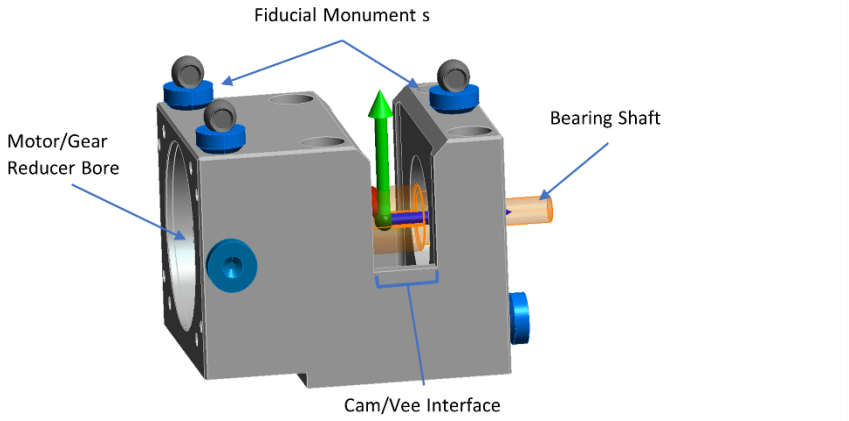

Figure 24. Fiducials for mover coordinate frames

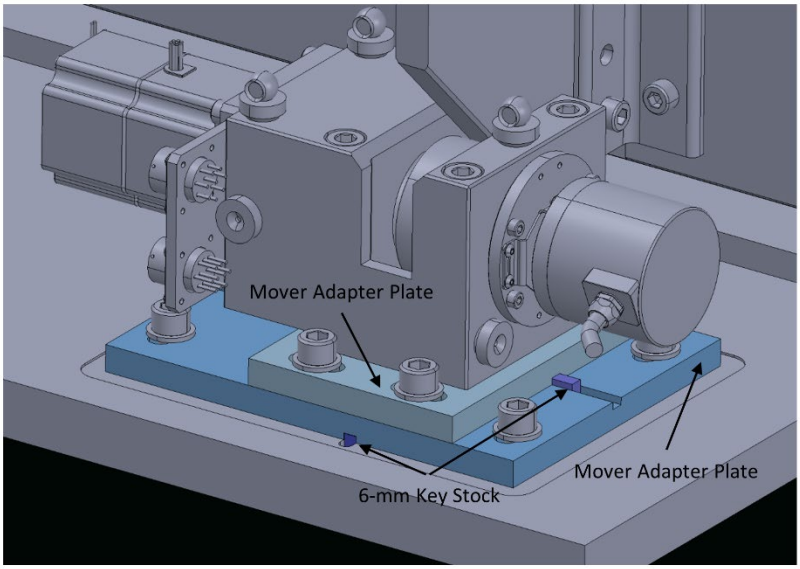

Figure 25. Mover base plates

3.1.5 Motion-verification sensors

Two types of external position verification sensors were used, each one requiring different control integration methods.

The first type of position sensor used was the Mitutoyo digital indicator model ID-H0530. These have a resolution of 0.5 µm and an accuracy of 1.5µm over 30-mm range. These were used to measure the position of the girder system when moving larger distances. These have an RS232 serial port, and we used a Mitutoyo serial multiplexer unit to connect all eight digital indicators to provide a single RS232 port for use by the control system. A Moxa 6100 terminal server was used to provide a serial-to-ethernet interface on which to read the position data.

The second type of position sensor used was a Micro-Epsilon induSensor Linear Variable Differential Transformer (LVDT) with a ±3-mm range. These LVDTs are fed an AC current from a compatible Micro-Epsilon controller (model MSC7802), which converts the LVDT position into 2-10 V analog signals that can be read by an external analog-to-digital converter (ADC). The ADC chosen for this was the Moxa E1240 16-bit ADC unit, which provides us with a position resolution of 0.15 μm. It is difficult to estimate the accuracy of this measurement system without characterizing the ADC; however, these sensors were only used for high-resolution tests over a narrow 200-μm (or 200-μrad) girder movement range, and efforts were made to reduce measurement noise by averaging the ADC value over multiple samples. In addition, the LVDT voltage-to-position conversion was calibrated using a Renishaw linear encoder system, which is described later.

To integrate the Micro-Epsilon equipment two rack mountable chassis were fabricated, each holding two MSC7802 controllers and a single Moxa E1240 unit. This catered for the eight LVDT sensors used in the project. A photograph of one of the opened chassis is shown in Figure 26, which also shows the Moxa serial-to-ethernet converter used to initially configure the Micro-Epsilon controllers.

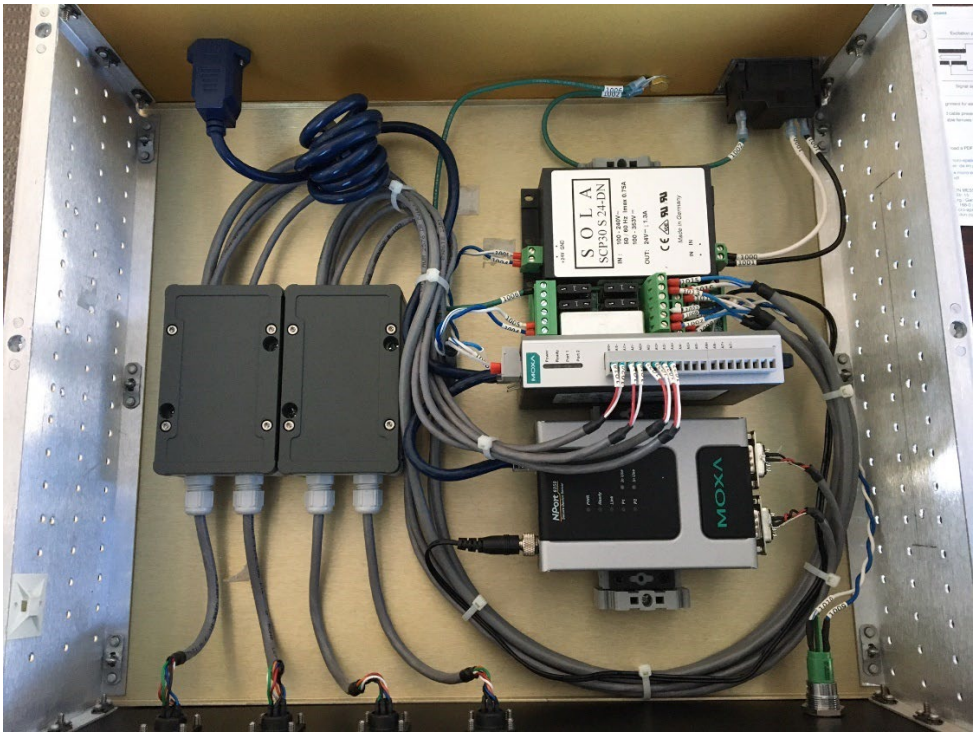

Figure 26: Chassis containing two Micro-Epsilon MSC7802 controller, power supply, readout and interface equipment.

The software for the Micro-Epsilon LVDT system involved using a device driver to interface to the Moxa ioLogik E1240 unit, which was responsible for converting the 2-10 V signal from the Micro-Epsilon controllers to an ADC count value. This software had already been developed for use at the SNS, so installation and setup were easy. Additional software was then developed to convert the ADC count back to voltage (a linear transformation), and then to calculate the position of the sensor.

The LVDT voltage-to-position conversion is not a simple linear relationship, so it was necessary to calibrate each sensor separately for the purposes of the mockup project. The LVDT sensors were each mounted on a motorized linear stage that could push against the end of the LVDT sensor. The stage position was read via a Renishaw linear absolute encoder with 50-nm resolution and accuracy of ±1.5 μm

over a 1-m length. A Python software script was then used to move the stage in 0.1mm steps, recording the LVDT voltage and the encoder position at each step, over a 6-mm range. Then a 5th-order polynomial function was used to provide a best fit to the position data, and the resulting coefficients were input into the control system software to provide voltage-to-position conversion. The quality of the fit was checked by re-calculating the position by using the voltage and actual (encoder) position data that was used to estimate the polynomial coefficients, and the difference between the calculated position and the actual position was found to be always less than 0.5µm.

The position data was also averaged over ten readings to reduce the effects of ADC noise. The position data was then displayed on the user interface and an example screenshot is shown in Figure 27.

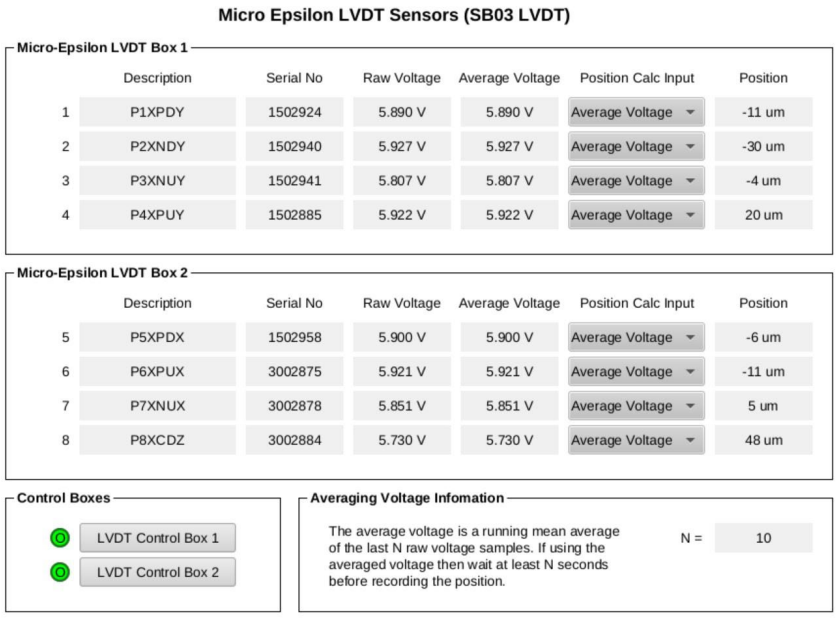

Figure 27. Micro-Epsilon LVDT position sensor user interface

The software developed for the Mitutoyo dial indicators is relatively simple. The indicators provide a RS232 serial interface to which ASCII commands can be sent to read back the position information. This was accomplished using a Mitutoyo RS-232 multiplexer (MIG) unit and a Moxa serial-to-ethernet converter. The software simply periodically (every few seconds) sent a command to read back the eight position values, and then displayed the results on the user interface, as shown in Figure 28.

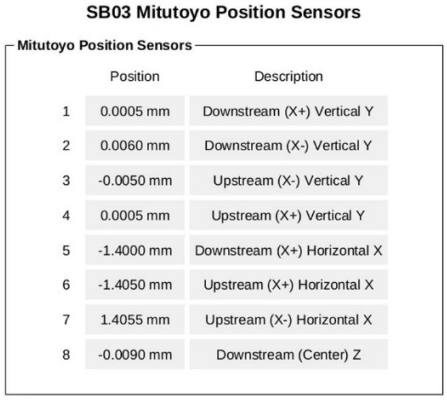

Figure 28. Mitutoyo position sensor user interface

The position values read from these sensors were recorded by the control system software as part of the scan applications described in section 2.3.2.4. The data recorded by the scans were used to generate the results described in the next section.

3.2 TESTING

For the initial system characterization (section 3.2.1) and the 10-μm/10-μrad step tests (section 3.2.2.1), the Mitutoyo indicators were needed in the motion-verification system for their larger measurement range. For the higher-precision step tests (sections 3.2.2.2 and 3.2.2.3), the Mitutoyo indicators were replaced with Micro-Epsilon LVDTs for their higher precision. In both cases, the sensors were installed in the approximate positions and orientations described in Section 2.4.

After installation, the position and orientation of each sensor was precisely mapped relative to the survey control network using a AT960 laser tracker. The position and orientation of each sensor was re-mapped when the sensors were changed.

To map the corresponding mirror planes, the girder was driven to its "home" position (where all movers are set at mid-range), and the mirror planes were precisely mapped relative to the survey control network, too. The mirror planes remained unchanged when sensors were swapped.

3.2.1 Initial system characterization

The system was initially characterized by running software scans in a single degree of freedom (DOF), for each of the possible motions: X, Y, Pitch, Yaw or Roll. The differences between the demand (setpoint) positions and the actual measured positions were then calculated and plotted, both for the individual DOF being scanned and for the incidental motions in the remaining DOF, including translation in Z. The scans of each DOF were performed in both directions, first in the positive direction and then in the negative direction. Additional testing was later done by moving multiple DOF at the same time and plotting the differences in the same way.

A scan of X across the full range of motion, from -2100 μm to +2100 μm in steps of 100 μm (in both directions) is shown in Figure 29. It shows that it is possible to position X accurately to ±8 μm, and the result is largely independent of direction except at large negative X values (which had the largest difference in time, as the scan was started at -2100 μm and the reverse scan ended at the same position).

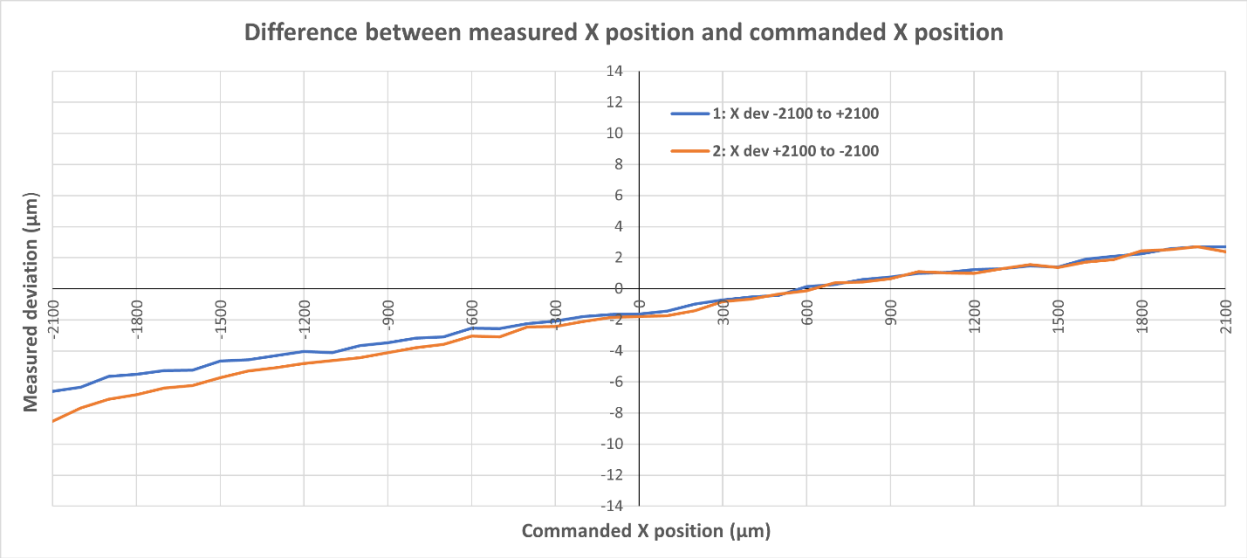

Figure 29. Scan of X between -2100 µm and +2100 µm in steps of 100 µm

Incidental motions in the other DOF were observed during the scan in X. These motions are shown in Figure 30. The vertical axis in Figure 30 is in microns for Y and Z, and in microradians for Pitch, Yaw, and Roll. One can see a large amount of Roll developing as X is moved to extreme values. In addition, some amount of motion in the Z direction is observed. The magnitude of the Roll and Z incidental motions decrease back to zero as X is moved back to zero.

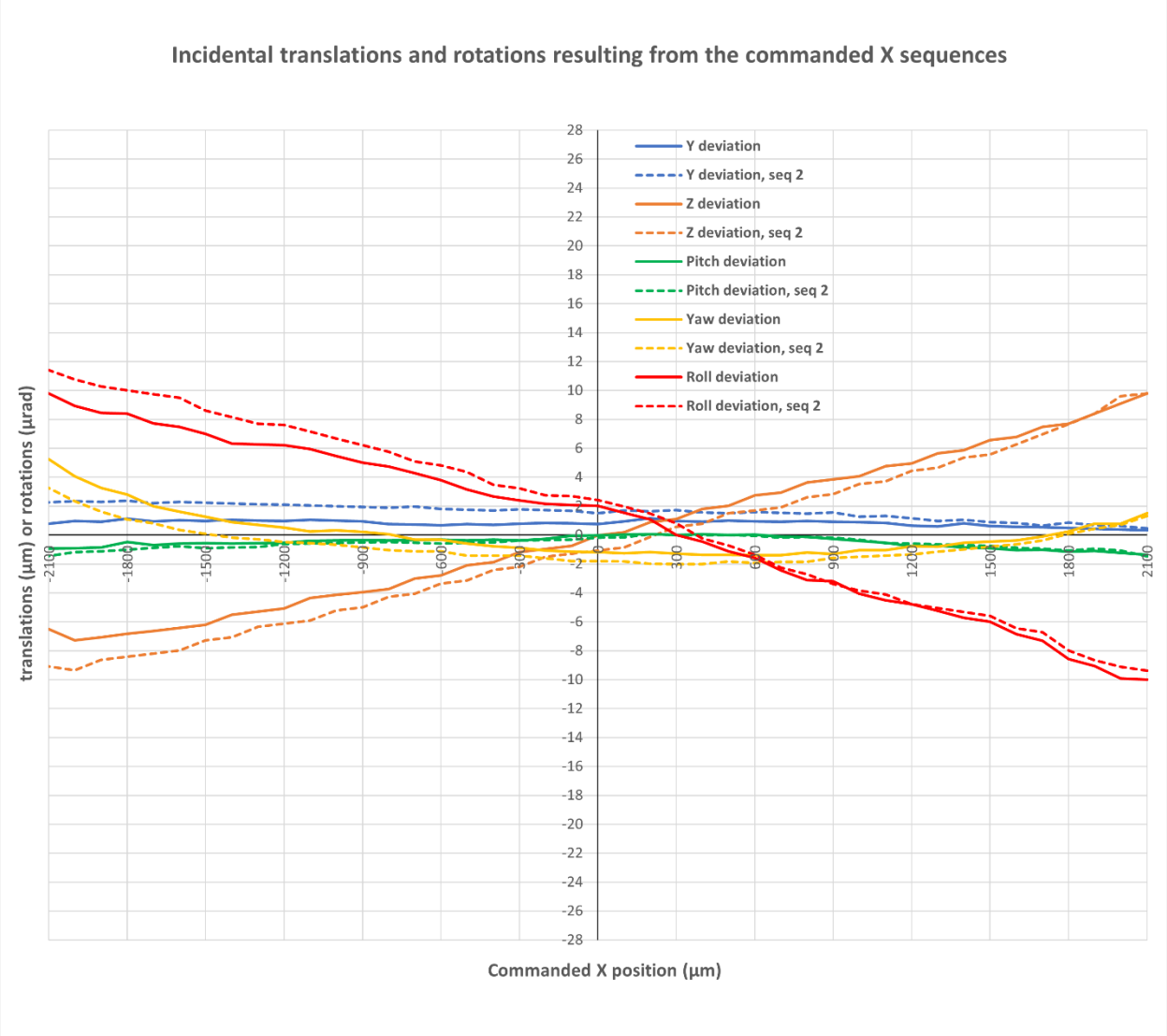

Figure 30. Incidental motions observed when scanning X between -2100 µm and +2100 µm

Similar results can be found for scanning Y across the full range of motion (-1400 µm to +1400 µm, in steps of 100 µm). The difference between the setpoint Y and the actual measured Y is shown in Figure 31, which shows that Y can be accurately positioned to within ±3 µm across the range of motion.

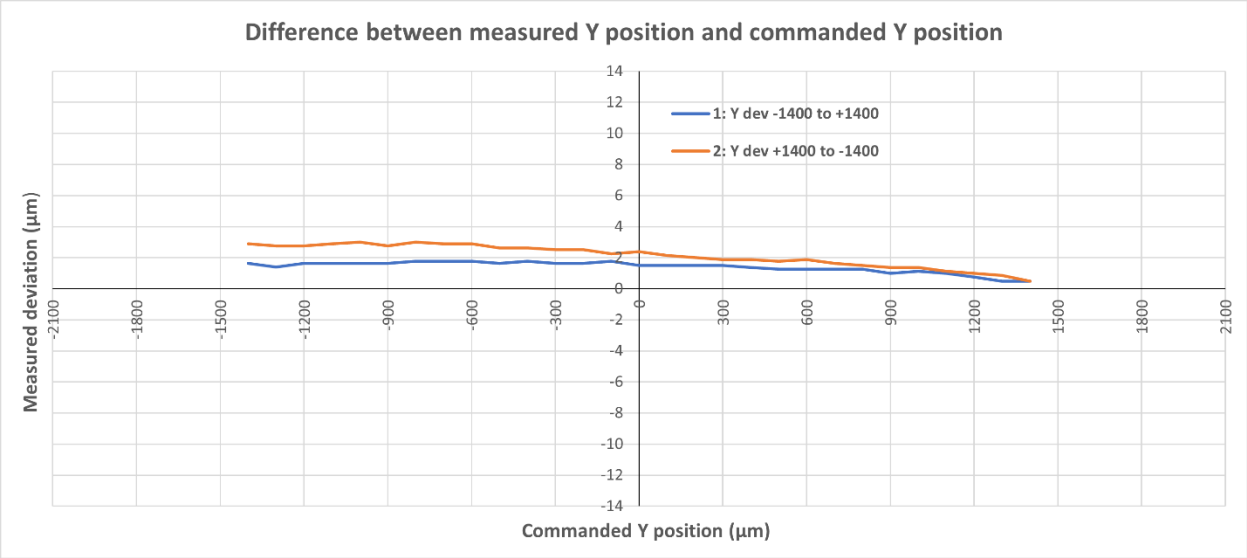

Figure 31. Scan of Y between -1400 µm and +1400 µm in steps of 100 µm

The incidental motions on X, Z, Pitch, Yaw, and Roll when scanning Y are shown in Figure 32. The incidental Roll is the largest unintended motion in this test.

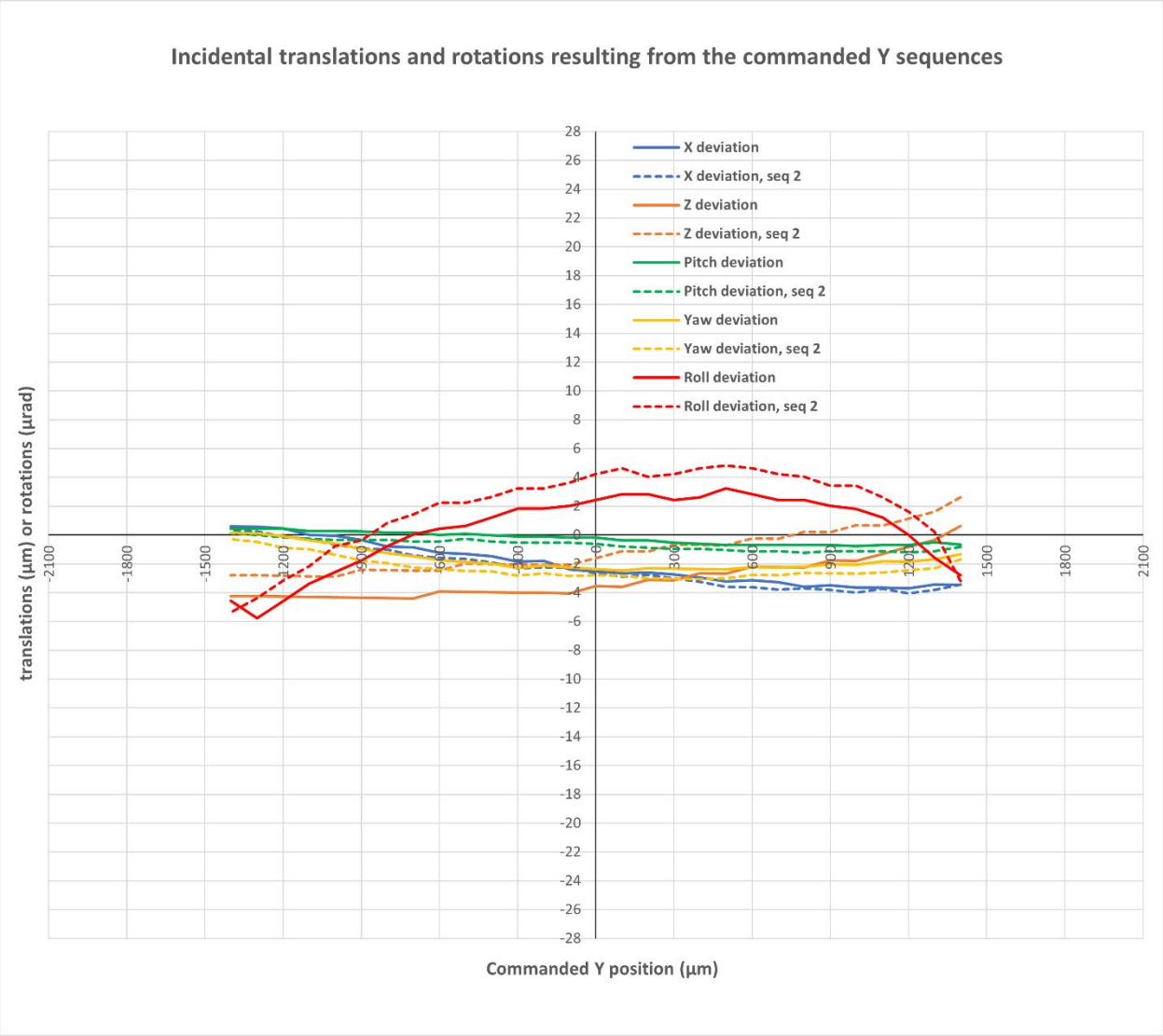

Figure 32. Incidental motions observed when scanning Y between -1400 µm and +1400 µm

These plots are reproduced in Appendix A, along with the same plots for scans of Pitch, Yaw and Roll. Similar results are obtained when performing the rotational movements, except that larger incidental motions are observed in some cases. In addition, when scanning Yaw, a large shift in Z is observed, which is not corrected when moving Yaw back to zero. There is also some hysteresis observed when reversing directions.

Similar results were obtained when scanning multiple DOF. For example, moving X and Y simultaneously between –1000 µm and +1000 µm in steps of 100 µm produced excellent results and shows that it is possible to position both X and Y to within ±2 µm across that narrower range of motion. A reduced range of motion had to used when moving multiple DOF. These results are shown in Figure 33 and Figure 34. The corresponding incidental motions on Z, Pitch, Yaw and Roll are shown in Figure 35.

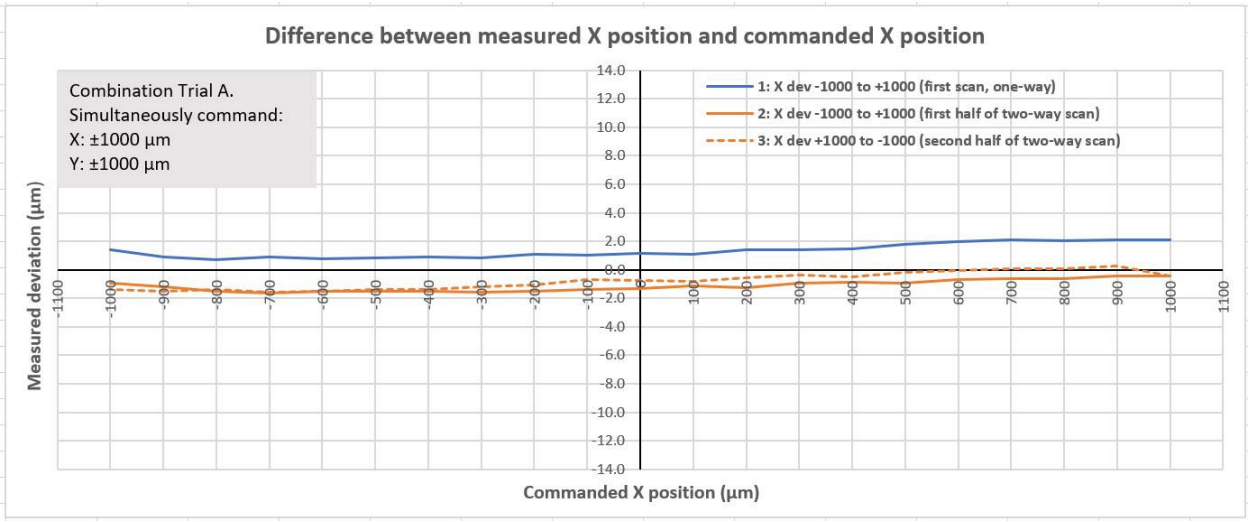

Figure 33. Difference between X setpoint and measured position between -1000 µm and +1000 µm when moving both X and Y

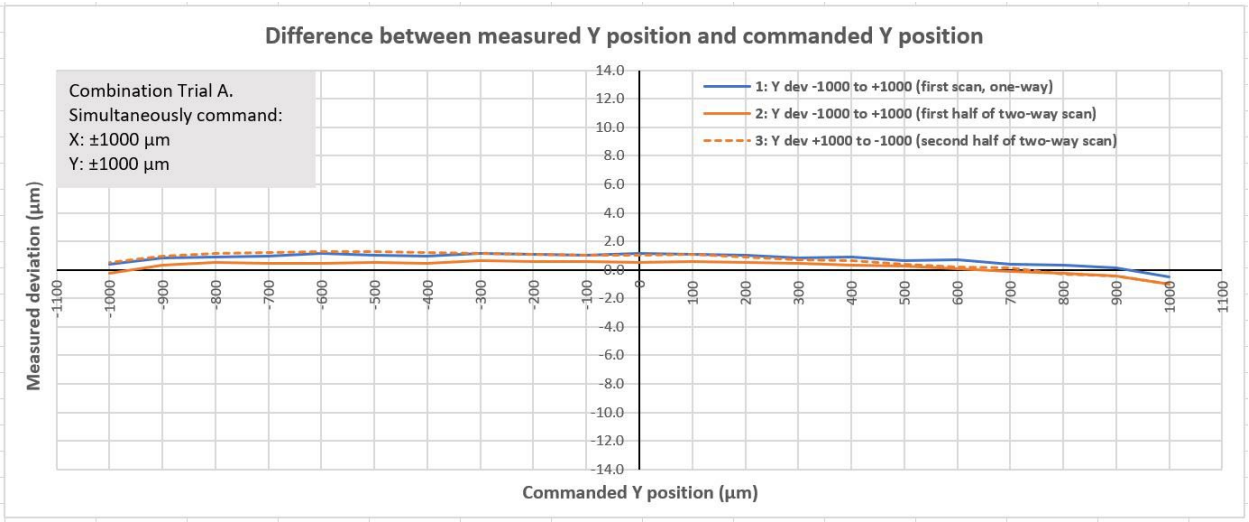

Figure 34. Difference between Y setpoint and measured position between -1000 µm and +1000 µm when moving both X and Y

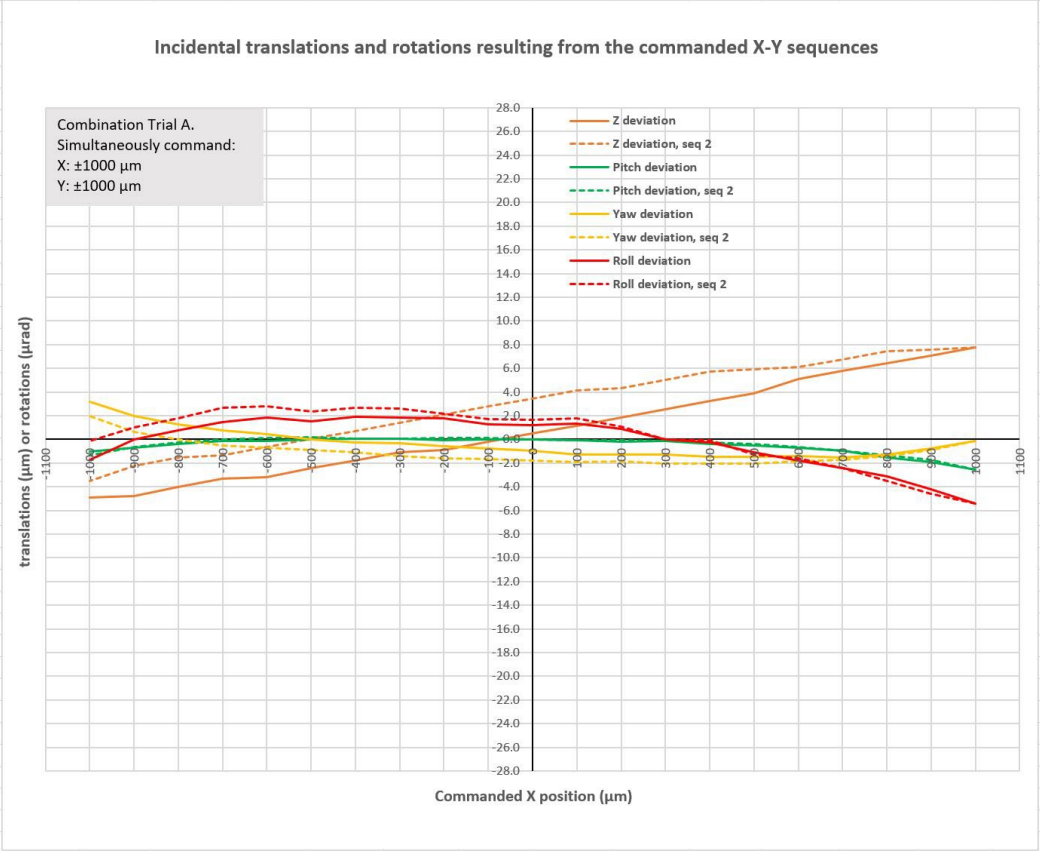

Figure 35. Incidental motions when scanning X and Y between -1000 µm and +1000 µm

The data in the plots in this section, and in Appendix A, show that it is possible to position any one of the DOF to within approximately ±10 µm for X and Y, or ±10 µrad for the angular motions Pitch, Yaw and Roll, across most of their ranges of motion. Towards the limits of the ranges of motion, the positioning errors increase and larger incidental motions can be observed. In particular, when moving Pitch, a large amount of Roll (25 µrad) was developed. The Yaw angular motion can also cause some level of positioning hysteresis in a few of the other DOF.

In the plots in Appendix A, it is also worth noting that the Y height position starts to increase as the testing progresses. This is suspected to be due to thermal effects caused by heat radiated from the stepper motors. This is discussed in more detail in section 3.2.3.

3.2.2 High-resolution system characterization

After the initial characterization of the system was completed, a series of tests was performed to characterize the high-resolution performance of the system. The focus of these tests was not global accuracy, but instead the relative accuracy of small, incremental steps. The first test was a series of 10-µm (or 10-µrad) steps commanded in each DOF. It was not deemed necessary to try to scan the full range of motion at this resolution. Instead, each DOF was scanned at just three relatively small bands: at each end of the range and at the center of the range. The results of this test are presented in section 3.2.2.1. Next, a series of 1-µm (or 1-µrad) steps was commanded in a small band near the center of the range for each DOF (section 3.2.2.2). Finally, a series of 0.5-µm steps was commanded in X and Y (section 3.2.2.3).

3.2.2.1 10-micron (and 10-microradian) step tests

The results of the 10-µm step tests were very similar to the initial system characterization results. Instead of testing the full range of each DOF, the ends and center of each DOF were scanned at 10-µm (or 10-µrad) intervals for 41 positions each. Drift in the Z parameter was observed again, primarily during the scans of pitch and yaw. Hysteresis was seen again between the two directions of the yaw scans and was also reflected in some of the incidental motions produced during the yaw scan (particularly roll and X translation). To measure the actual translation step sizes produced by the mover system, successive positions were differenced without overlap, so each one-way set of 41 positions yields only 20 measured steps. The last position in each set is discarded since it is unpaired. The results of the 10-µm step tests in X are shown below in Figure 36, Figure 37, and Figure 38. The results of the scans in the other DOF are presented in Appendix B.

Figure 36. Scan of X in three bands between -2100 µm and +2100 µm, with step size of 10 µm.

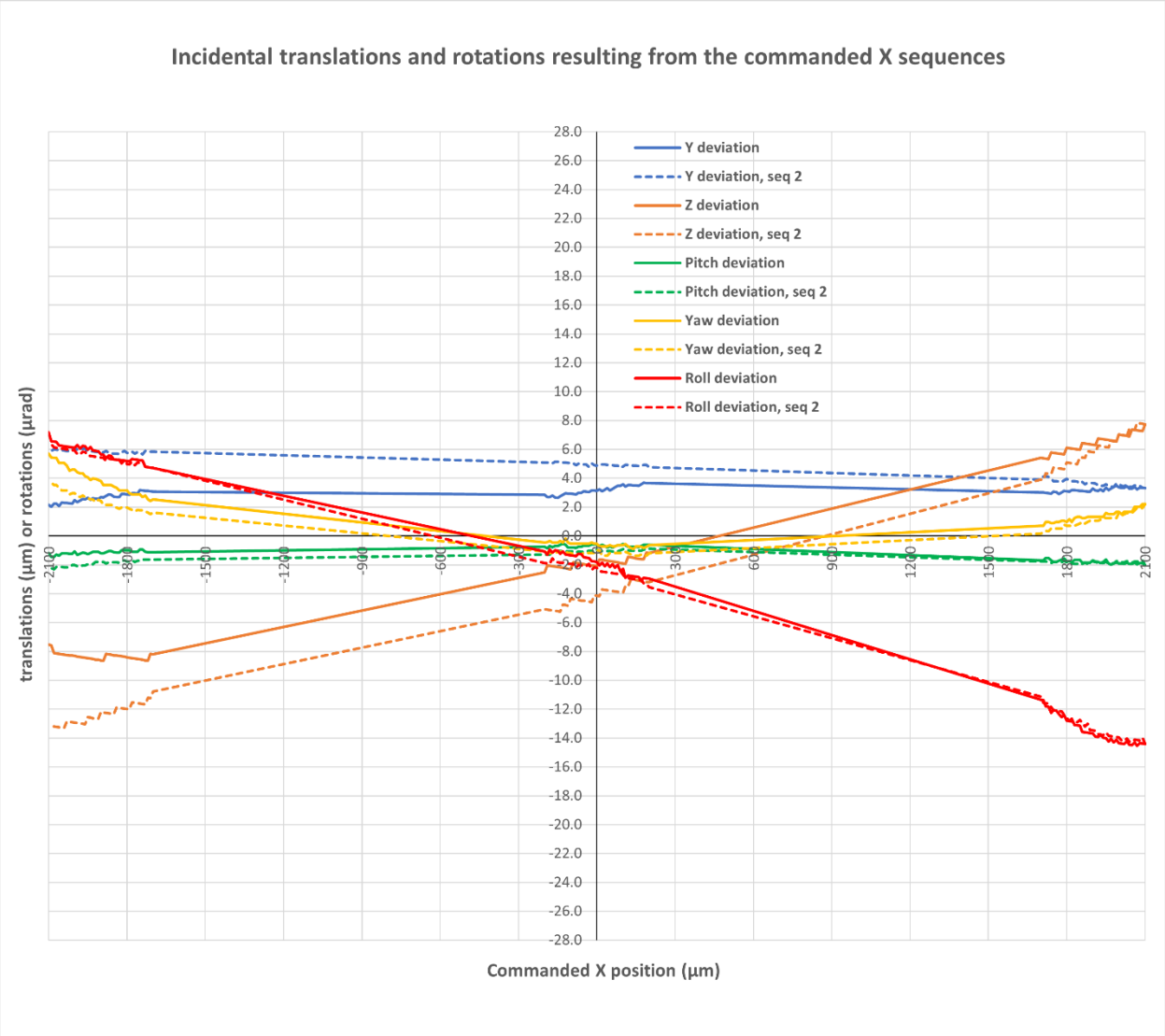

Figure 37. Incidental motions when scanning both directions in X, in three bands between -2100 µm and +2100 µm, with step size of 10 µm

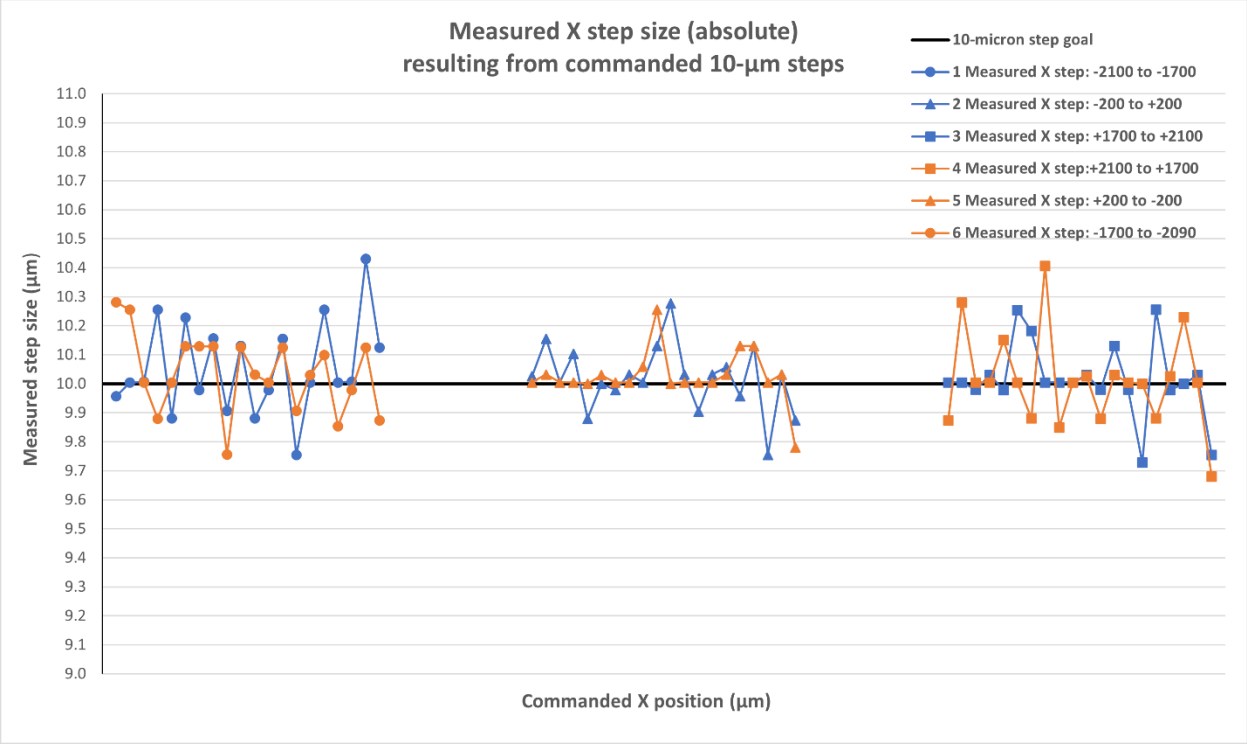

Figure 38. Computed step sizes (nominally 10 µm) when scanning both directions in X, in three bands between –2100 µm and +2100 µm.

3.2.2.2 1-micron (and 1-microradian) step tests

Since the desired resolution of this test was close to the resolution limit of the Mitutoyo indicators, we switched to the Micro-Epsilon LVDT sensors for motion verification. Because of the smaller usable range of the LVDTs, the end-of-range portions of each DOF were not examined and the testing was carried out on a band of ±100 µm (or ±100 µrad) at the middle of the range of each DOF.

To measure the actual translation step sizes produced by the mover system, positions were measured at commanded 1-µm intervals between -100 µm and +100 µm, and then back to -100 µm again, for a total of 201 positions in each direction. These positions were first processed in the usual way, finding the six best-fit translation/orientation parameters corresponding to each position. Then the resulting translation parameters were differenced to compute the measured step sizes. To calculate statistically independent step sizes from these measured positions, successive pairs were differenced without overlap, so each one-way set of 201 positions yields only 100 measured steps. The last position in each set is discarded since it is unpaired.

For testing the rotation step sizes, an analogous process was used, measuring at commanded 1-µrad intervals. The resulting rotation parameters were processed and differenced in the same way, providing 100 independent measured angular steps for each one-way set of 201 positions.

For ease of comparison, the negative steps of the second half of each test were converted to positive steps in the statistics below. There were no actual cases of a commanded positive step yielding a measured negative step, or vice versa.

Table 3 summarizes the results of the 1-µm (1-µrad) step testing for all five DOF, scanned in both directions. The computed root mean square (rms) values in the table, while very low, are actually

pessimistic estimates of the step size uncertainty since they are still inflated by the uncertainty of the LVDT readings from which they were determined. The uncertainty of the LVDT readings has not been quantified.

Table 3. Statistical results from tests of commanded 1-µm and 1-µrad steps.

Test	n	Mean step size (µm or µrad)	Median step size (µm or µrad)	Min (µm or µrad)	Max (µm or µrad)	rms (µm or µrad)
X: -100 to +100 µm	100	0.99	0.99	0.78	1.14	0.067
X: +100 to -100 µm	100	1.00	1.01	0.78	1.17	0.068
Y: -100 to +100 µm	100	1.00	1.00	0.81	1.15	0.062
Y: +100 to -100 µm	100	0.99	0.99	0.87	1.12	0.054
Pitch: -100 to +100 µrad	100	1.00	1.00	0.83	1.13	0.050
Pitch: +100 to -100 µrad	100	0.99	0.99	0.89	1.10	0.049
Yaw: -100 to +100 µrad	100	0.97	0.97	0.81	1.16	0.068
Yaw: +100 to -100 µrad	99*	0.97	0.97	0.80	1.11	0.061
Roll: -100 to +100 µrad	100	1.00	0.99	0.70	1.38	0.156
Roll: +100 to -100 µrad	100	0.98	0.98	0.69	1.37	0.134

***The first computed step in the negative-direction yaw test was excluded from the summary statistics as an extreme outlier: 0.41 µm. This outlier step is probably due to hysteresis at the change in scan direction from positive to negative.**

For commanded motions of ≤ 1 µm or ≤ 1 µrad, we are close to the mover full-step resolution of 0.015°, and so we are relying on the motion control micro-stepping resolution of 0.000234°, although in practice we are only able to accurately position to ±1 encoder count, which is 0.0027°. As an example, a 1-µrad change in Pitch from nominal zero requires rotating the movers 0.022°, and a 1-µm increase in Y height from nominal zero requires a 0.027° change, both of which are between 1 and 2 full motor steps.

However, the results above make it clear that performing very precise 1-µm and 1-µrad steps is possible and suggests that smaller incremental motions can also be made reliably. A test of 0.5-µm steps is described in section 3.2.2.3.

In addition to examining the accuracy of the individual step sizes, the measured position deviations and incidental motions were checked in the same way as the initial system characterization. The same kinds of effects were found, but since this test covered a much smaller range of motion, the effects were mostly scaled down. Hysteresis was present in yaw and roll, but at a smaller magnitude. Translation in Z was present during pitch scans, but at a smaller magnitude. The exception was incidental motion in Y; it was present at about the same magnitude observed during the initial system characterization. The effect seems to be related to how long the scans took, rather than range covered, which provides further evidence that this is a thermal effect from motor heating. This is explored in more detail in section 3.2.3.

3.2.2.3 0.5-micron step tests

Encouraged by the results of the 1-µm step tests, we attempted a similar test with 0.5-µm steps. Motion verification was again performed using the Micro-Epsilon LVDT sensors. The test was an abbreviated version of the 1-µm test procedure; steps in only X and Y were checked, and only over a range of ±20 µm at the middle of the X and Y ranges.

The testing and data processing was performed in the same way as for the 1-µm tests. Positions were measured at commanded 0.5-µm intervals between -20 µm and +20 µm, and then back to -20 µm again,

for a total of 81 positions in each direction. Then the six best-fit translation/orientation parameters were found for each position, and the resulting translation parameters were differenced to compute the measured step sizes. To calculate statistically independent step sizes from these measured positions, successive pairs were differenced without overlap, so each one-way set of 81 positions yields only 40 measured steps. The last position in each set was discarded since it was unpaired. Negative steps of the second half of each test were converted to positive steps in the statistics and graphs below. There were no actual cases of a commanded positive step yielding a measured negative step, or vice versa. Figure 39 shows that the mover system can command accurate 0.5-µm translations in X, and Figure 40 shows the same for translations in Y. All these step results are tabulated in Table 4. It was rare to see a measured step size differ by more than 0.1 µm from the commanded 0.5-µm value. And, as noted with the 1-µm step tests, some of the variation in the step size is due to the uncertainty in the LVDT readings, so the step size uncertainties shown below are too pessimistic.

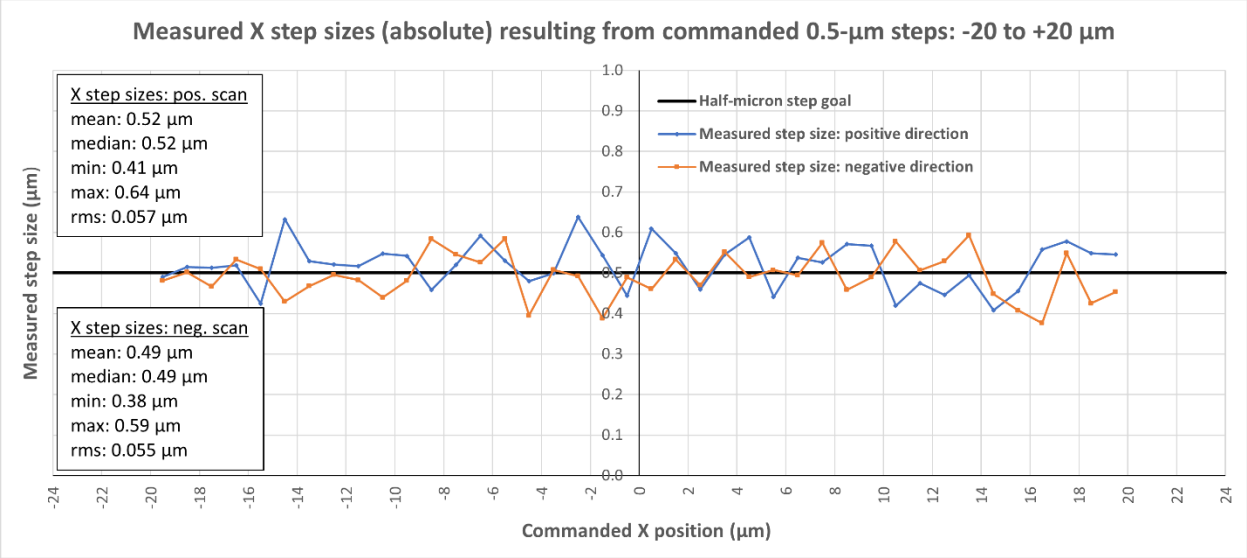

Figure 39. Measured step sizes resulting from commanded 0.5-µm steps in X between -20 µm and +20 µm, in both directions (absolute values of negative steps are shown for ease of comparison).

Figure 40. Measured step sizes resulting from commanded 0.5-µm steps in Y between -20 µm and +20 µm, in both directions (absolute values of negative steps are shown for ease of comparison).

Table 4. Statistical results from tests of how accurately the mover system can perform 0.5-µm steps.

Test	n	Mean step size (µm)	Median step size (µm)	Min (µm)	Max (µm)	rms (µm)
X: -20 to +20 µm	40	0.52	0.52	0.41	0.64	0.057
X: +20 to -20 µm	40	0.49	0.49	0.38	0.59	0.055
Y: -20 to +20 µm	40	0.51	0.51	0.39	0.59	0.046
Y: +20 to -20 µm	40	0.49	0.49	0.42	0.59	0.041

Figure 41 shows the deviations between the commanded X positions and the measured X positions during the step tests (rather than the step sizes themselves). Over this very small range, between -20 µm and +20 µm, the deviations don't exceed 0.25 µm. However, the analogous comparison for the commanded-versus-measured Y deviations shown in Figure 42 clearly shows the gradual height gain due to heating of the motor housings. This is discussed in more detail in section 3.2.3.

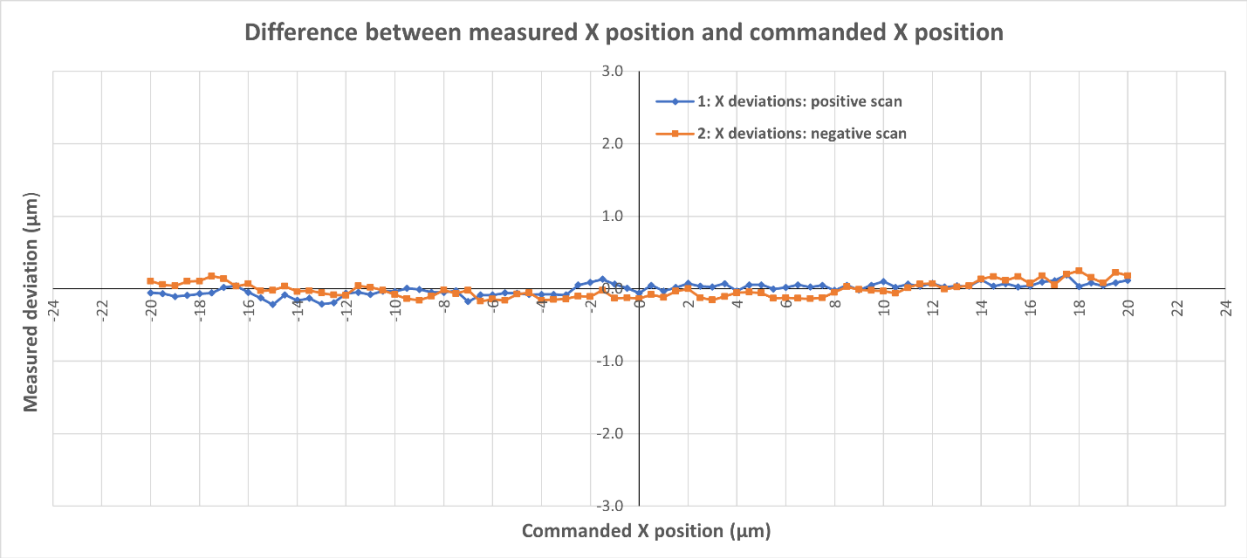

Figure 41. Scan of X between -20 µm and +20 µm in steps of 0.5 µm.

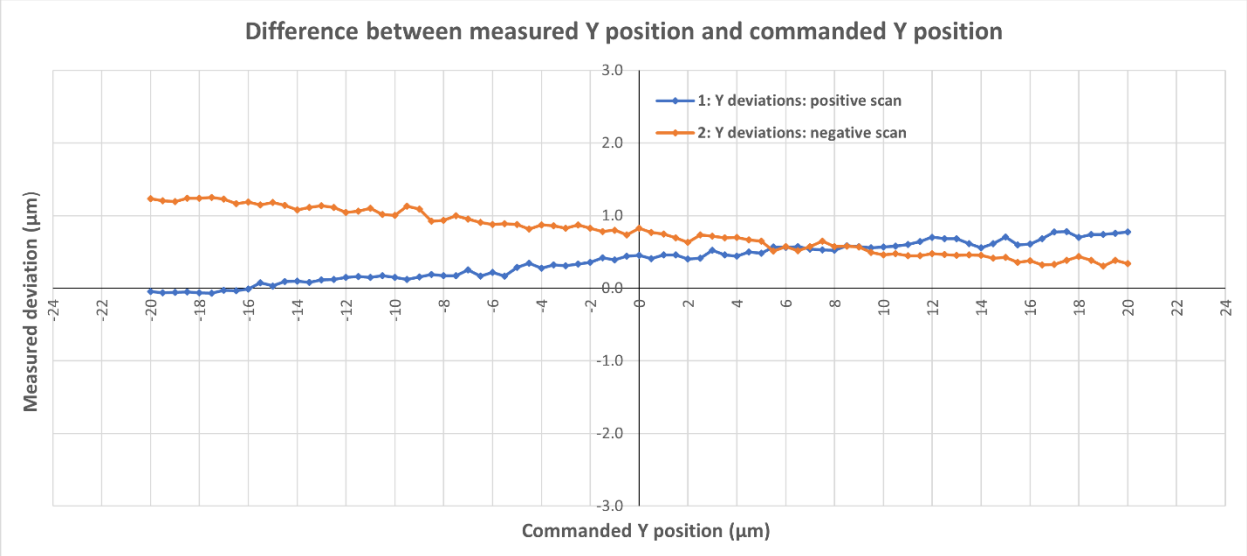

Figure 42. Scan of Y between -20 µm and +20 µm in steps of 0.5 µm.

The incidental motions in other DOF during the X- and Y-scans are shown in Figure 43 and Figure 44, respectively. Once again thermal effects can be seen in the incidental Y deviations during the X scans. Hysteresis can be seen in the roll parameter, too, during the X scans. The most notable incidental motion during the Y scan is a small amount of drift in Z.

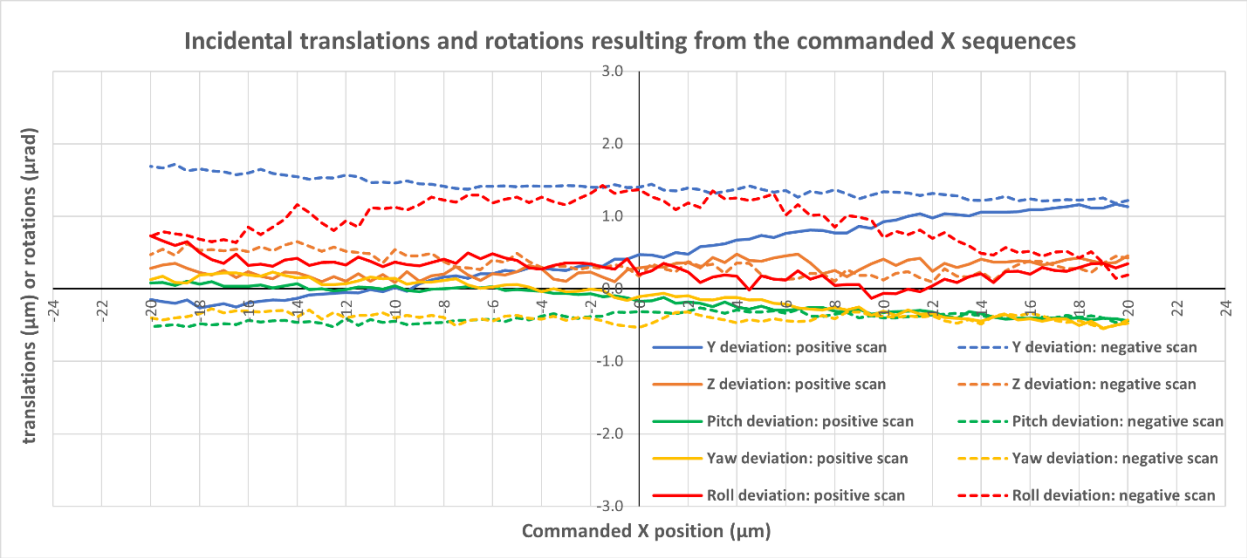

Figure 43. Incidental motions observed when scanning X between -20 µm and +20 µm in steps of 0.5 µm.

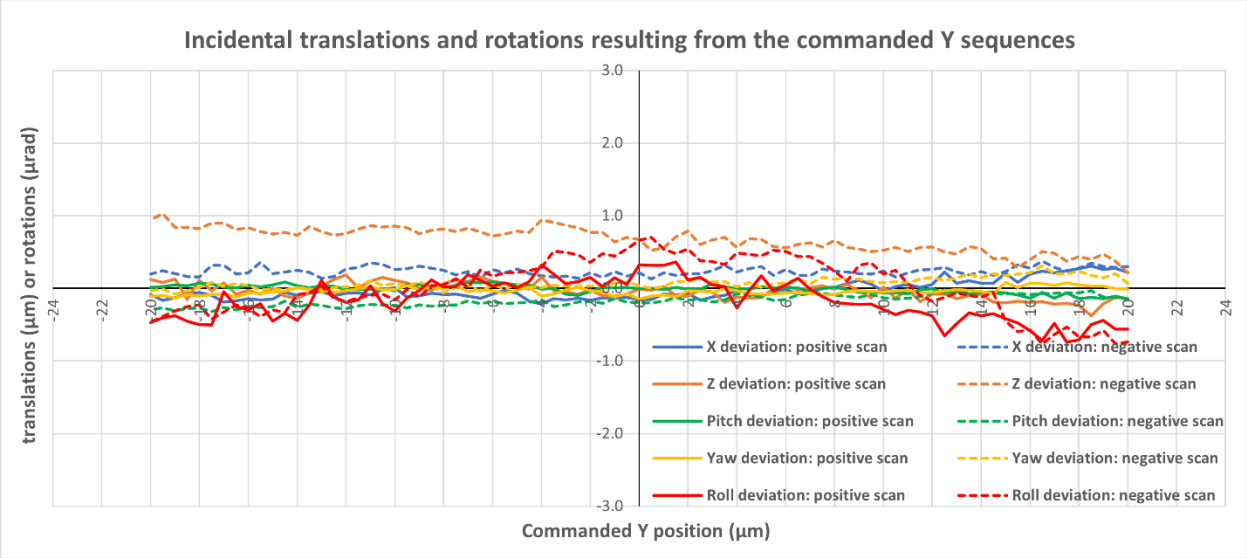

Figure 44. Incidental motions observed when scanning Y between -20 µm and +20 µm in steps of 0.5 µm.

3.2.3 Thermal stability tests

When the system is at rest and not actively being moved, it is expected that some amount of temperature variation will cause movement due to thermal expansion and contraction of the mover assemblies and the girder itself. To try to quantify this movement, the air temperature in the room and the surface of the mover assemblies was continuously monitored. In addition to two air temperature sensors, surface mount sensors were attached to all four mover bodies, and we placed one sensor directly on the body of the stepper motor in mover 1. Figure 45 shows the ±0.5 °C temperature variation from several of these sensors over a period of seven days.

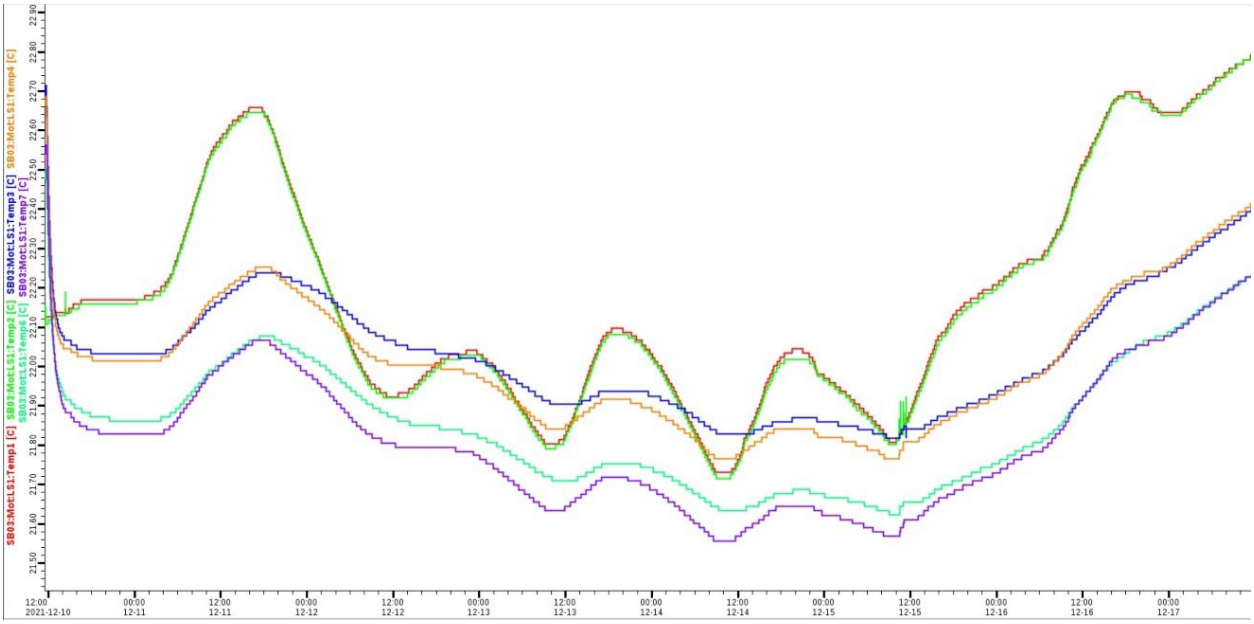

Figure 45. Air and mover surface temperature variation over 7 days

To see the effect this has on the movement of the girder we can plot the positions of the LVDT sensors over the same seven-day period. Figure 46 shows the vertical LVDT sensor positions with several microns (up to 5 µm) deviations over that same time period. It is worth noting that the two X negative side sensors show a positive change when the temperature increases, but the X positive side sensors show a negative change, which indicates there are angular tilts developing as the temperature changes. Similar results were seen for the horizontal displacement sensors, as well as changes in girder length seen by the Z axis sensor (of up to 30 µm) as seen in Figure 47.

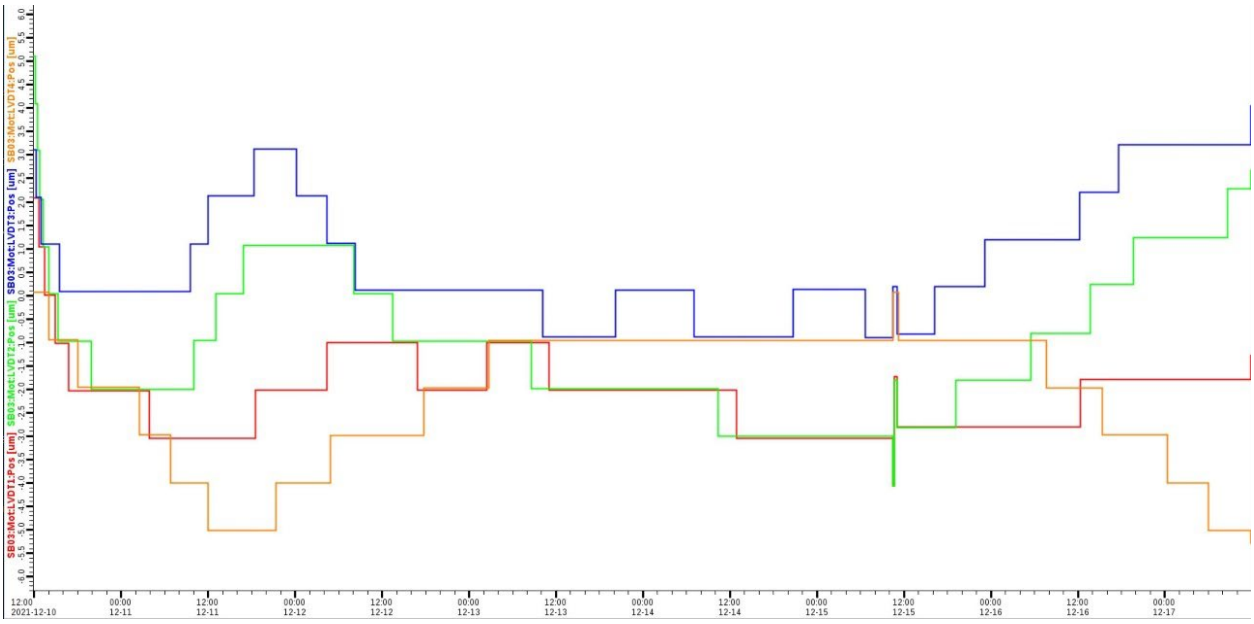

Figure 46. Vertical LVDT sensor positions over seven days

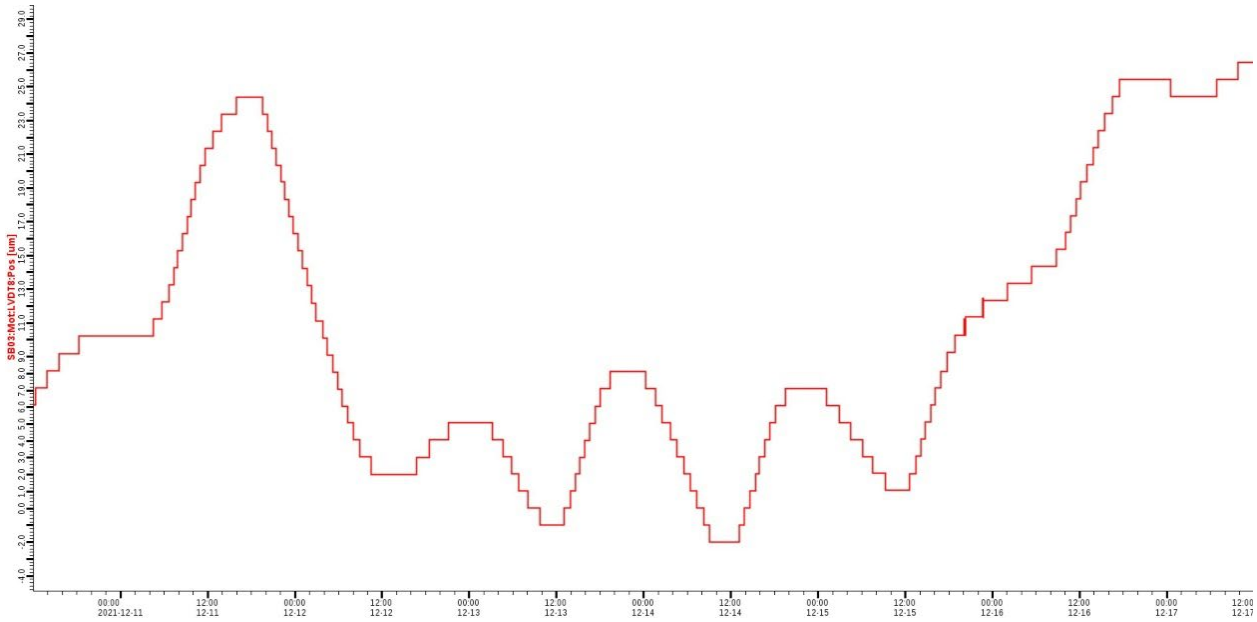

Figure 47. Beam direction (Z) girder length change over 7 days

From the above discussion it is clear that movements of at least a few microns is possible when the temperature is allowed to vary by ±0.5 °C. This amount of movement is larger than the smallest DOF step size obtainable by the movers, and so thermal effects must be considered when positioning the system with small step sizes.

We also aimed to characterize the thermal behavior of the system due to heat radiated from the stepper motors. The system was left idle for several hours to ensure thermal equilibrium is reached, and all the LVDT sensors were reset to read 0.0 µm. Then, all five motors were turned on so that full holding current (2.0 A) was present in the motor windings. The mover-1 motor surface temperature immediately started rising from 21 °C and reached 38.5 °C after one hour. The mover body temperatures also started rising from 21 °C and reached 24.5 °C after one hour. During the temperature rise of the mover bodies we observed an increase in the Y height sensor positions from 0.0 µm to 6-9.5 µm for the upstream sensors (movers 1 & 2) and to 13-17.5 µm for the downstream sensors (movers 3, 4 and 5). It is suspected that increased Y height change is seen at the downstream end of the girder due to the additional motor heating in the double mover. These results are shown in Figure 48, which has annotations describing the temperature and Y height sensor changes.

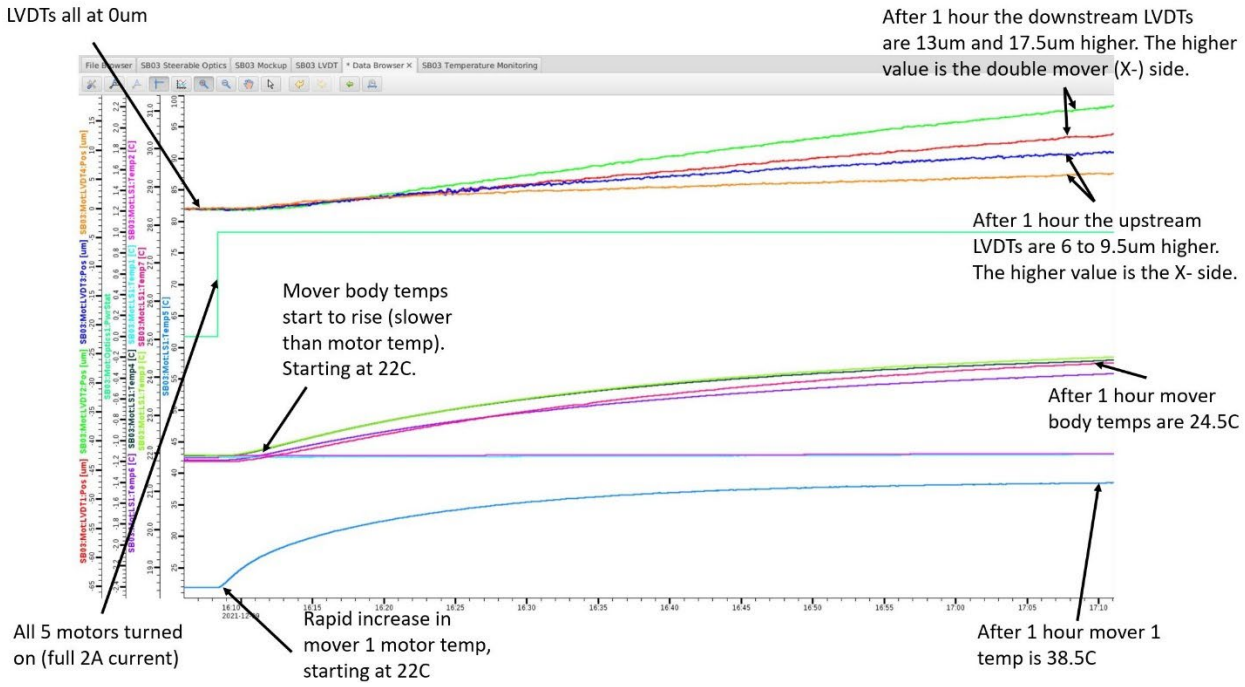

Figure 48. Temperature rise and Y height sensor increase with all 5 motors on

After one hour the five motors were turned off and it was observed that the cooling period and Y height reduction back to almost 0.0 µm took at least 4.5 hours. This is shown in Figure 49.

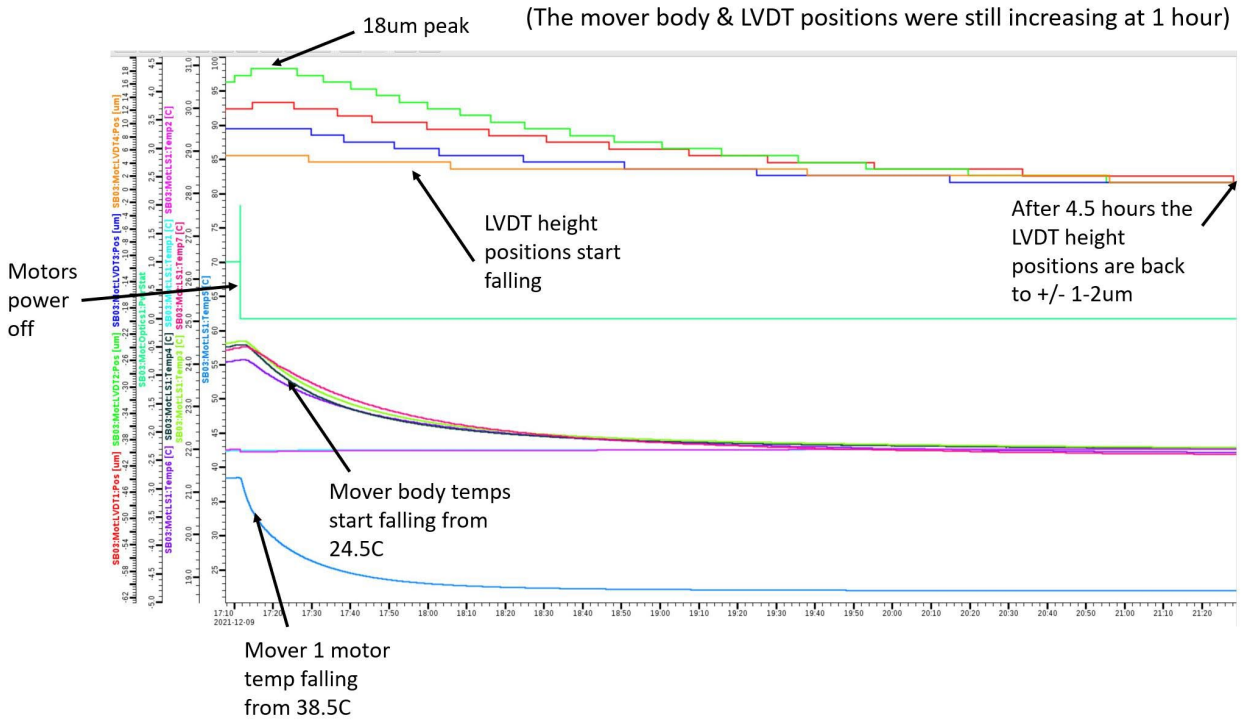

Figure 49. Temperature reduction and Y height change several hours after turning motor power off

The test described above is somewhat an extreme case, in that usually the motor power would be turned off between moves and most series of moves would not result in such a temperature increase. However, temperature changes and Y height changes of this magnitude may be reached if the system is continually moved around over a period of several hours without allowing a cooling off period between moves.

A single move that may take 5 seconds to complete can result in the motor body temperature increasing by 0.15 °C over a period of several minutes, and it can take one hour to cool back to the original temperature. Such a small temperature rise does not lead to any change in the mover body temperatures or change in Y height. However, any additional moves within the one-hour time period can result in a cumulative heating effect which eventually would start to affect the mover bodies and cause an increase in height. This is illustrated in Figure 50 which shows that the Y height sensors detected a 1-5 µm increase in height when the motors were turned on and off repeatedly 100 times, with each cycle being 5s on and 45s off, which simulates the effect of moving the girder around 100 times. In this case it took around 1.5 hours to cool off and reduce the Y height back to almost nominal zero.

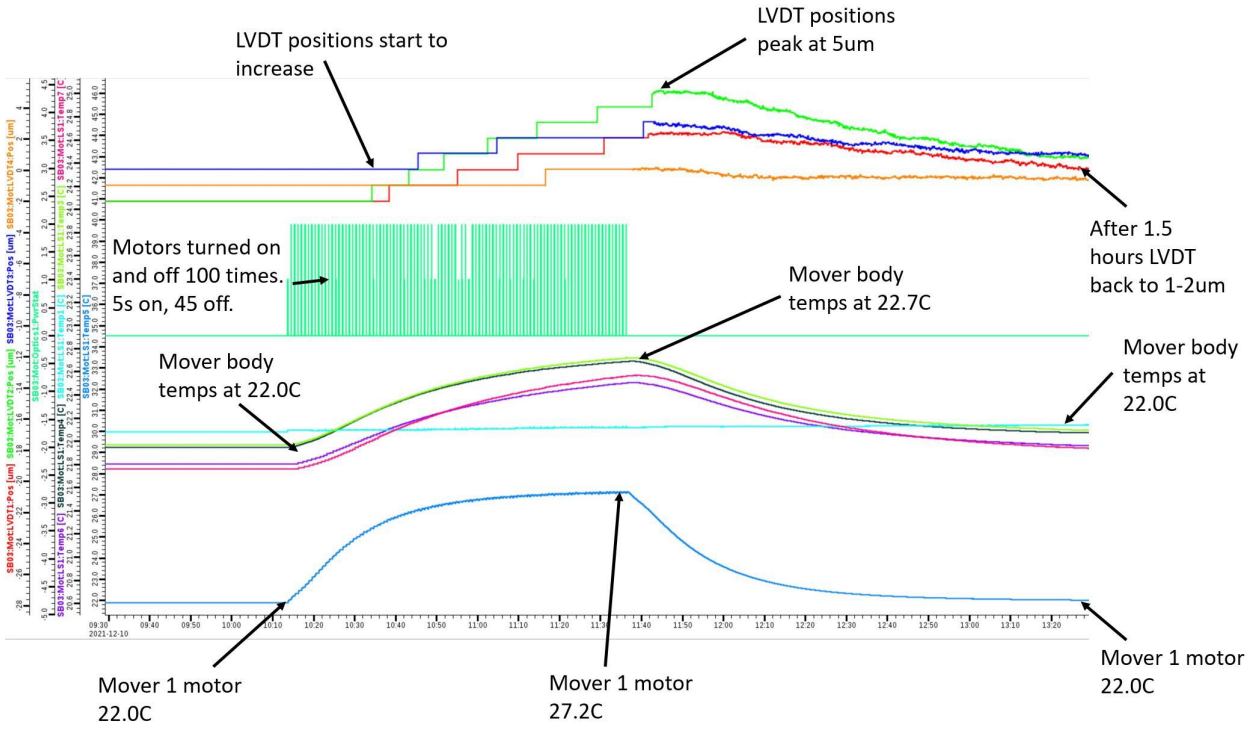

Figure 50. Cumulative heating effect when turning the motors on and off multiple times

The thermal effects discussed in this section are specific to the size, environment and materials used in the construction of the mockup project.

3.2.4 Repeatability testing

At the conclusion of the high-precision testing, a test was performed to determine: (1) how well the system could return to its "home" position after a lengthy series of moves, and (2) how much the home position repeatability would be affected by a day-long span of ordinary indoor temperature fluctuations.

The test began by driving the girder to its home position and zeroing the Micro-Epsilon LVDTs. Then the system was commanded to perform a series of 100 random moves, each involving all five DOF, within the space of -100 µm ≤ translation ≤ +100 µm, and -100 µrad ≤ rotation ≤ +100 µrad. At the conclusion

of each set of random moves, the system was commanded to return to its home position and the LVDT readings were then recorded. This whole sequence was repeated three times on the first day, and then seven more times on the following day. All ten of the recorded return-to-home positions were then compared against the original home position recorded on the first day. The full test took almost 26 hours, but no movements were made in the overnight span.

The system reliably returned to the same position, within a few microns/microradians, with only two notable differences. First, the Z position drifted by 11 µm, and showed a correlation to the temperature of the girder. This is just thermal expansion of the girder itself as the air temperature varied. Second, the Y position showed an increasing trend beginning at the start of movements each day; this is probably another example of thermal expansion in the motor housings. There are also some fluctuations in the roll angle that might be attributable to differential heating among the housings. These results are shown in Figure 51.

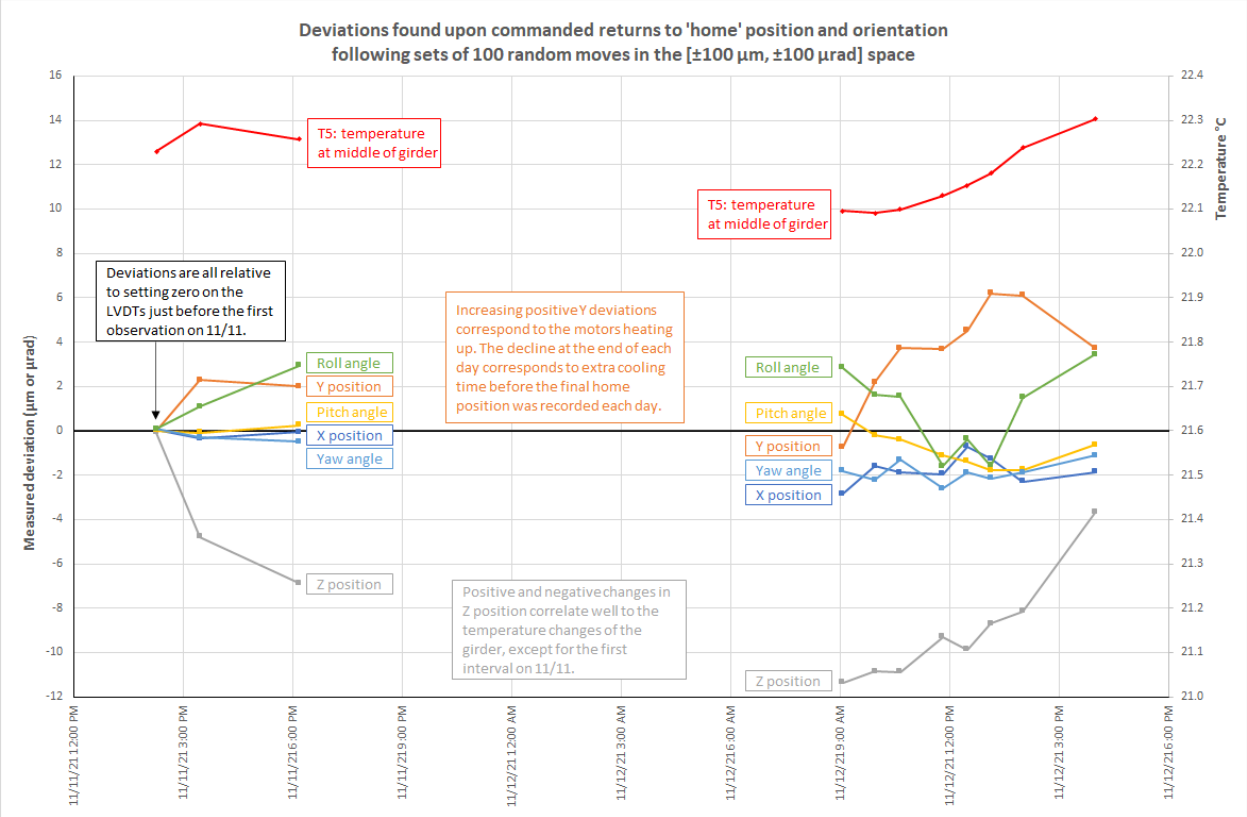

Figure 51. Repeatability of returning to the home position after lengthy series of moves.

4. SUMMARY & CONCLUSIONS

During the assembly and testing of the system, some notable points emerged. Below is a summary of the results.

Reliability of control system and hardware. To collect, verify and analyze the data presented in this report, a total of 139 automated scans were performed, on 18 separate days, over a period of almost 4 months. This is a total of 8717 individual moves on either a single or multiple degree of freedom. This resulted in 43,585 motor and motor brake operations across the 5 movers, which shows the system has been reliable and no degradation in performance was seen during this time. The actual number of moves

performed is somewhat higher, as the system was initially commissioned and tested manually before data collection scans were started.

Accuracy throughout range. The mover system was able to produce translations with an accuracy exceeding 10 μm and rotations with an accuracy exceeding 10 μrad throughout its working range.

Half-micron steps. The system reliably produced translations as small as 0.5 μm on command. The smallest step sizes were tested only in the centermost 40 μm of the X and Y translation ranges, but 10-μm steps were successfully tested out to the full range of the movers, and there's no reason to suspect that the smaller steps wouldn't work similarly.

Z drift. Large (±600 μm) incidental translations along the Z axis occurred during scans of pitch and yaw. These translations were separate from the expected tangential motions of these angular scans, and they were verified with a laser tracker as a check. These Z translations can accumulate; at one point in the testing the girder was found to have moved 820 μm downstream. A similar Z-drift phenomenon is described by Bowden et al. in their description of the FFTB at SLAC [1], so this was not unexpected, although the magnitude of the drift is larger than anticipated. There was no physical restraint mechanism on the mockup to prevent this motion. As part of the proposed modifications on the next version of the mover design, implementing better mover bearing restraints and a restraint on the girder itself should significantly improve performance in this area.

Roller shift. During testing, the girder wings were observed to be translating in Z relative to the rollers on which they were resting. It was not clear whether this was from the roller moving within its housing or the girder/wing moving on the roller. This effect is probably related to the Z drift phenomenon.

Hysteresis. Single-DOF scans in both yaw and roll showed different results when run in opposite directions. It's not clear why this occurred, but it might be handled procedurally in a real-life situation by always making test scans and alignment adjustments from the same direction (e.g., always from negative side towards the positive side of the parameter in question).

Y drift. Heat from the mover motors was found to cause thermal expansion, slowly raising the girder during scans. The effect was not uniform among the movers, so small changes were seen not only in Y, but also in the pitch and roll parameters. If similar scanning is intended to be used during actual operation of the mover system (e.g., to provide feedback on aiming an optic), then for the best results some form of remediation should be found, perhaps by increasing pauses between steps to let heat dissipate, or by active cooling, or by designing the housing with a material having a lower coefficient of thermal expansion.

Girder expansion. The mockup girder was made of aluminum 6061. When the girder was monitored for temperature-related motions on the weekend of November 6-7, 2021, the girder increased in length by about 90 μm due to temperature drifts in the room.

Shimming. During alignment of the movers on the base plate, shimming was used to align the movers to their intended positions in Y, pitch, and roll. However, shimming is not a very precise alignment technique, and it doesn't adequately support the very high angular precision of the TDC determination.

Mover fiducialization. While preparing to assemble the mockup, the determination of eccentricity and TDC angular offset was done separately from the fiducialization of the mover housing. It would be more efficient and more precise to combine these two procedures. Also, the manufacturer-provided fiducial points were delivered covered in paint, which had to be removed to provide a repeatable contact surface for the SMRs used with the laser tracker. In the future, manufacturers should be told not to allow paint on

fiducial surfaces. Seating the magnets deep enough within the fiducial nests was difficult due to the workability time limit of the epoxy used. Other brands should be tested to avoid lumpy epoxy problems.

Roll weakness. Excluding unintended Z drift, the roll parameter was the least precisely controlled motion produced by the system. This is evident in the deviation plots (particularly large incidental motions during scans of other DOF) and in the step-size tests. This is to be expected, given the relatively close spacing of the cam rollers in the X direction and the height of the imaginary optic reference point above the rollers. These factors serve to magnify any small remaining errors in eccentricity, or in angular offset of the rollers, or in thermal expansion from the mover motors. If more precision is needed in the roll parameter, the rollers could be relocated farther apart in X. The incidental motions could also be reduced by designing the system so that the roller/girder contact surfaces are close to the height of the optic.

5. FUTURE WORK

The design and testing information documented in this report summarize the characterization studies of the steerable optic mockup system and validate its ability to position and orient large neutron optics at micron levels of precision and resolution. But the most applicable demonstration would be to use this system to install and align an actual optic in a neutron beamline. To deploy a specific optic would require reconfiguration of the steerable optic system, likely with a shorter girder custom designed for the optic it supports along with corresponding changes in the positions of the movers along the girder. The actual operation of the system would not change because the mover locations are stored in a data file read by the control system at startup, and any geometric reconfigurations would be captured in that file. Thus, multiple variations of the steerable optic system can easily be supported in actual beamline applications. Discussions are underway to identify a potential optic and a specific beamline at SNS or HFIR for this next phase of testing.

As with most mechanical systems, there are some improvements to the mover design which would be incorporated into future versions. The use of gear reducer component sets in the housings resulted in relatively tight tolerances on some of the machined features, and the machine shop had some difficulty in achieving them. By selecting the modular version of the gear reducer that incorporates its own housing, the complexity and precision required in the mover housings could be reduced, at the expense of a larger mover housing being required.

This mockup system was designed to mimic the original SLAC mover design as much as possible, so it incorporated 1.5 mm of eccentricity. In an actual beamline deployment, the amount of eccentricity (and associated optic adjustability) must be defined based on the application-specific requirements. If the purpose of the steerable optic system is only to provide final alignment of the optic along with future position/orientation changes, then 1.5 mm may be sufficient; however, if the system's intended use is to compensate for floor settlement, then additional range may be required. There are examples of systems with larger eccentricities; it’s primarily a matter of choosing different bearings and a matching gear reducer and designing the machined blocks to house them. Of course, the overall mover size would subsequently increase, so that would have to be considered in the beamline design as well.

For future deployment at the STS, the control system hardware will be updated to conform to STS standards. This will likely involve using a different, more modern, motion controller as well as cable and cable adaptor simplifications. It is also possible to simplify some of the internals of the motion control chassis. The control system software will mostly remain the same for deployment at the STS, as it was initially designed to enable easy integration with an existing or future EPICS-based Instrument control system. Therefore, apart from minor software maintenance, the only software changes that are expected are to deal with the future hardware changes.

For the installation and commissioning of steerable optics at the STS, additional development will be needed to build an automated mover alignment station that can be used to align and calibrate each mover before it is installed.

---

[1] G. Bowden, P. Holik, S.R. Wagner, G. Heimlinger, R. Settles, "Precision Magnet Movers for the Final Focus Test Beam," Nuclear Instruments and Methods in Physics Research A, volume 368 (1996), 579-592.
[2] G. Bowden, P. Holik, S.R. Wagner, "Precision Magnet Movers for the Final Focus Test Beam," SLAC-PUB-95-6132.
[3] Andreas Streun, "Algorithms for dynamic alignment of the SLS storage ring girders", SLS-TME-TA-2000-0152.

APPENDIX A. INITIAL SYSTEM CHARACTERIZATION PLOTS

The plots in this section show the results of scanning each degree of freedom (DOF) over their maximum ranges and comparing the setpoint positions to the actual measured positions. These tests were performed in both directions, starting at the most negative position, and moving to the most positive position, and then back to the most negative position. The corresponding incidental motions on the other DOF are also shown. The dial indicators used to measure the actual positions were not reset between each scan and so any residual incidental motion that remained from a scan impacts the later scans. The plots are presented in the order in which the scan data was collected.

The complete list of data collection scans are detailed in the below table. The plots are then presented in the same order.

Scan ID	DOF Parameter	Start Position	End Position	Step Size
1	X	-2100	2100	100
2	X	2100	-2100	-100
3	Y	-1400	1400	100
4	Y	1400	-1400	-100
5	Pitch	-1800	1800	100
6	Pitch	1800	-1800	-100
7	Yaw	-2600	2600	100
8	Yaw	2600	-2600	-100
9	Roll	-3900	3900	100
10	Roll	3900	-3900	-100
11	X & Y	-1000	1000	100
12	X & Y	1000	-1000	-100
13	X, Y & Pitch	-700	700	100
14	X, Y & Pitch	700	-700	-100
15	X, Y, Pitch & Yaw	-500	500	100
16	X, Y, Pitch & Yaw	500	-500	100
17	X, Y, Pitch, Yaw & Roll	-500	500	100
18	X, Y, Pitch, Yaw & Roll	500	-500	100

Scans 1 & 2: X moving between –2100 µm and +2100 µm in steps of 100 µm:

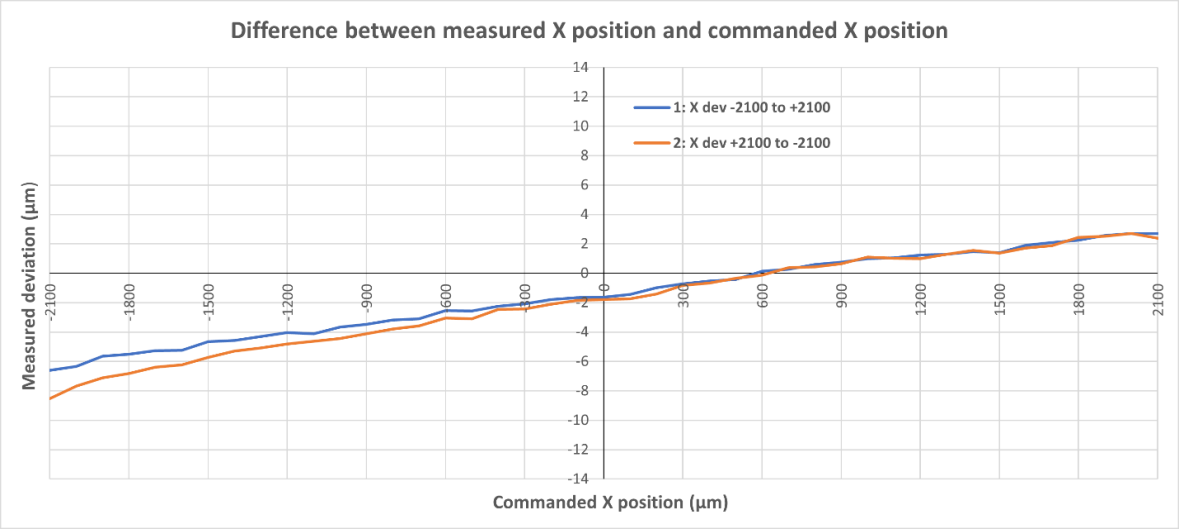

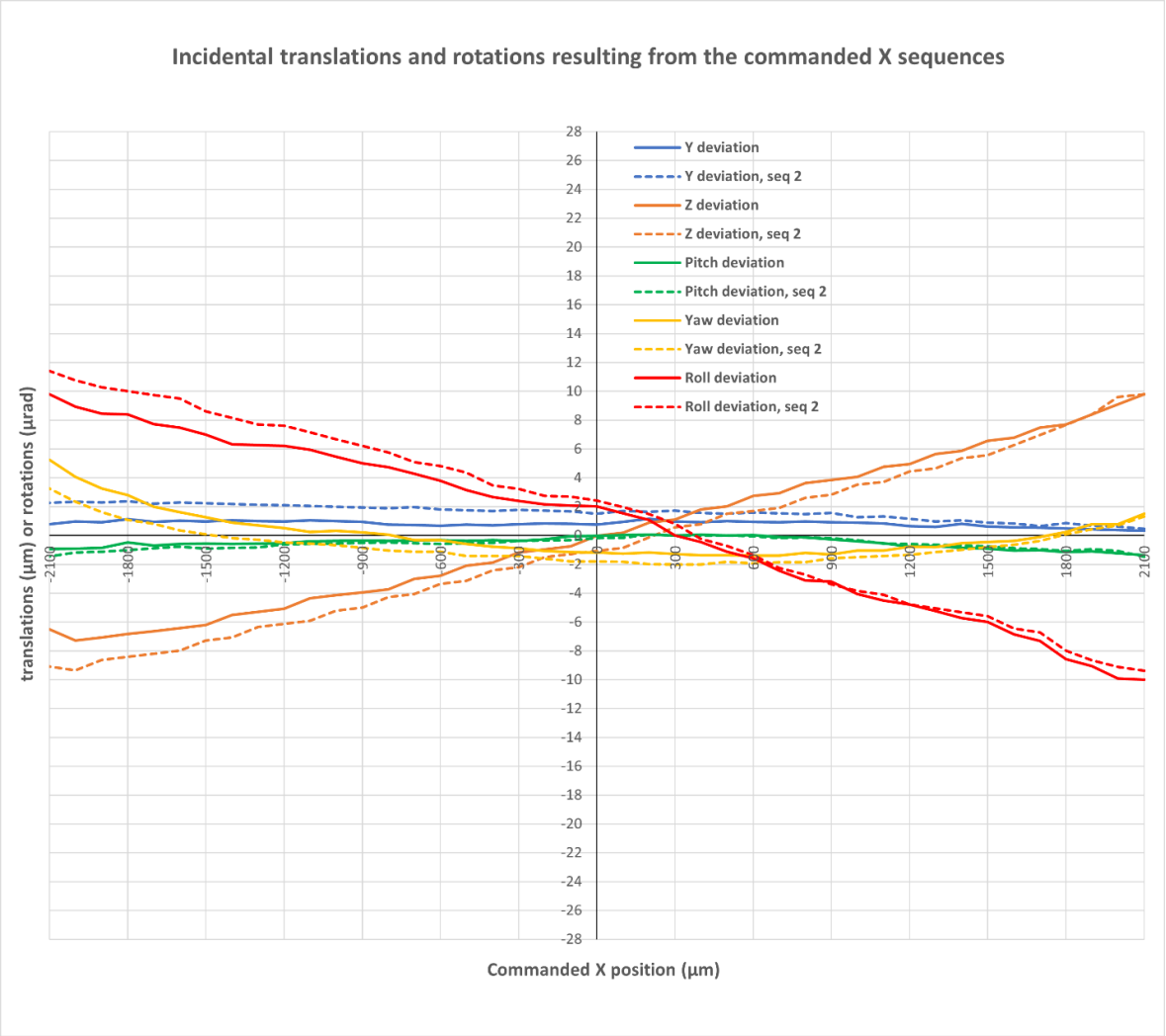

Scans 3 & 4: Y moving between –1400 µm and +1400 µm in steps of 100 µm:

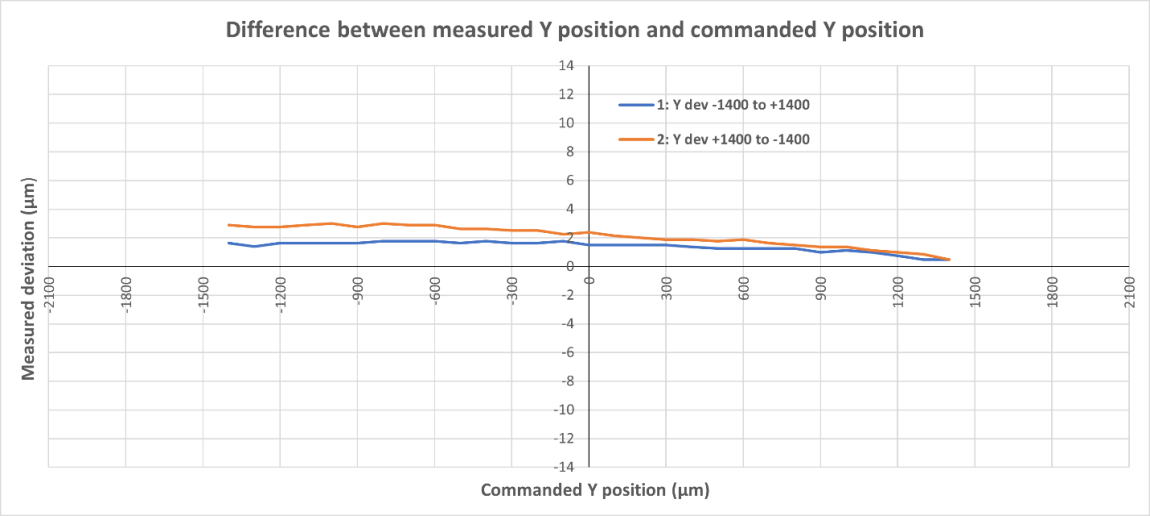

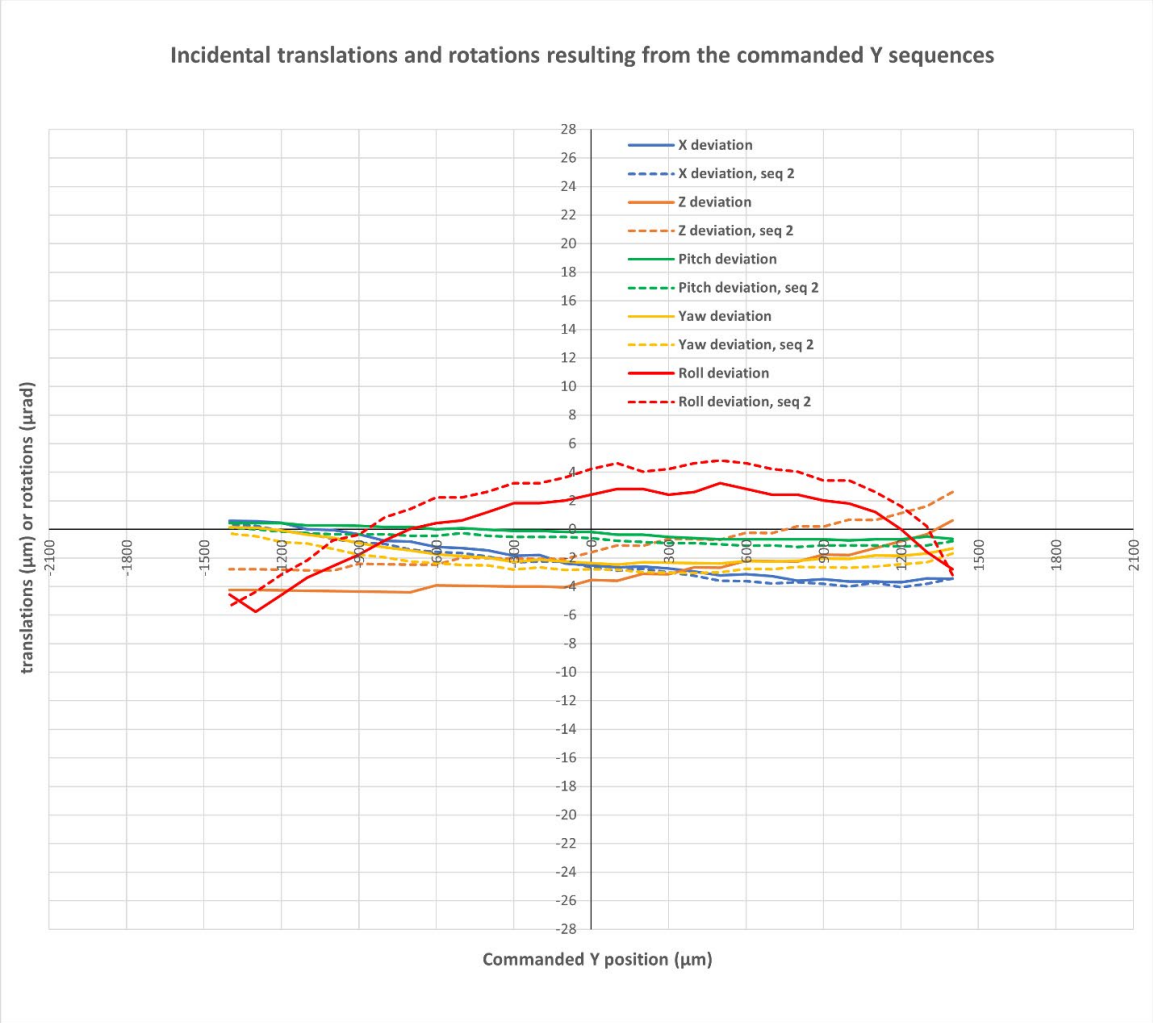

Scans 5 & 6: Pitch moving from –1800 µrad to +1800 µrad in steps of 100 µrad:

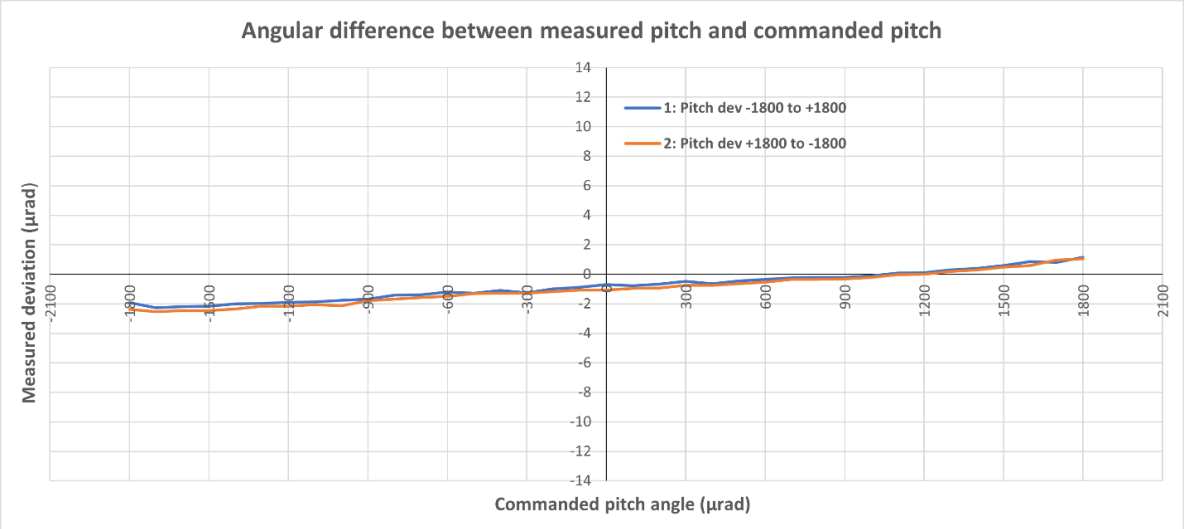

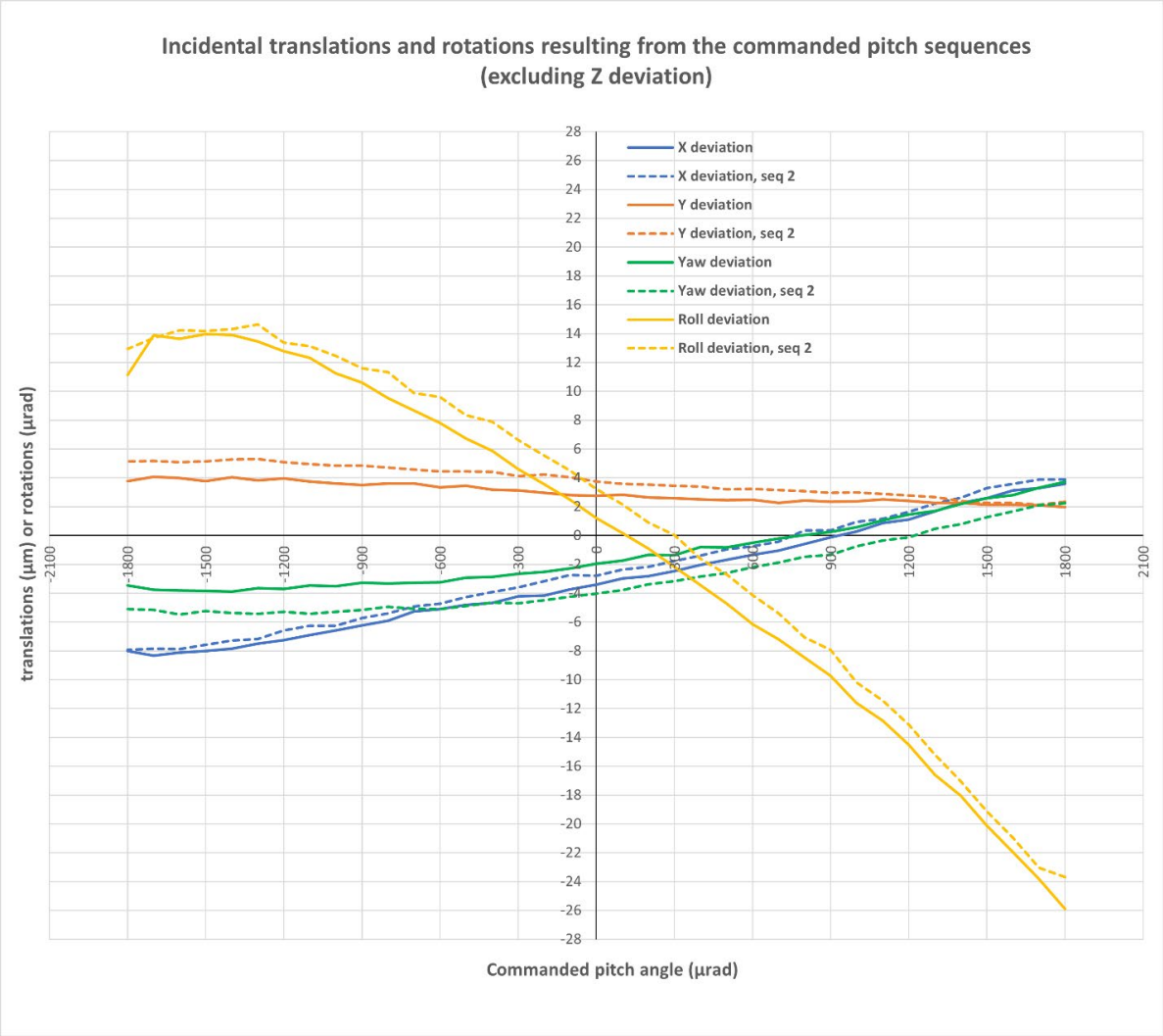

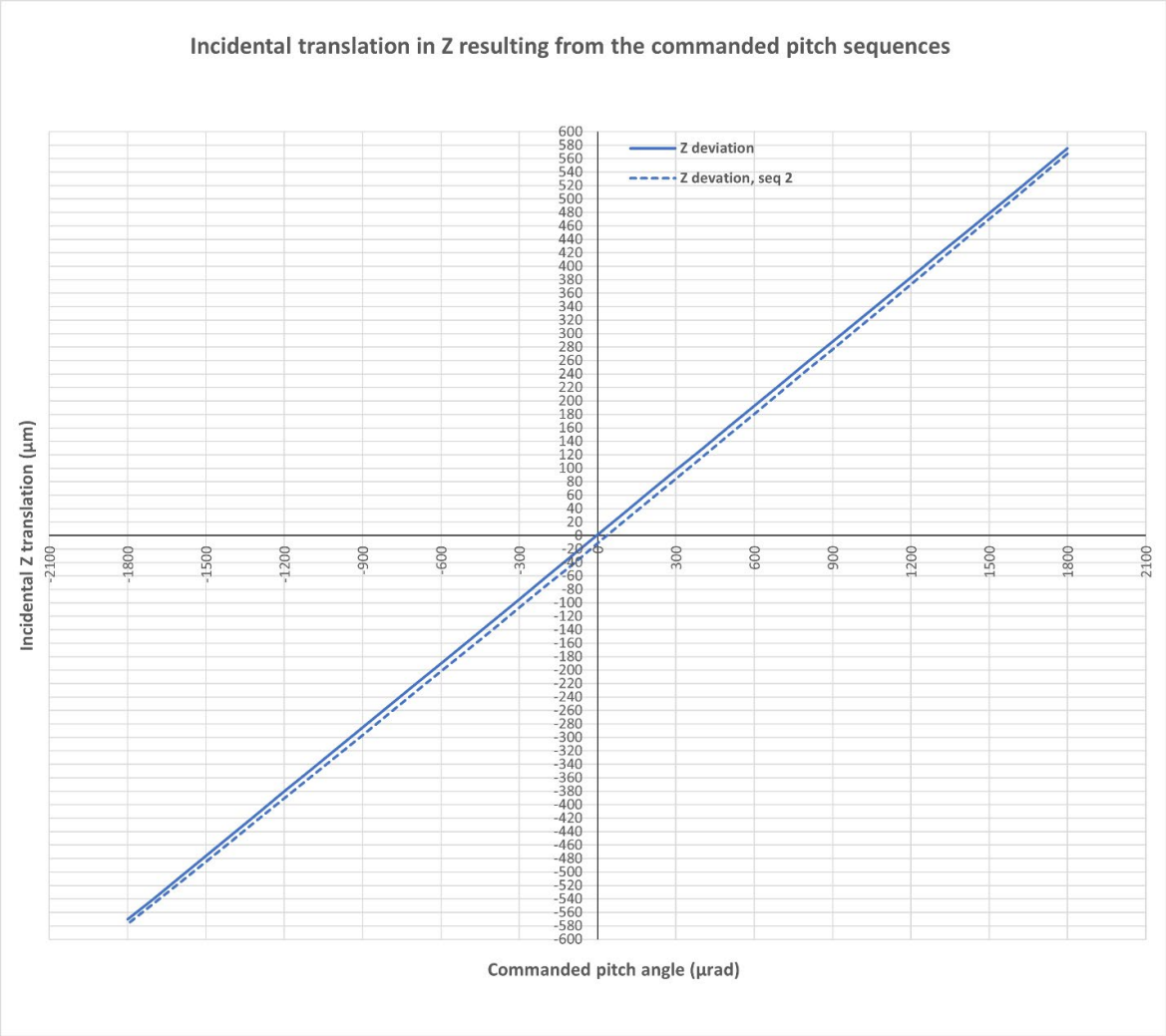
Incidental translation in Z resulting from the commanded pitch sequences
Z deviation
Z devation, seq 2
Incidental Z translation (µm)
Commanded pitch angle (µrad)
600
580
560
540
520
500
480
460
440
420
400
380
360
340
320
300
280
260
240
220
200
180
160
140
120
100
80
60
40
20
0
-20
-40
-60
-80
-100
-120
-140
-160
-180
-200
-220
-240
-260
-280
-300
-320
-340
-360
-380
-400
-420
-440
-460
-480
-500
-520
-540
-560
-580
-600
-2100
-1800
-1500
-1200
-900
-600
-300
0
300
600
900
1200
1500
1800
2100

Scans 7 & 8: Yaw moving from –2600 µrad to +2600 µrad in steps of 100 µrad:

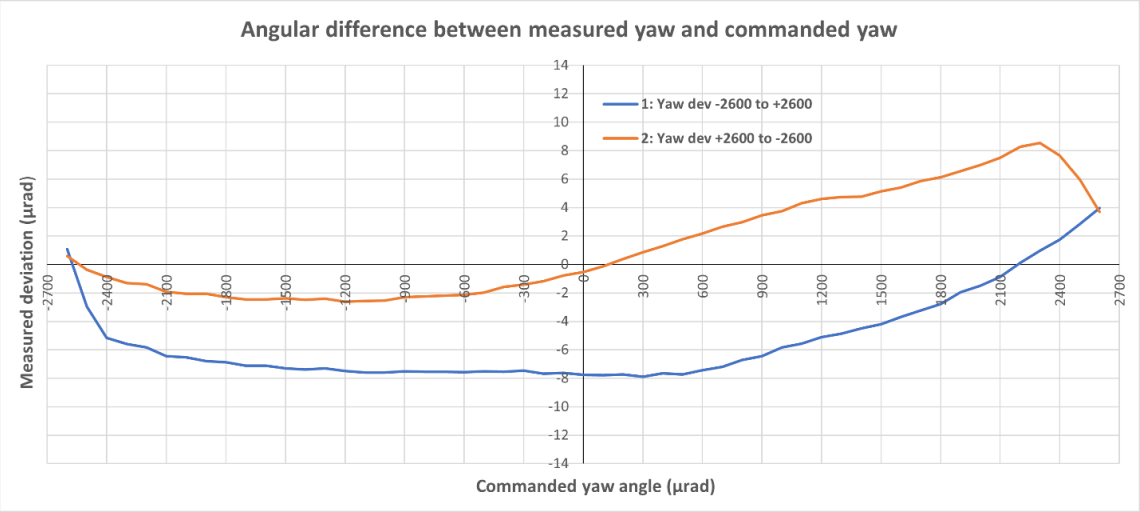

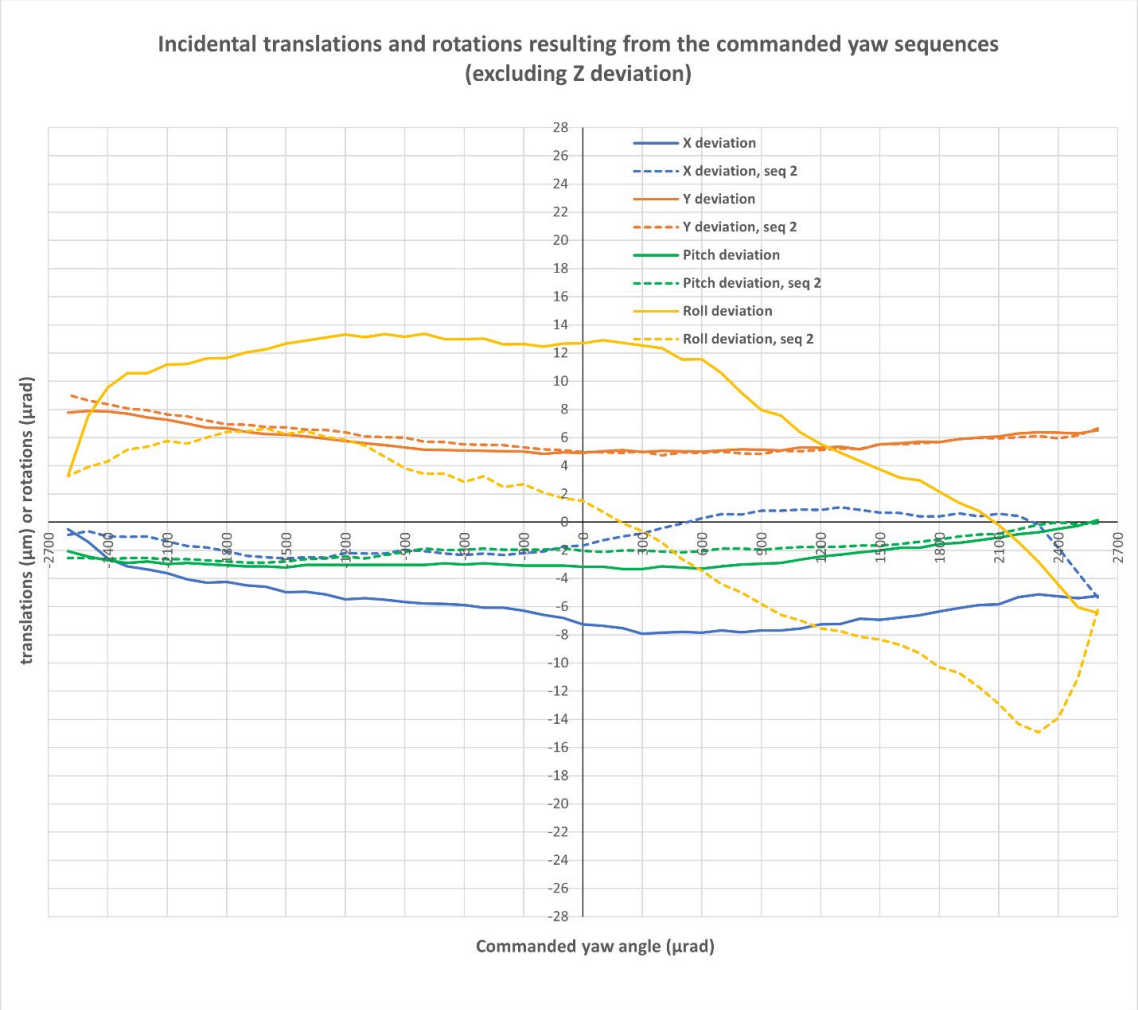

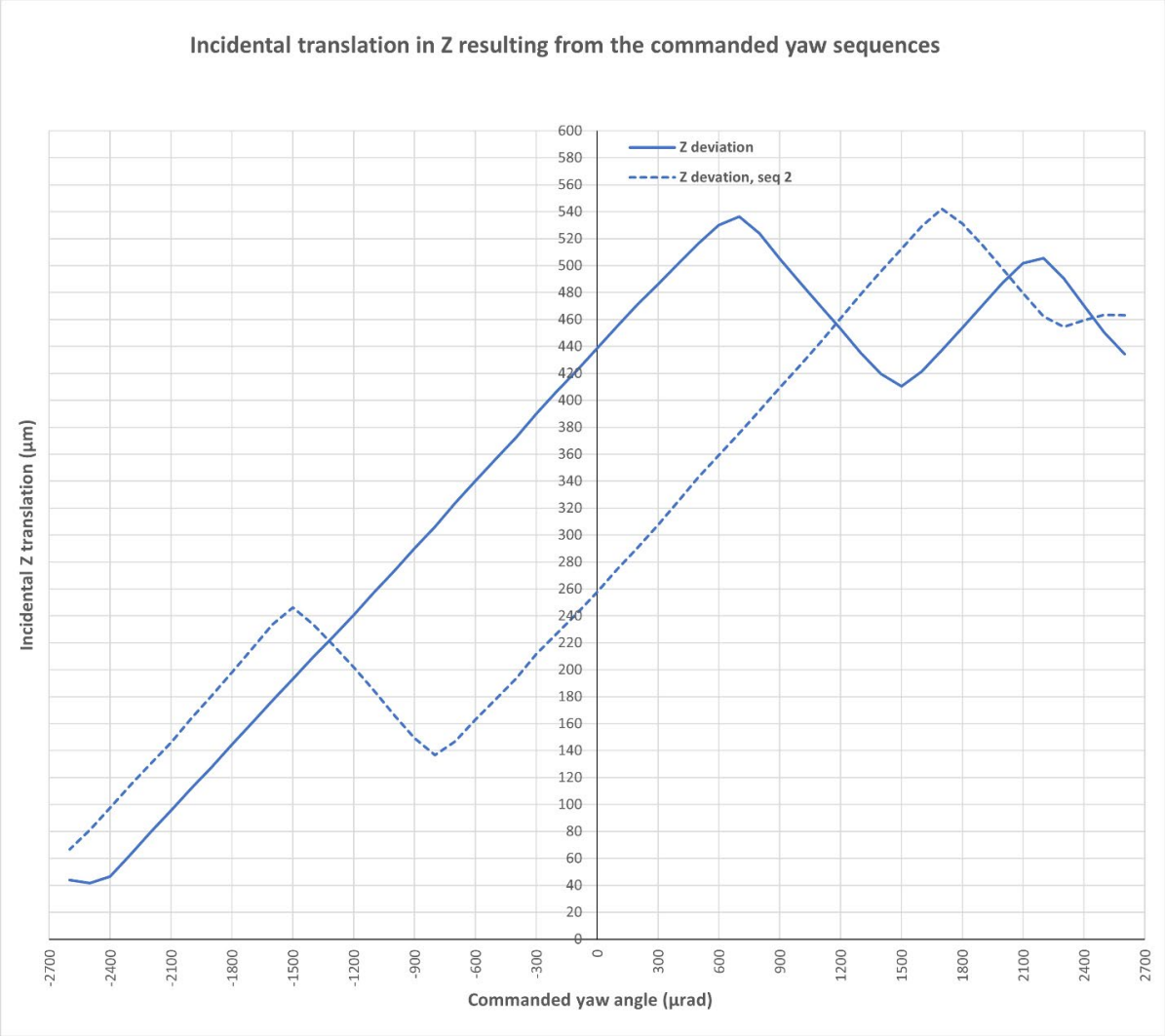
Incidental translation in Z resulting from the commanded yaw sequences
Z deviation
Z devation, seq 2
Incidental Z translation (µm)
Commanded yaw angle (µrad)
600
580
560
540
520
500
480
460
440
420
400
380
360
340
320
300
280
260
240
220
200
180
160
140
120
100
80
60
40
20
0
-2700
-2400
-2100
-1800
-1500
-1200
-900
-600
-300
0
300
600
900
1200
1500
1800
2100
2400
2700

Scans 9 & 10: Roll moving from –3900 µrad to +3900 µrad in steps of 100 µrad:

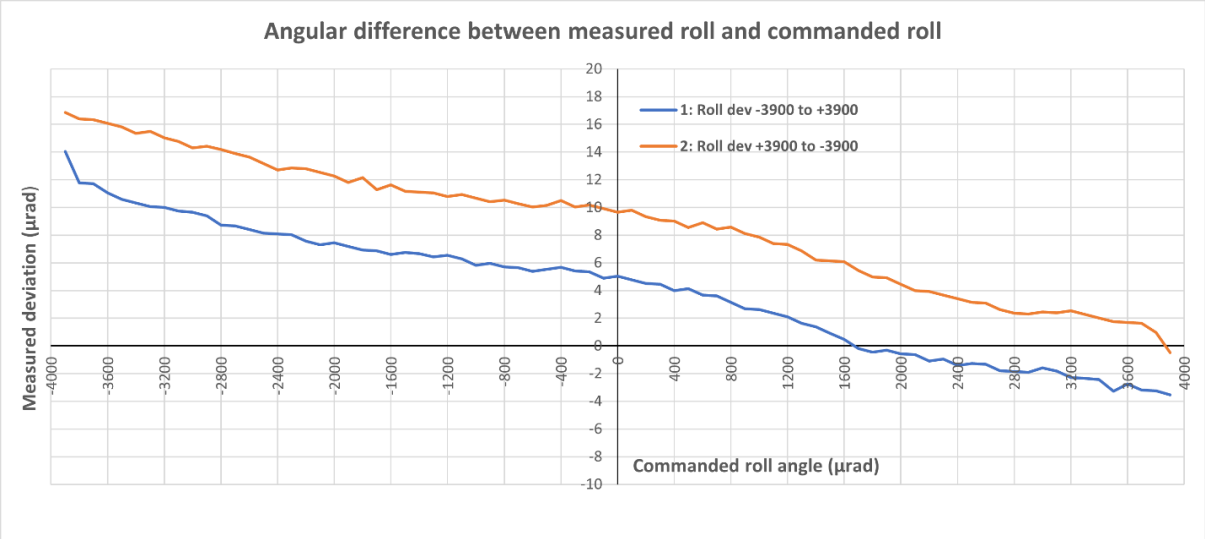

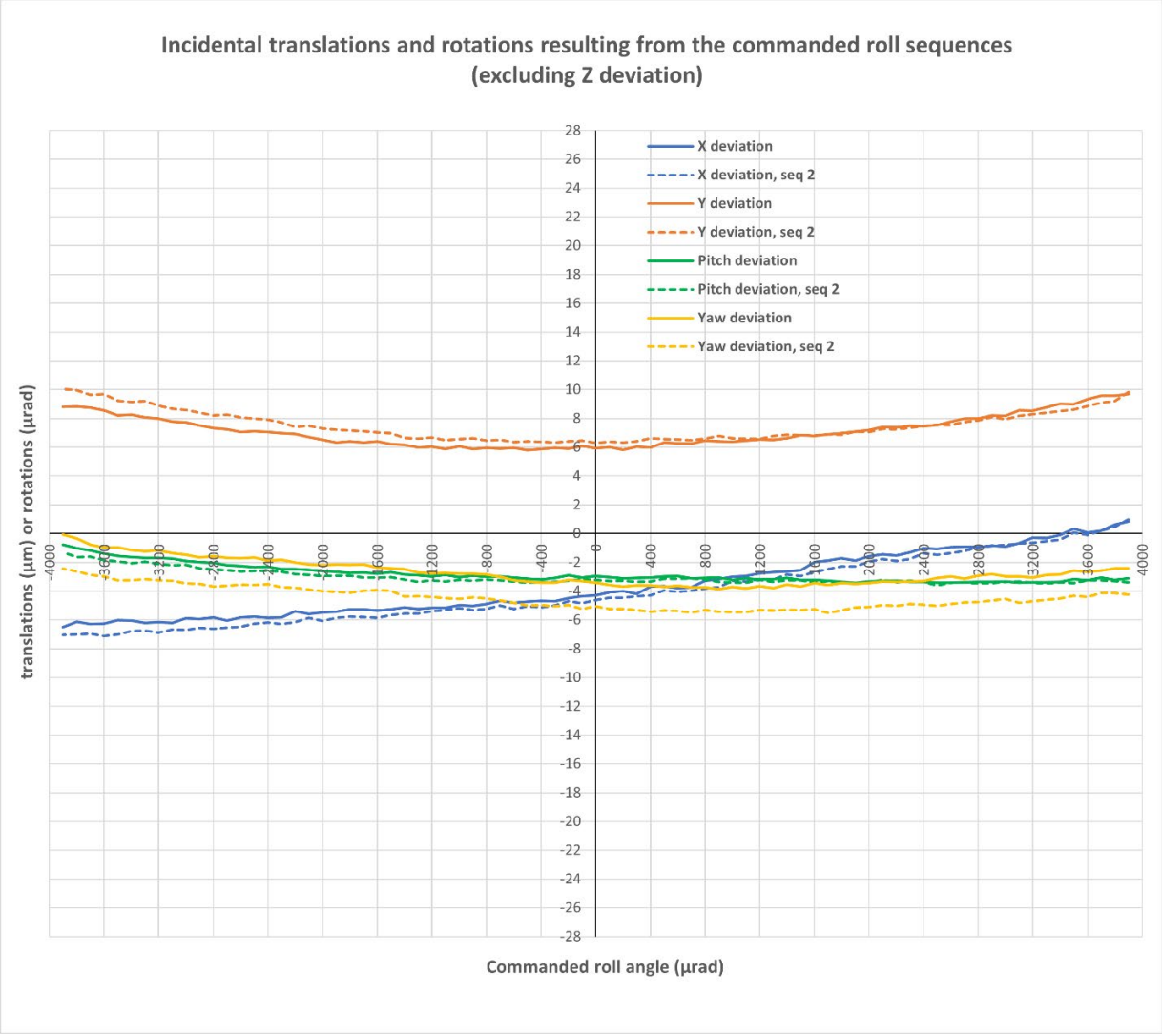

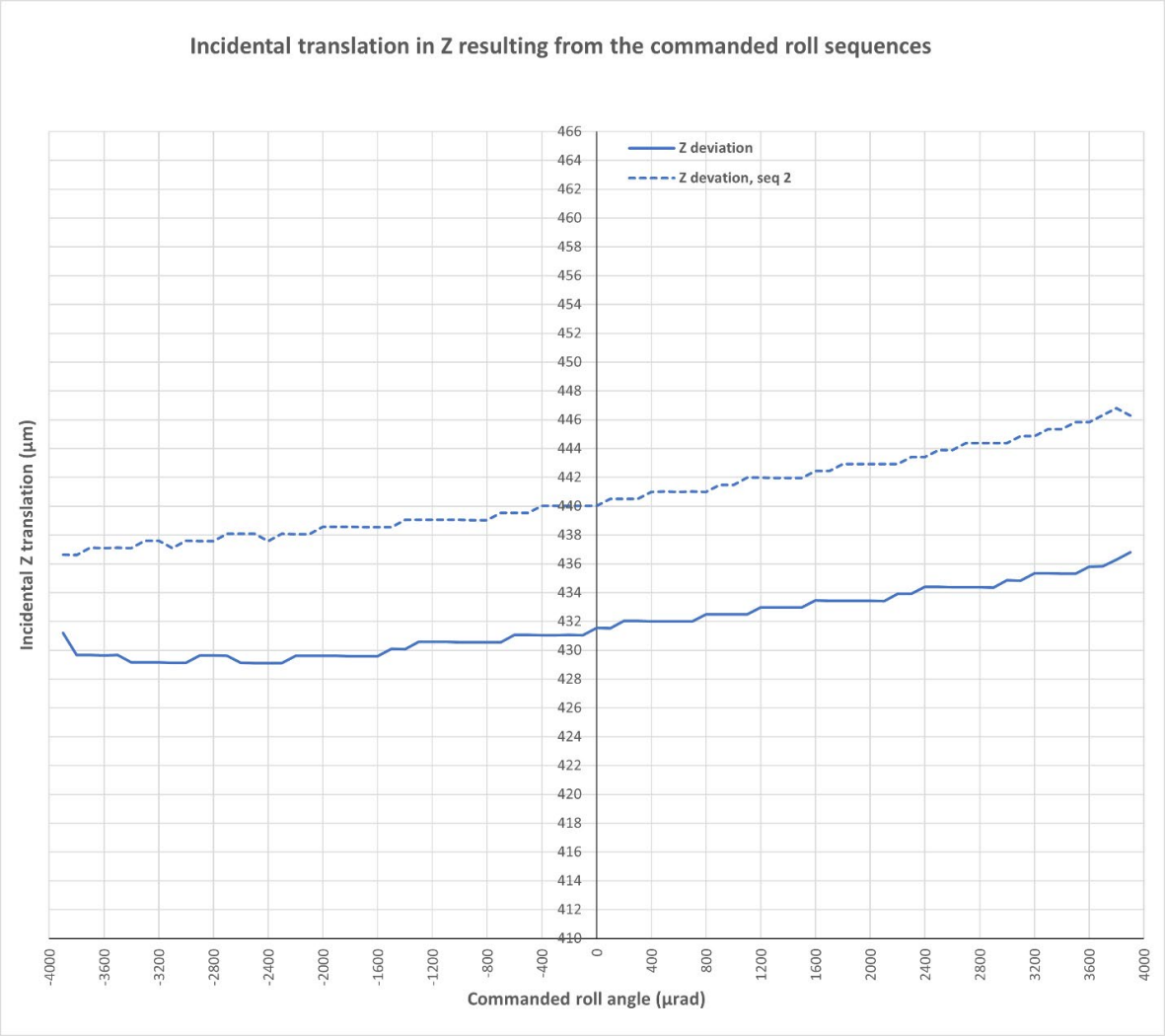
Incidental translation in Z resulting from the commanded roll sequences
Z deviation
Z devation, seq 2
Incidental Z translation (µm)
Commanded roll angle (µrad)
466
464
462
460
458
456
454
452
450
448
446
444
442
440
438
436
434
432
430
428
426
424
422
420
418
416
414
412
410
-4000
-3600
-3200
-2800
-2400
-2000
-1600
-1200
-800
-400
0
400
800
1200
1600
2000
2400
2800
3200
3600
4000

Scans 11 & 12: X and Y moving from –1000 µm to +1000 µm in steps of 100 µm:

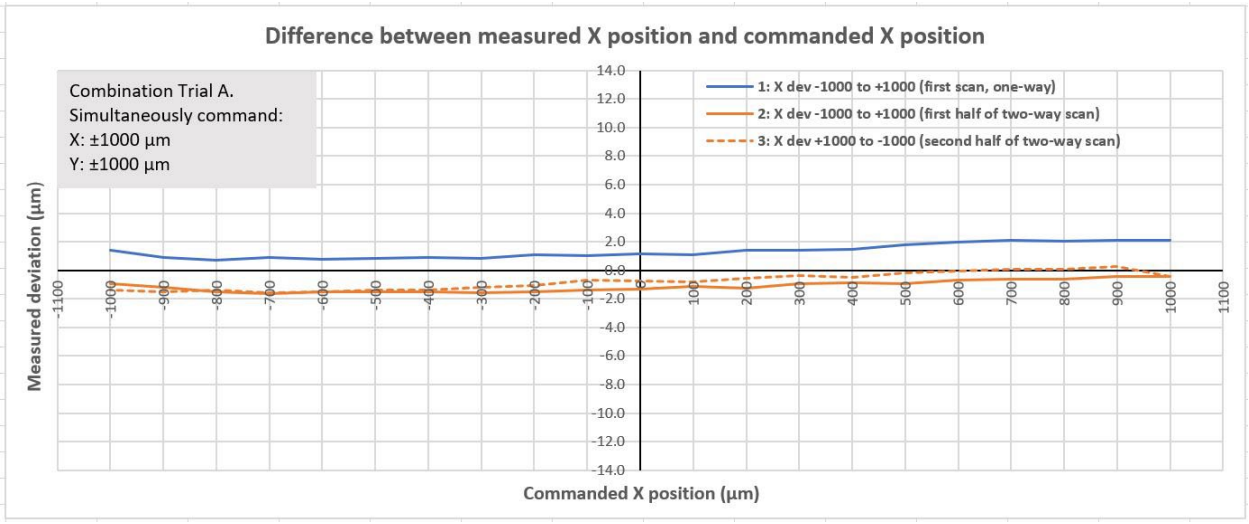

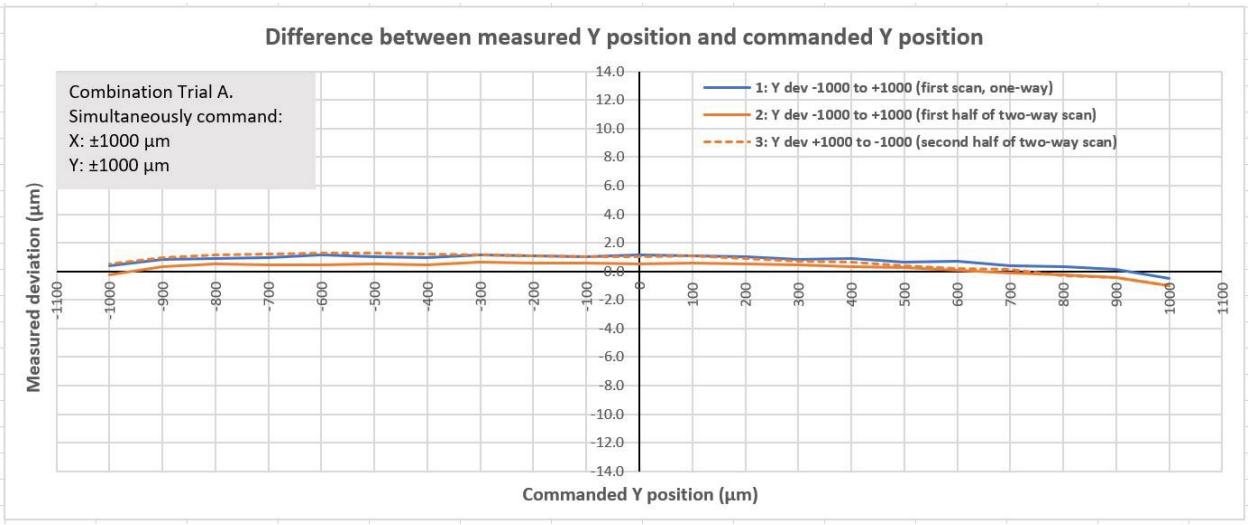

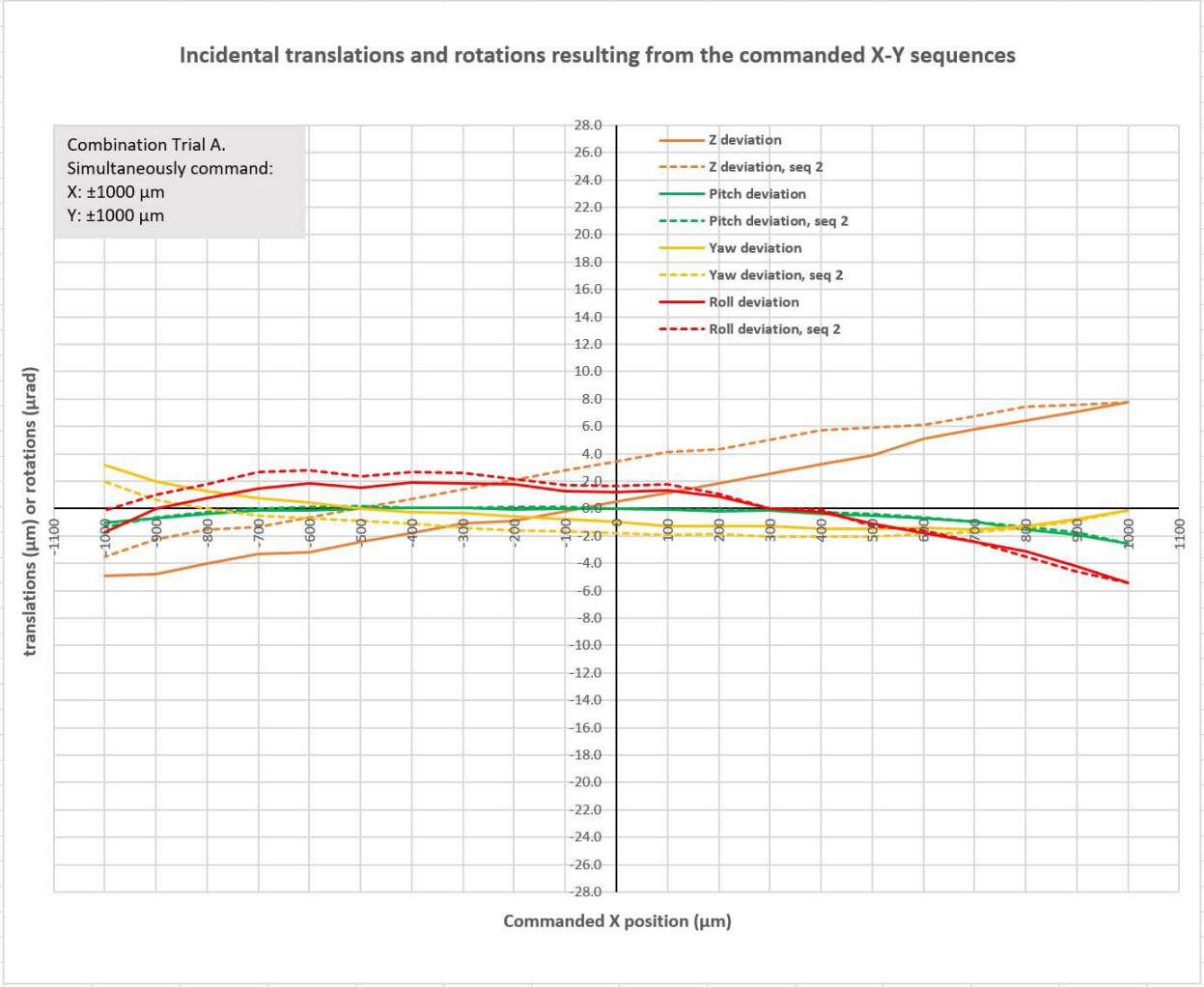
Incidental translations and rotations resulting from the commanded X-Y sequences
Combination Trial A.
Simultaneously command:
X: ±1000 µm
Y: ±1000 µm
Z deviation
Z deviation, seq 2
Pitch deviation
Pitch deviation, seq 2
Yaw deviation
Yaw deviation, seq 2
Roll deviation
Roll deviation, seq 2
translations (µm) or rotations (µrad)
Commanded X position (µm)

Scans 13 & 14: X, Y and Pitch moving from –700 µm/µrad to +700 µm/µrad in steps of 100 µm/µrad :

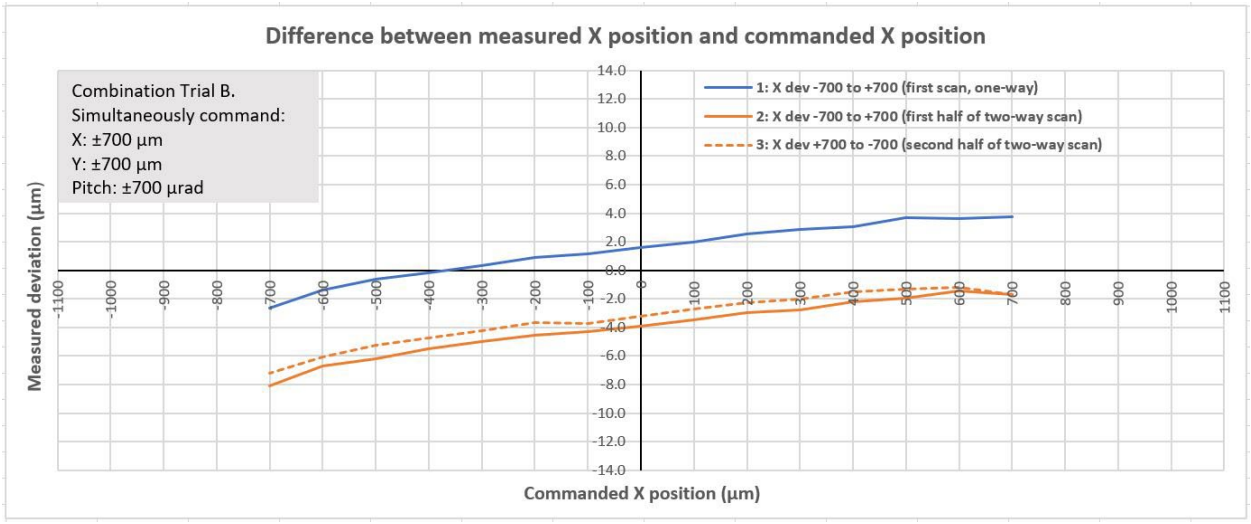

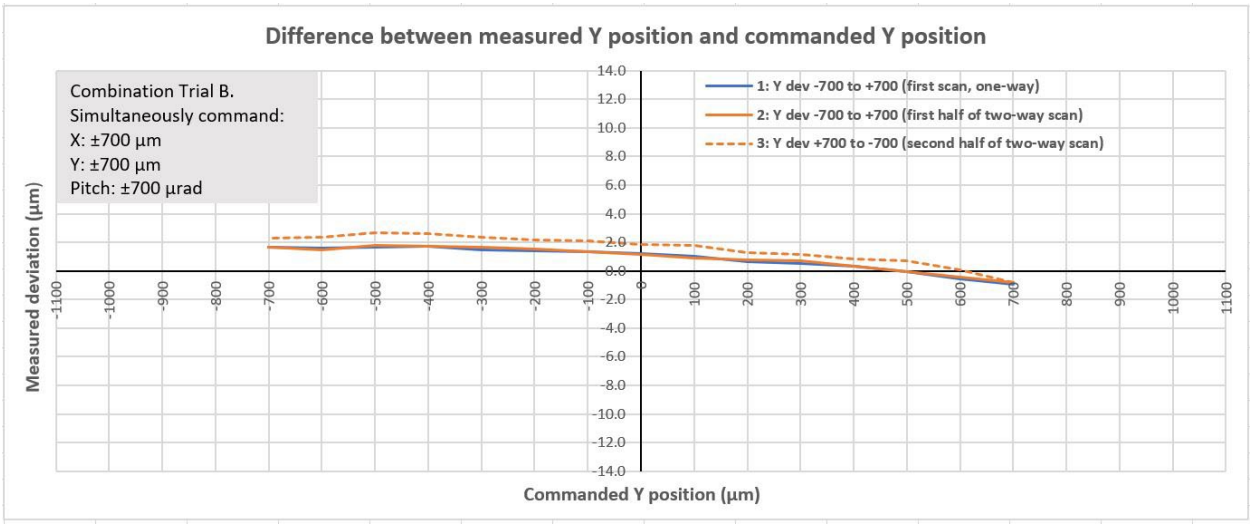

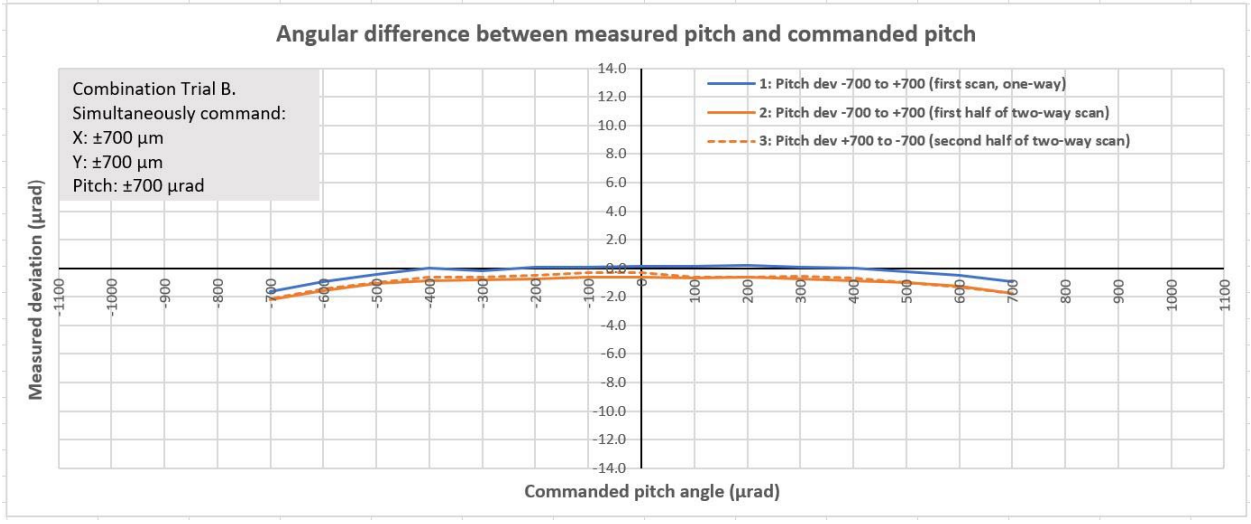

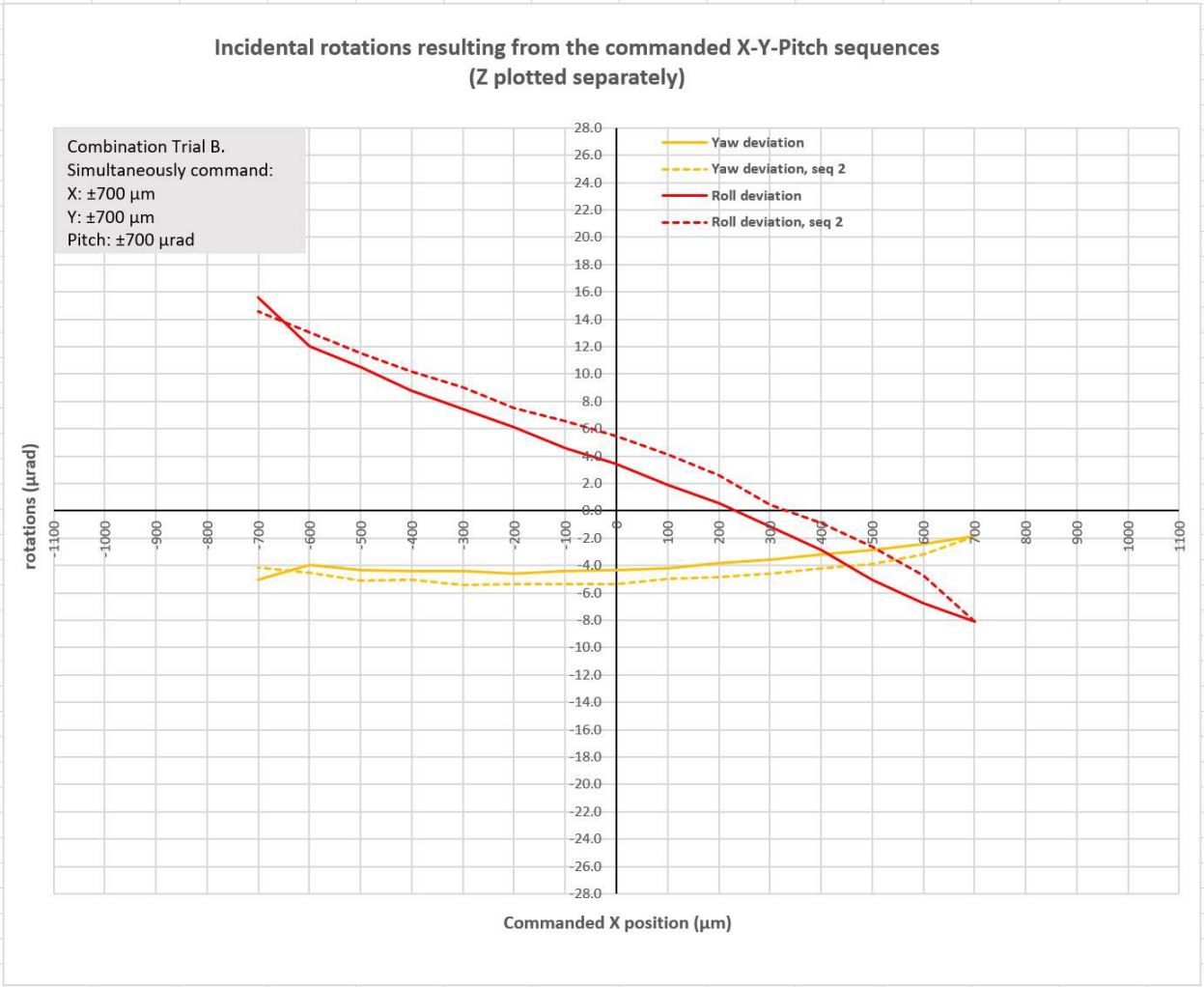
Incidental rotations resulting from the commanded X-Y-Pitch sequences
(Z plotted separately)
Combination Trial B.
Simultaneously command:
X: ±700 µm
Y: ±700 µm
Pitch: ±700 µrad
Yaw deviation
Yaw deviation, seq 2
Roll deviation
Roll deviation, seq 2
rotations (µrad)
Commanded X position (µm)

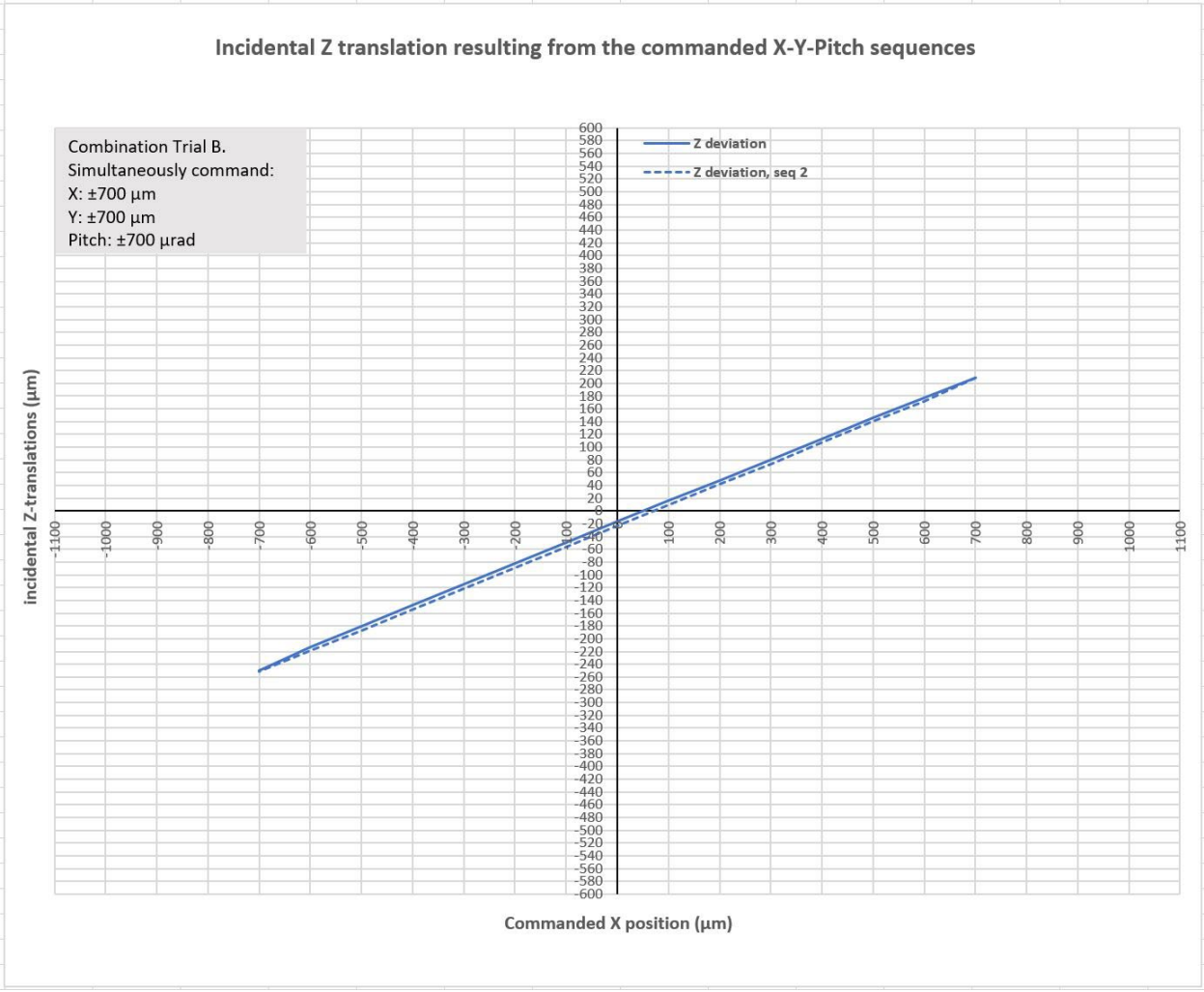
Incidental Z translation resulting from the commanded X-Y-Pitch sequences
Combination Trial B.
Simultaneously command:
X: ±700 µm
Y: ±700 µm
Pitch: ±700 µrad
Z deviation
Z deviation, seq 2
incidental Z-translations (µm)
Commanded X position (µm)

Scans 15 & 16: X, Y, Pitch & Yaw moving from –500 µm/µrad to 500 µm/µrad in steps of 100 µm/µrad:

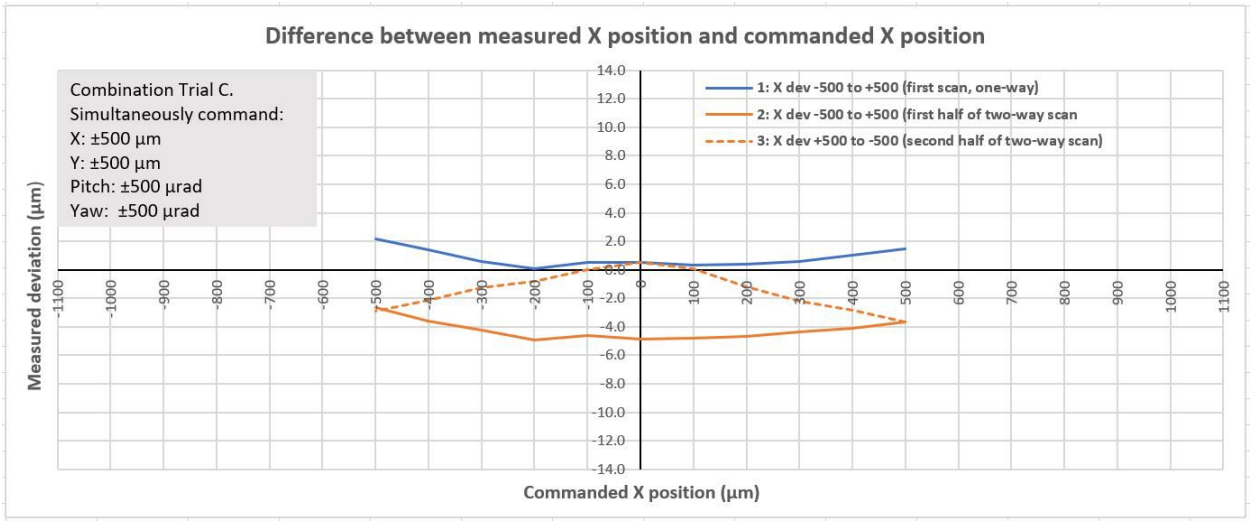

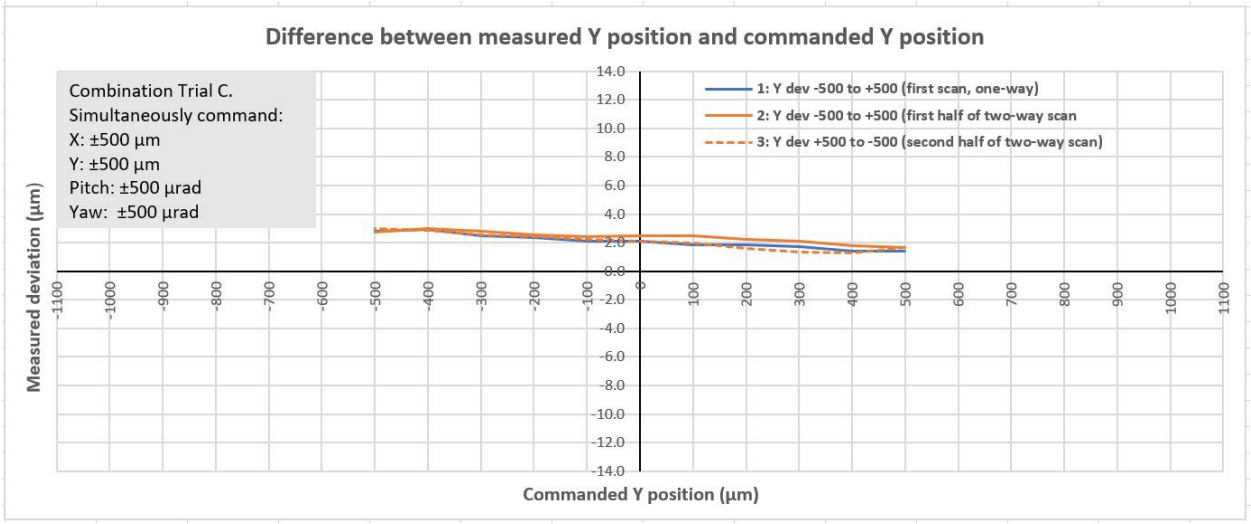

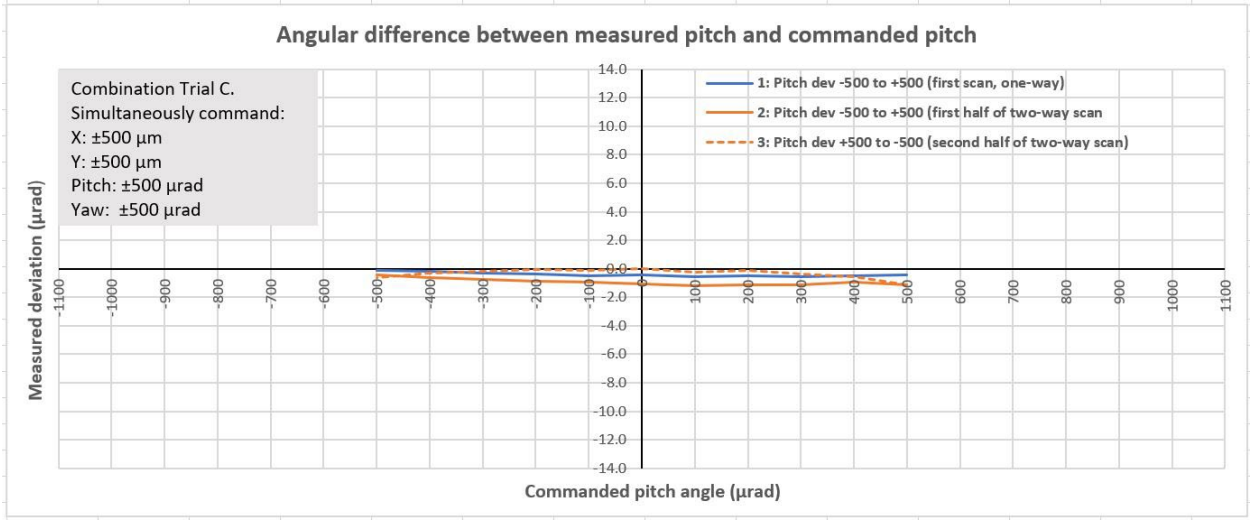

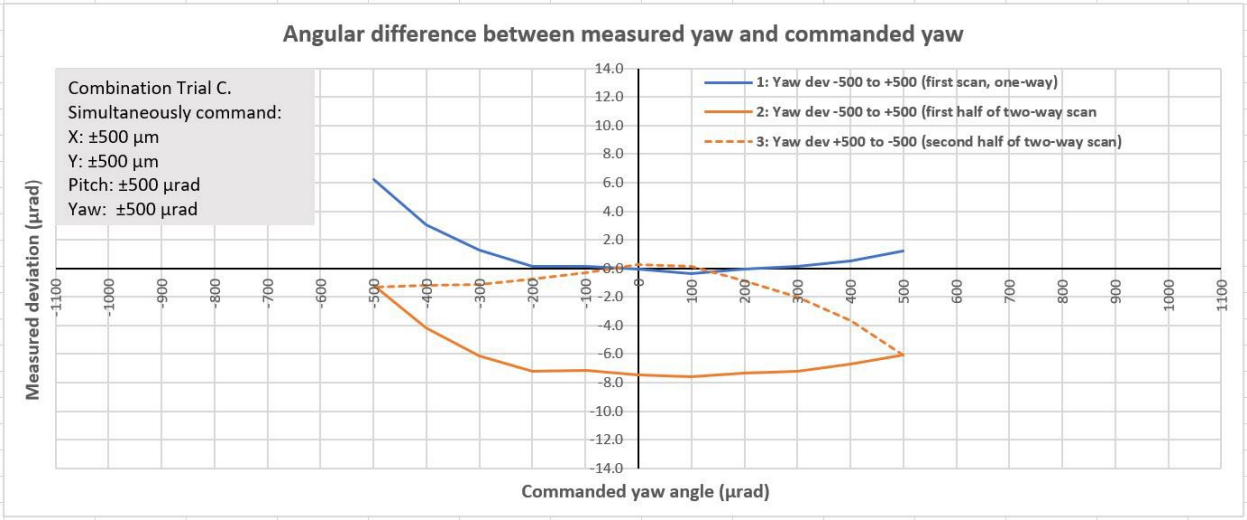
Angular difference between measured yaw and commanded yaw
Combination Trial C.
Simultaneously command:
X: ±500 µm
Y: ±500 µm
Pitch: ±500 µrad
Yaw: ±500 µrad
1: Yaw dev -500 to +500 (first scan, one-way)
2: Yaw dev -500 to +500 (first half of two-way scan
3: Yaw dev +500 to -500 (second half of two-way scan)
Measured deviation (µrad)
Commanded yaw angle (µrad)

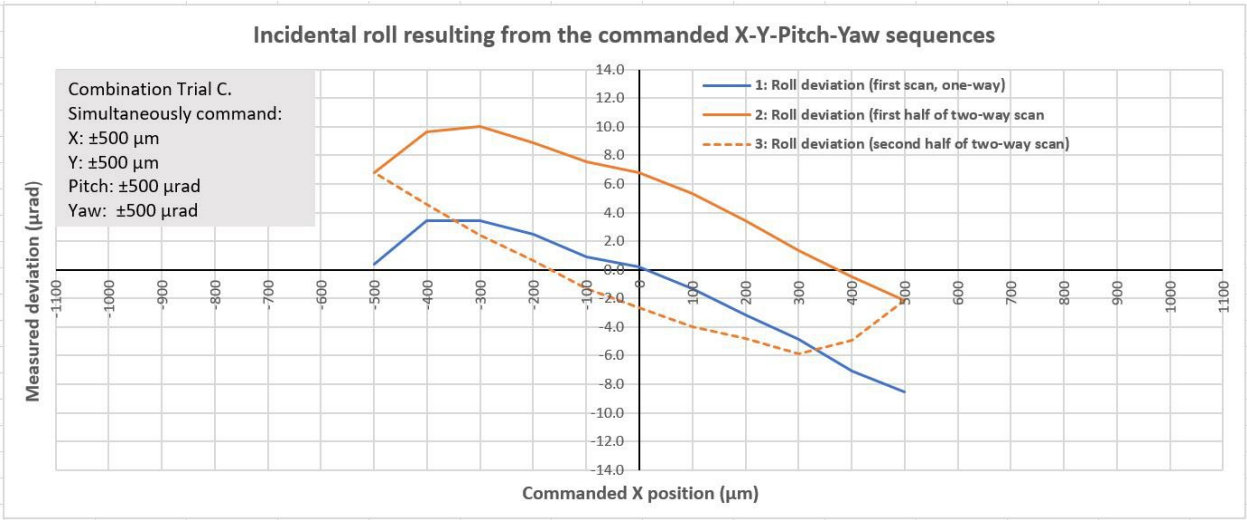
Incidental roll resulting from the commanded X-Y-Pitch-Yaw sequences
Combination Trial C.
Simultaneously command:
X: ±500 µm
Y: ±500 µm
Pitch: ±500 µrad
Yaw: ±500 µrad
1: Roll deviation (first scan, one-way)
2: Roll deviation (first half of two-way scan
3: Roll deviation (second half of two-way scan)
Measured deviation (µrad)
Commanded X position (µm)

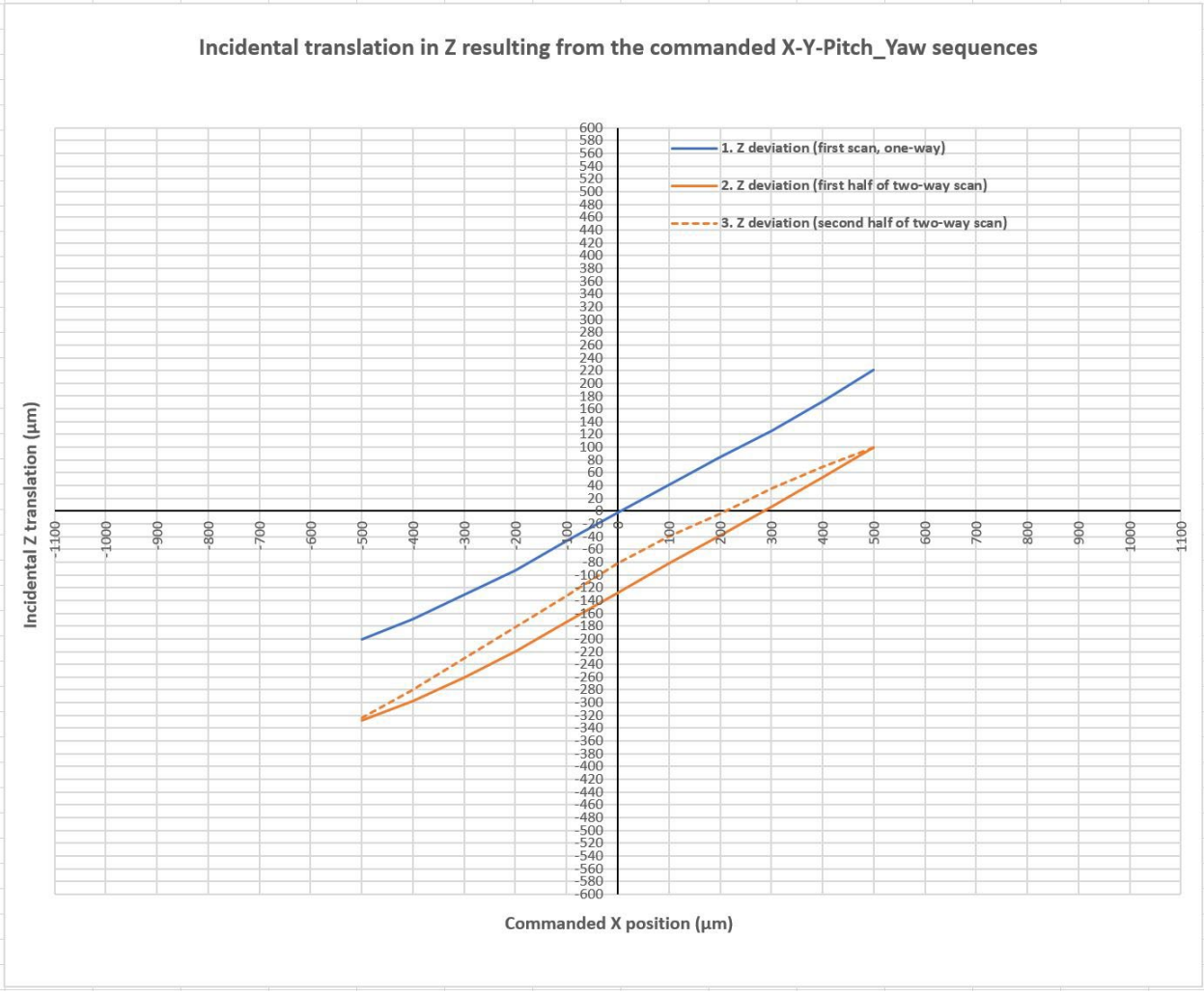
Incidental translation in Z resulting from the commanded X-Y-Pitch_Yaw sequences
1. Z deviation (first scan, one-way)
2. Z deviation (first half of two-way scan)
3. Z deviation (second half of two-way scan)
Incidental Z translation (µm)
Commanded X position (µm)

Scans 17 & 18: X, Y, Pitch, Yaw & Roll moving from –500 µm/µrad to +500 µm/µrad in steps of 100 µm/µrad :

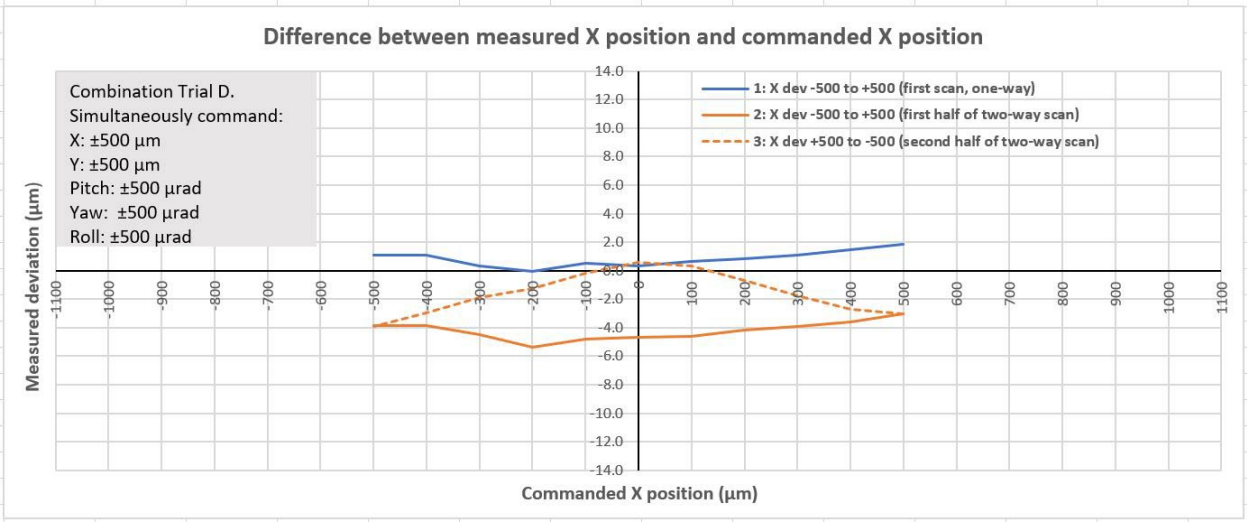

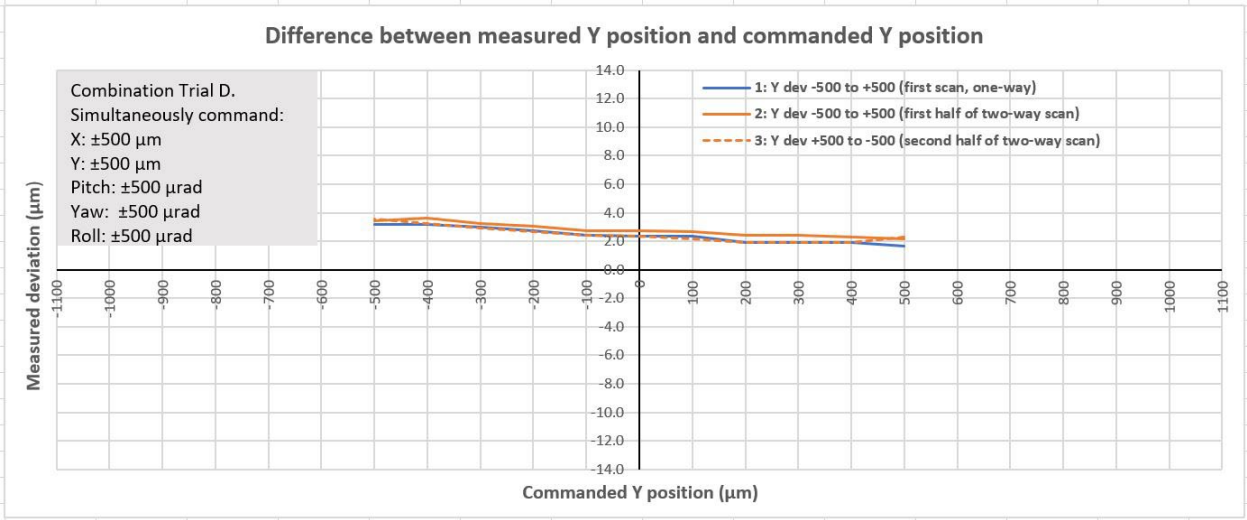

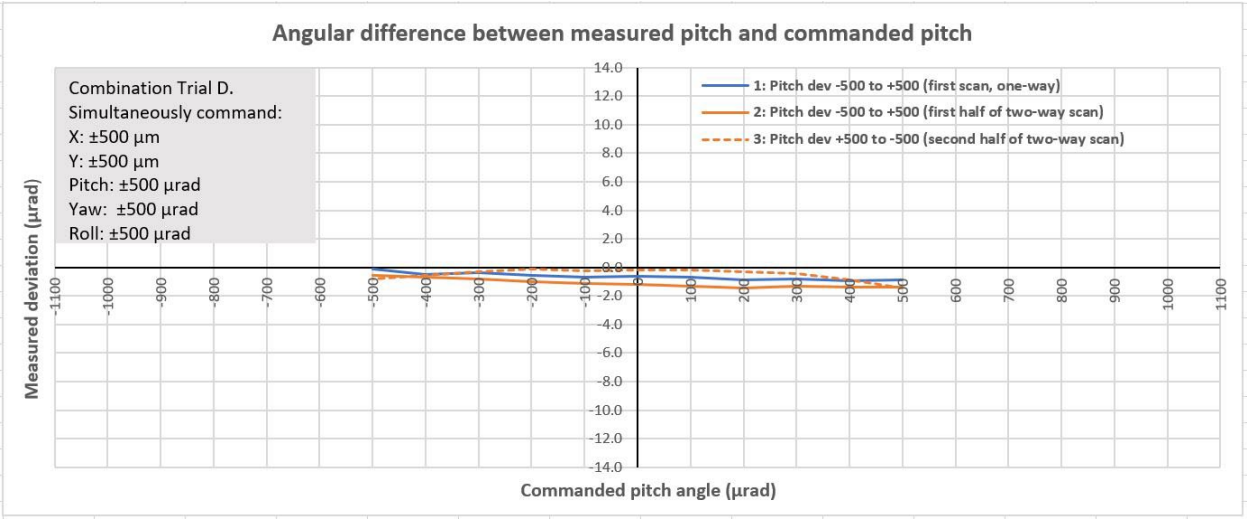

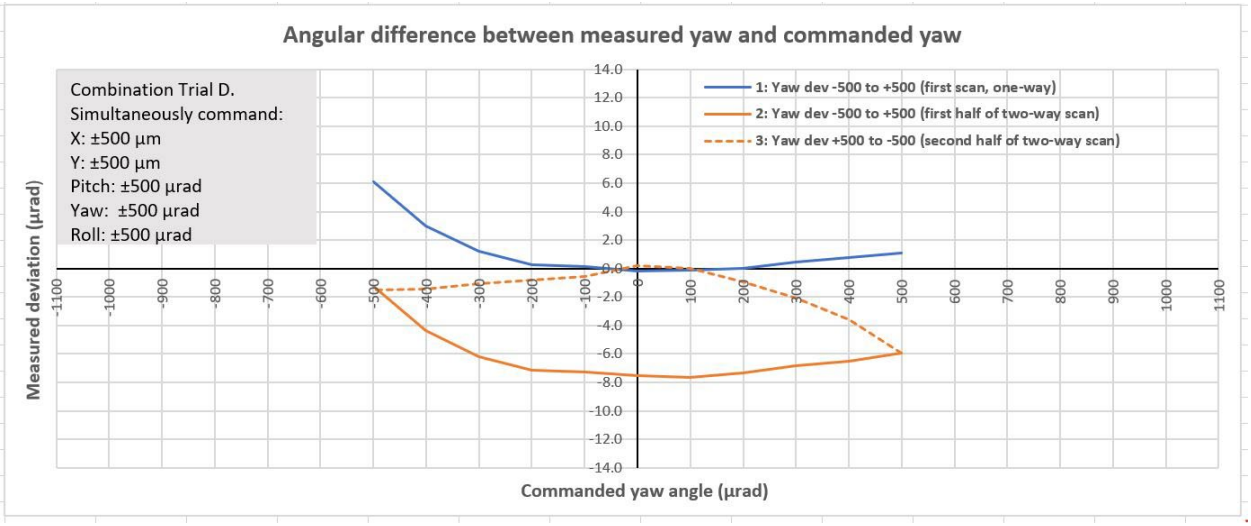
Angular difference between measured yaw and commanded yaw
Combination Trial D.
Simultaneously command:
X: ±500 µm
Y: ±500 µm
Pitch: ±500 µrad
Yaw: ±500 µrad
Roll: ±500 µrad
1: Yaw dev -500 to +500 (first scan, one-way)
2: Yaw dev -500 to +500 (first half of two-way scan)
3: Yaw dev +500 to -500 (second half of two-way scan)
Measured deviation (µrad)
Commanded yaw angle (µrad)

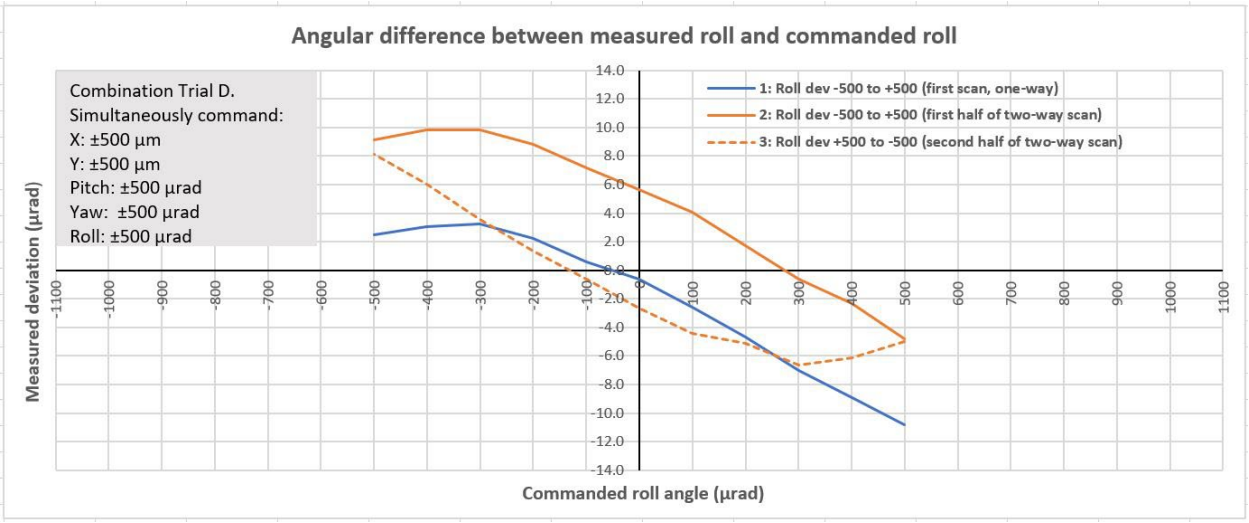
Angular difference between measured roll and commanded roll
Combination Trial D.
Simultaneously command:
X: ±500 µm
Y: ±500 µm
Pitch: ±500 µrad
Yaw: ±500 µrad
Roll: ±500 µrad
1: Roll dev -500 to +500 (first scan, one-way)
2: Roll dev -500 to +500 (first half of two-way scan)
3: Roll dev +500 to -500 (second half of two-way scan)
Measured deviation (µrad)
Commanded roll angle (µrad)

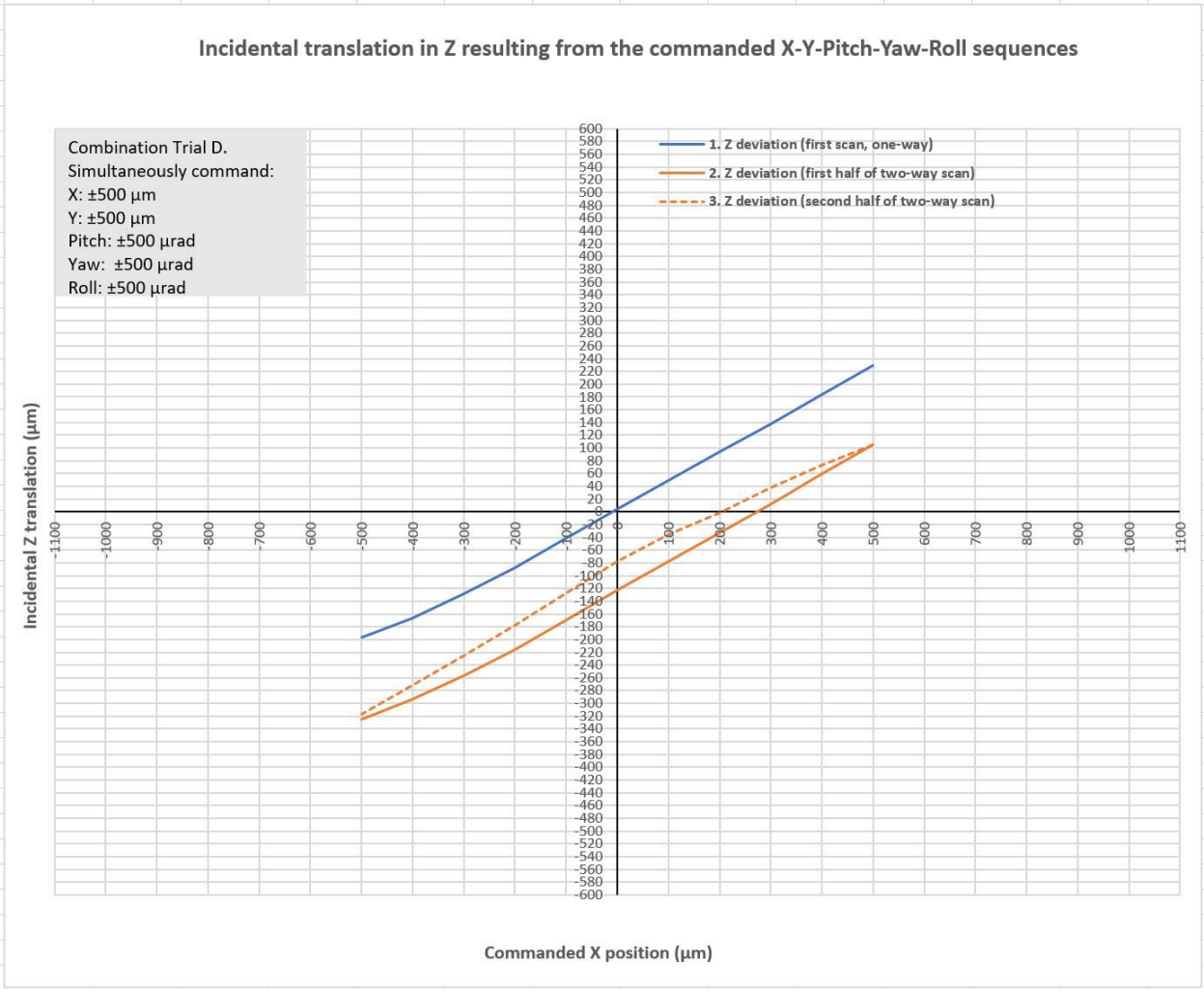
Incidental translation in Z resulting from the commanded X-Y-Pitch-Yaw-Roll sequences
Combination Trial D.
Simultaneously command:
X: ±500 µm
Y: ±500 µm
Pitch: ±500 µrad
Yaw: ±500 µrad
Roll: ±500 µrad
1. Z deviation (first scan, one-way)
2. Z deviation (first half of two-way scan)
3. Z deviation (second half of two-way scan)
Incidental Z translation (µm)
Commanded X position (µm)

APPENDIX B. HIGH-RESOLUTION SYSTEM CHARACTERIZATION PLOTS

The plots in this section show the results of scanning each degree of freedom (DOF) in smaller steps: 10 µm or 10 µrad. Each DOF was scanned at just three relatively small bands: at each end of the range and at the center of the range. The setpoint positions are differenced against the actual measured positions. These tests were performed in both directions, starting at the most negative position, and moving to the most positive position, and then back to the most negative position. The corresponding incidental motions on the other DOF are also shown. Additionally, the measured step sizes are computed and plotted. The plots are presented in the order in which the scan data was collected.

The complete list of data collection scans is detailed in the below table. The plots are then presented in the same order.

Scan ID	DOF Parameter	Band 1	Band 2	Band 3	Step Size
1 P	X	-2100 to -1700	-200 to +200	+1700 to +2100	10
2 P	X	+2100 to +1700	+200 to -200	-1700 to -2100	-10
3 P	Y	-1400 to -1000	-200 to +200	+1000 to +1400	10
4 P	Y	+1400 to +1000	+200 to -200	-1000 to -1400	-10
5 P	Pitch	-1800 to -1400	-200 to +200	+1400 to +1800	10
6 P	Pitch	+1800 to +1400	+200 to -200	-1400 to -1800	-10
7 P	Yaw	-2600 to -2200	-200 to +200	+2200 to +2600	10
8 P	Yaw	+2600 to +2200	+200 to -200	-2200 to -2600	-10
9 P	Roll	-3900 to -3500	-200 to +200	+3500 to +3900	10
10 P	Roll	+3900 to +3500	+200 to -200	-3500 to -3900	-10

Scans 1 P & 2 P: X moving between –2100 µm and +2100 µm:

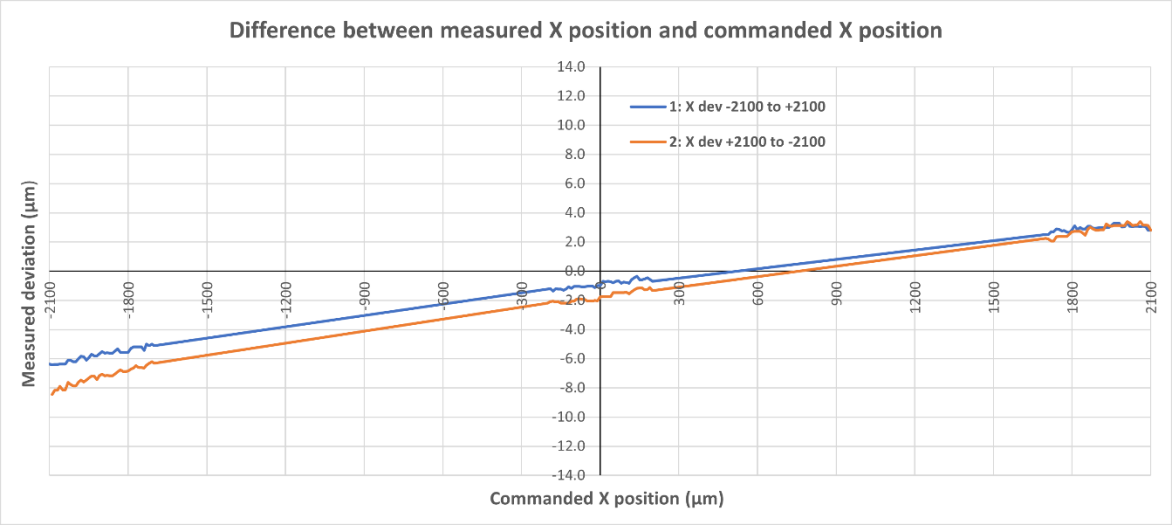

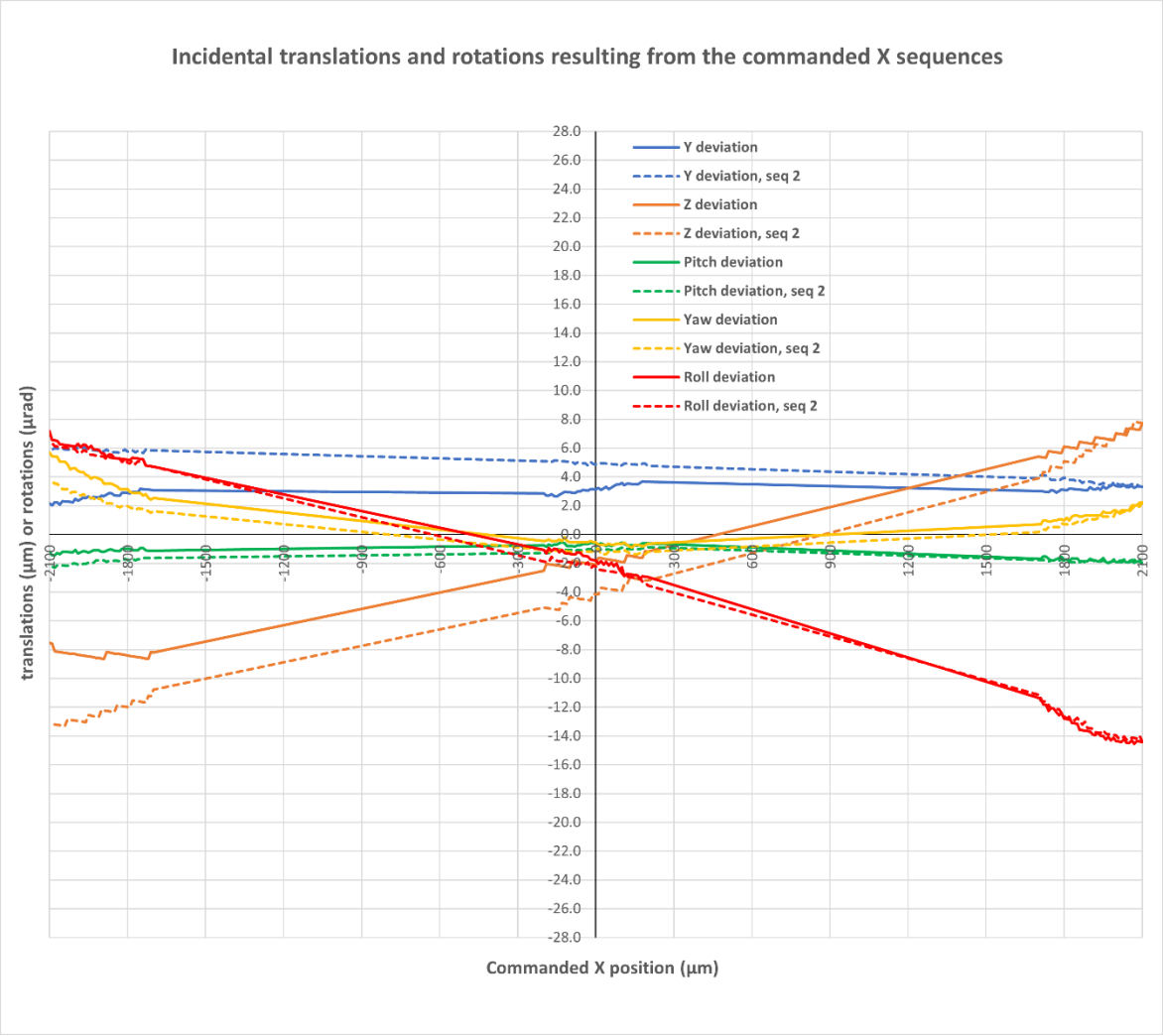

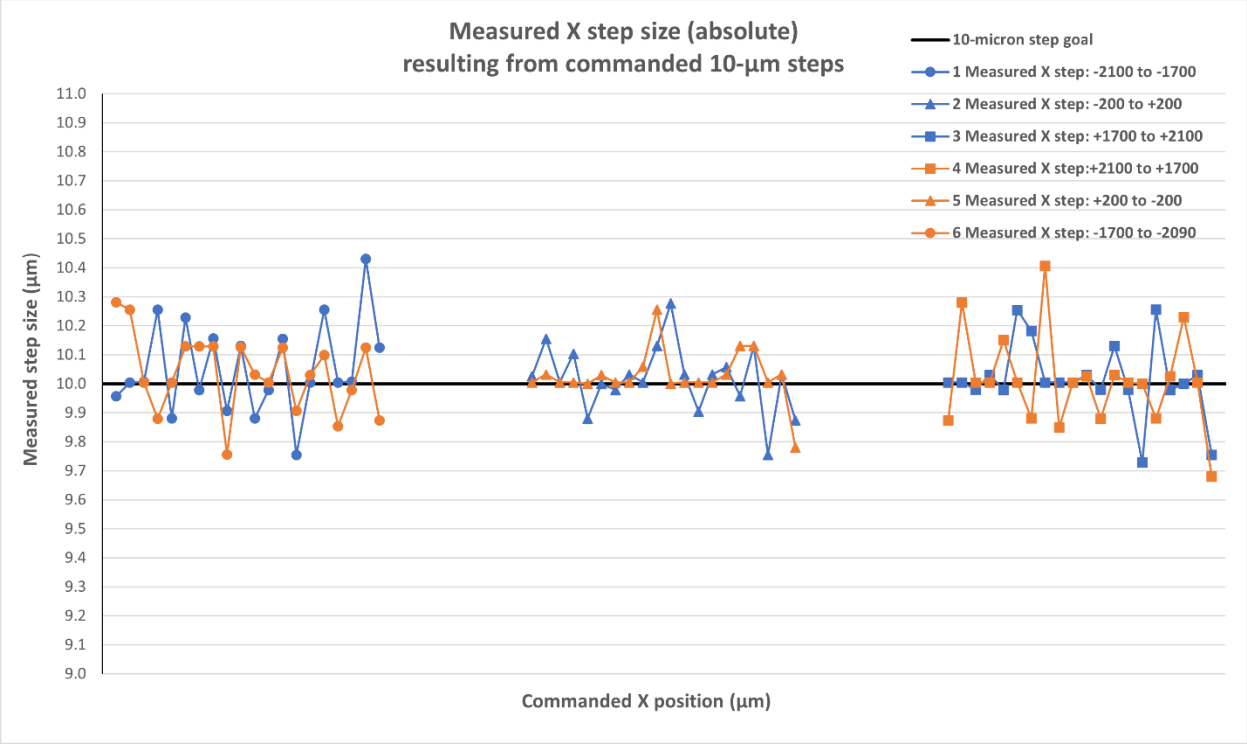
Measured X step size (absolute)
resulting from commanded 10-µm steps
10-micron step goal
1 Measured X step: -2100 to -1700
2 Measured X step: -200 to +200
3 Measured X step: +1700 to +2100
4 Measured X step:+2100 to +1700
5 Measured X step: +200 to -200
6 Measured X step: -1700 to -2090
Measured step size (µm)
11.0
10.9
10.8
10.7
10.6
10.5
10.4
10.3
10.2
10.1
10.0
9.9
9.8
9.7
9.6
9.5
9.4
9.3
9.2
9.1
9.0
Commanded X position (µm)

Scans 3 P & 4 P: Y moving between –1400 µm and +1400 µm:

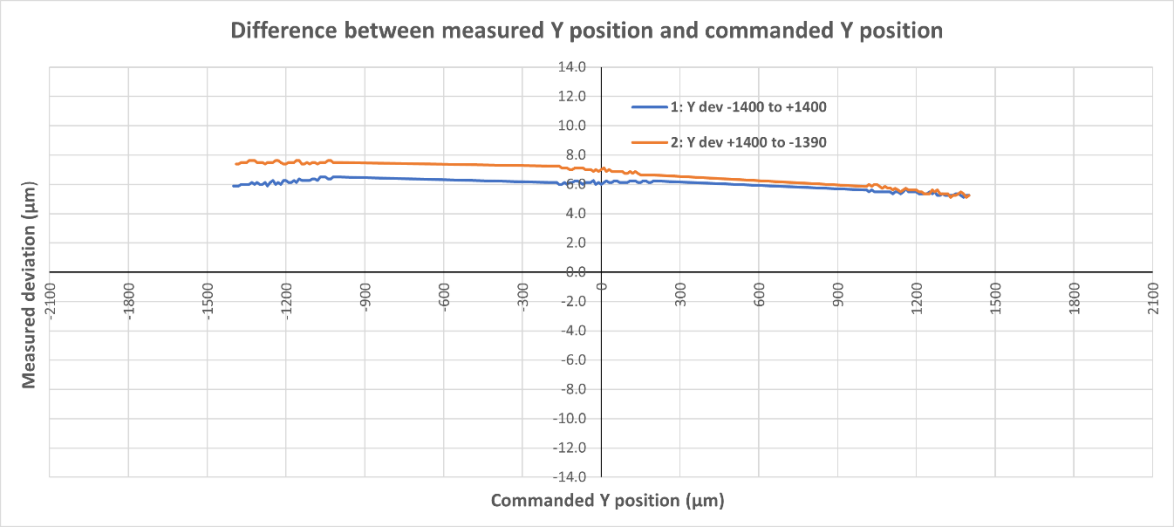

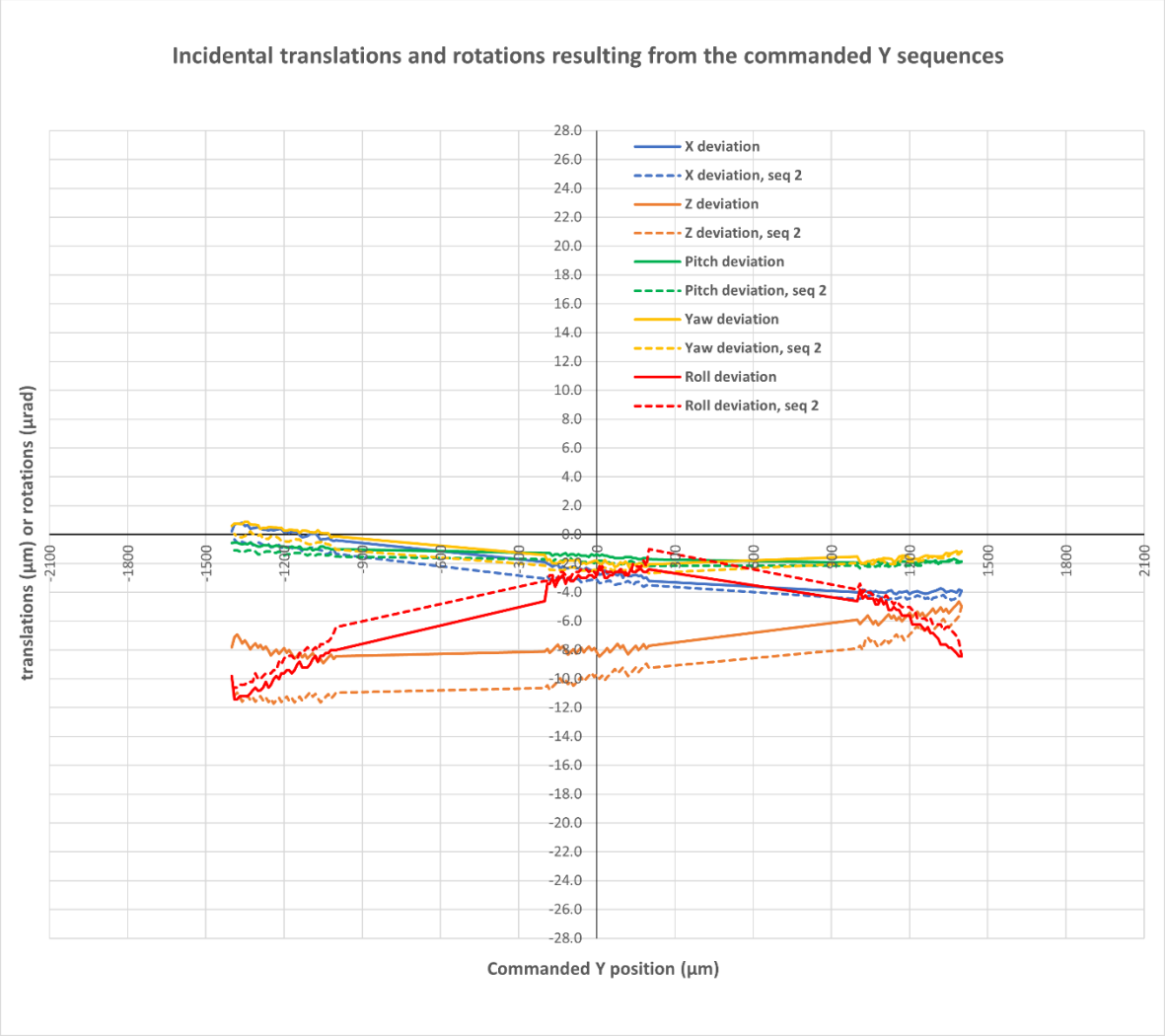

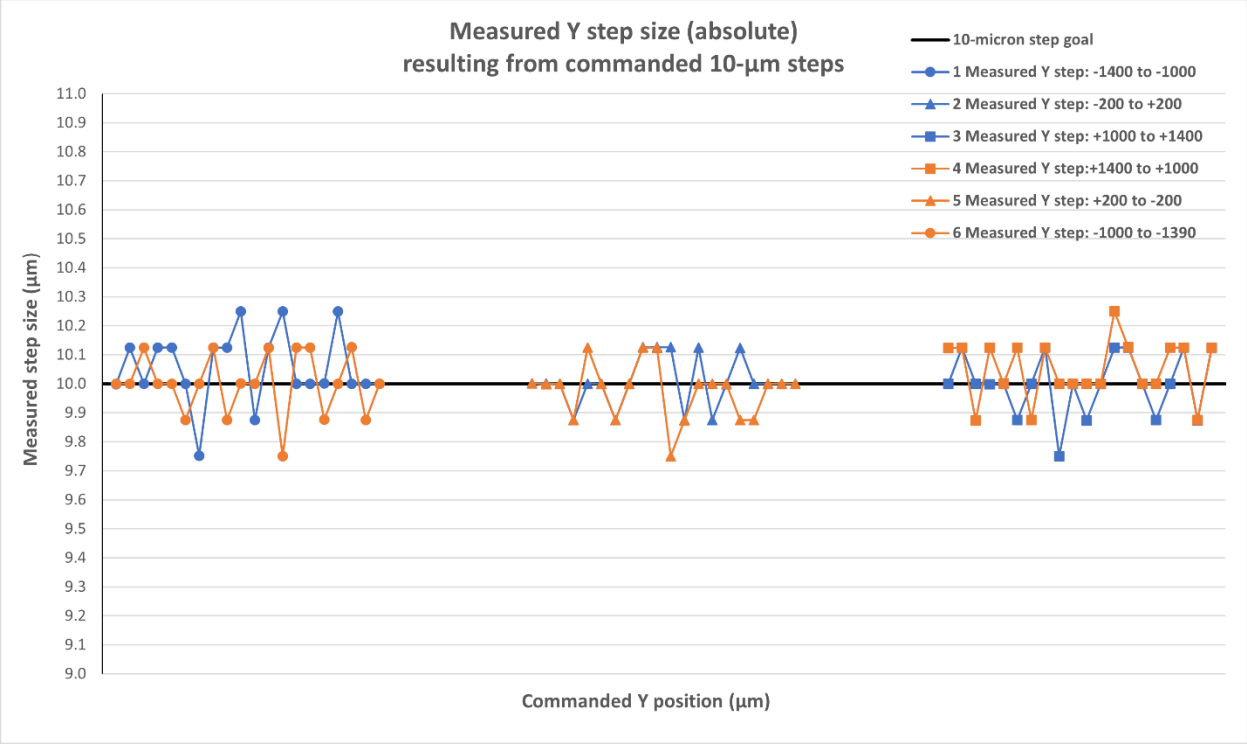
Measured Y step size (absolute)
resulting from commanded 10-µm steps
10-micron step goal
1 Measured Y step: -1400 to -1000
2 Measured Y step: -200 to +200
3 Measured Y step: +1000 to +1400
4 Measured Y step:+1400 to +1000
5 Measured Y step: +200 to -200
6 Measured Y step: -1000 to -1390
Measured step size (µm)
11.0
10.9
10.8
10.7
10.6
10.5
10.4
10.3
10.2
10.1
10.0
9.9
9.8
9.7
9.6
9.5
9.4
9.3
9.2
9.1
9.0
Commanded Y position (µm)

Scans 5 P & 6 P: Pitch moving between –1800 µrad and +1800 µrad:

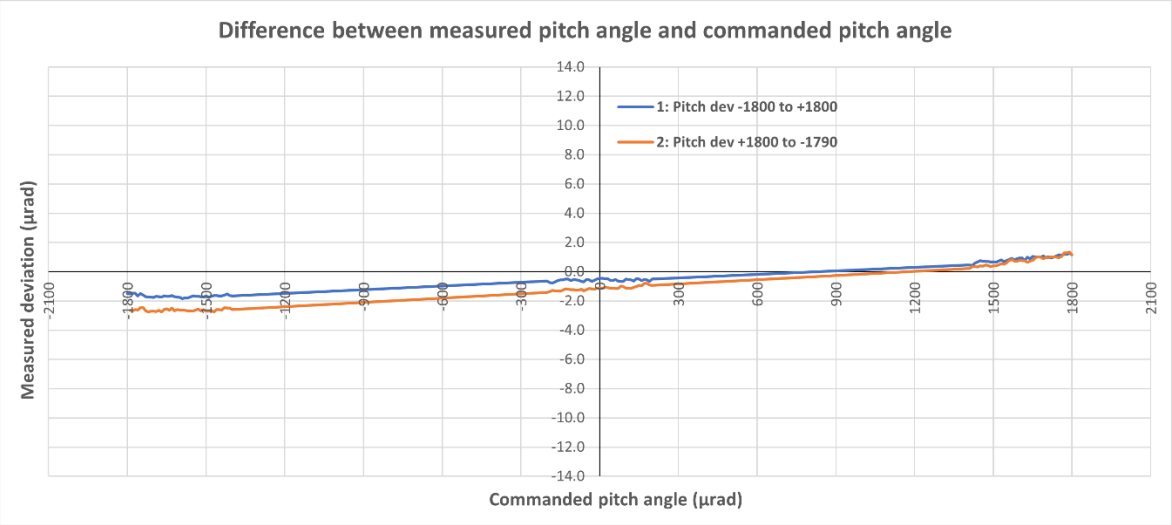

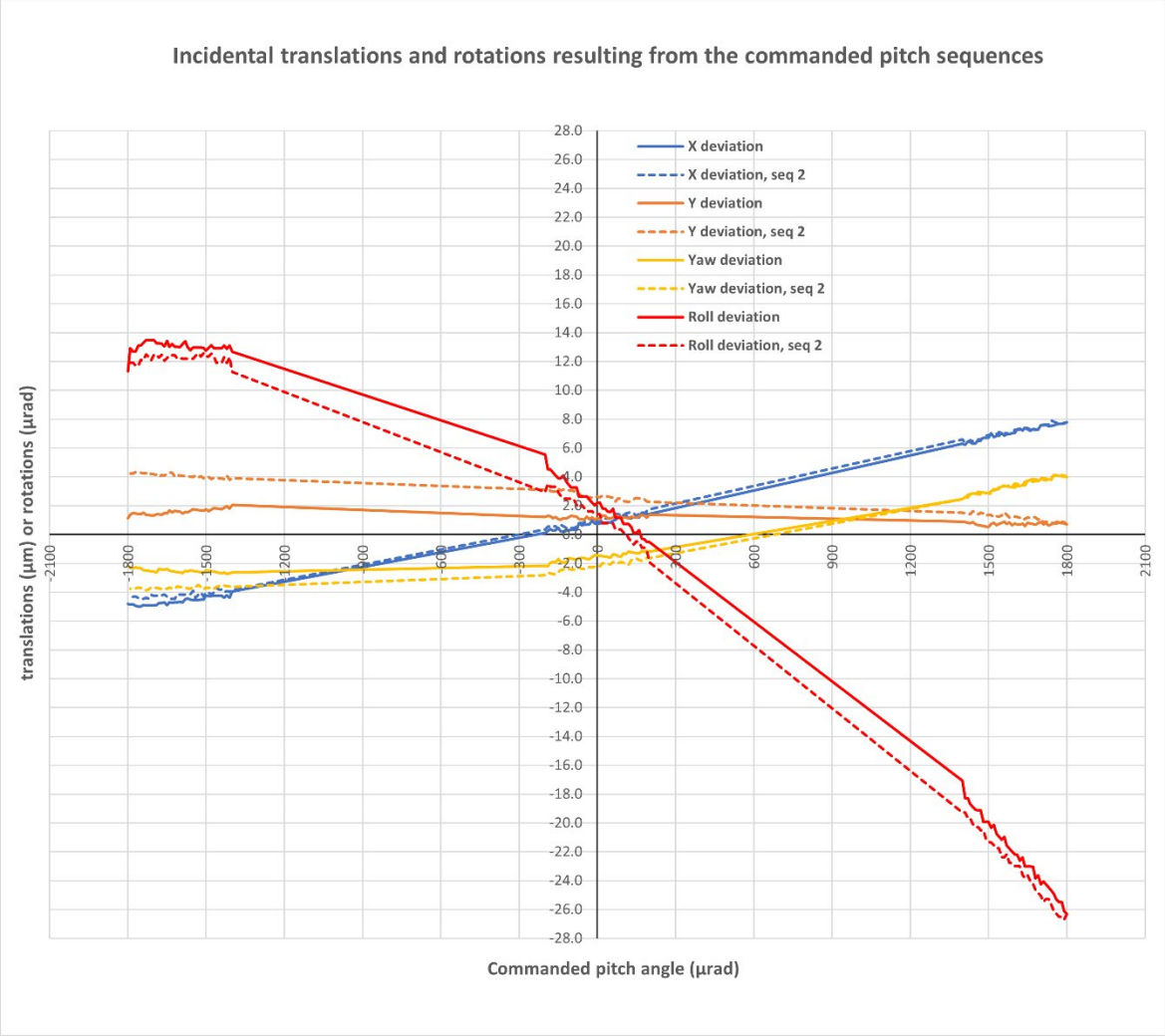

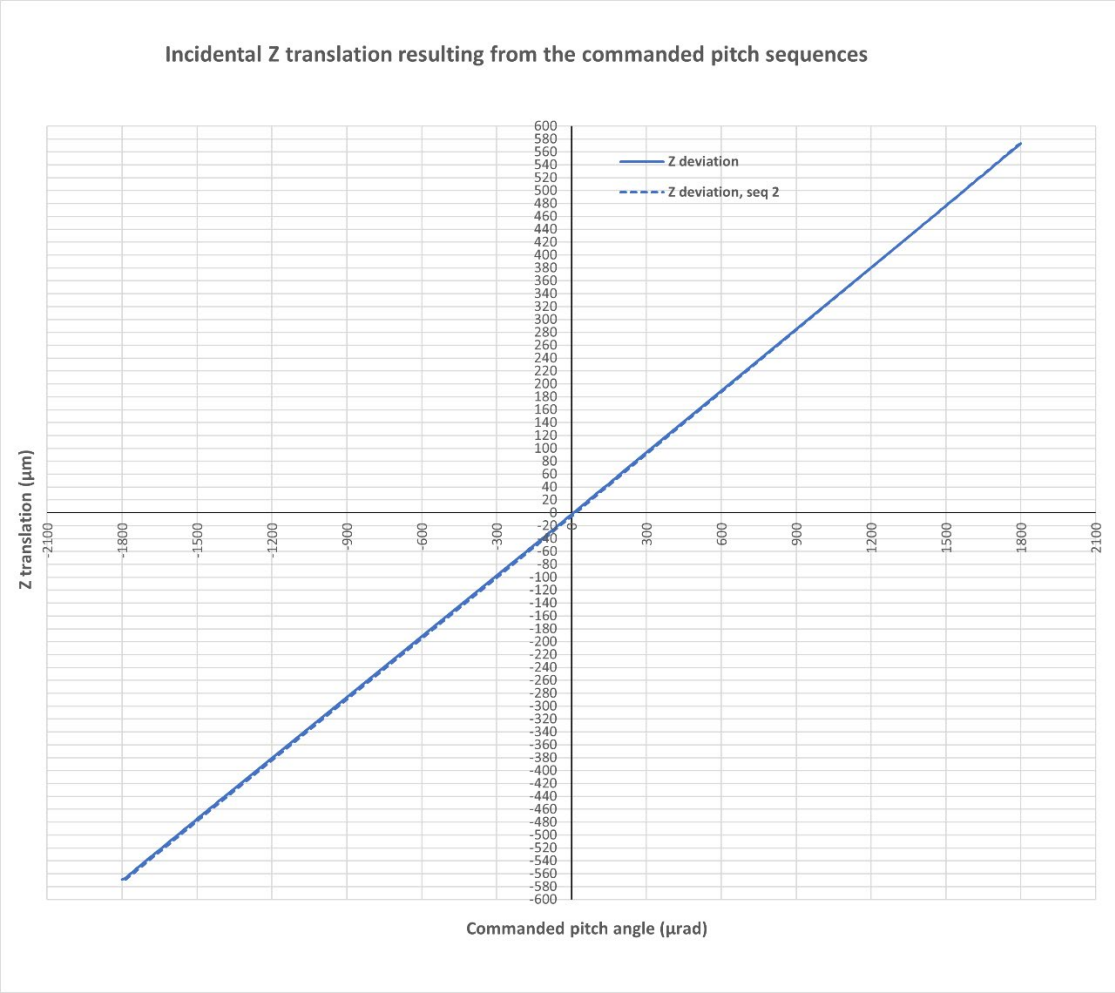
Incidental Z translation resulting from the commanded pitch sequences
Z deviation
Z deviation, seq 2
Z translation (µm)
Commanded pitch angle (µrad)

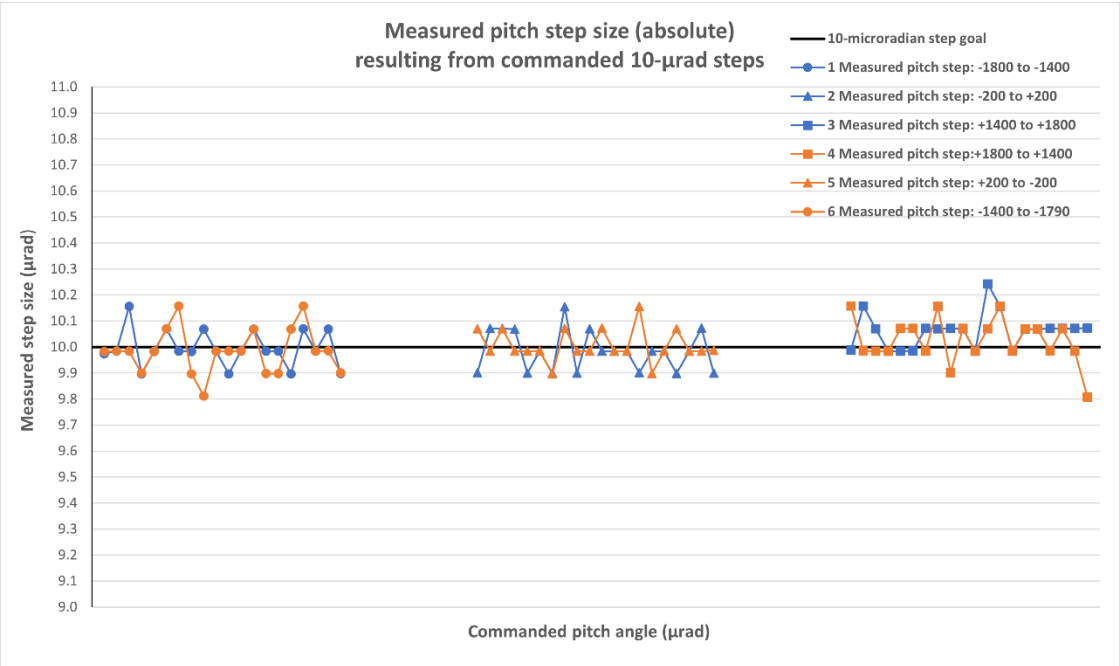
Measured pitch step size (absolute)
resulting from commanded 10-µrad steps
10-microradian step goal
1 Measured pitch step: -1800 to -1400
2 Measured pitch step: -200 to +200
3 Measured pitch step: +1400 to +1800
4 Measured pitch step:+1800 to +1400
5 Measured pitch step: +200 to -200
6 Measured pitch step: -1400 to -1790
Measured step size (µrad)
Commanded pitch angle (µrad)

Scans 7 P & 8 P: Yaw moving between –2600 µrad and +2600 µrad:

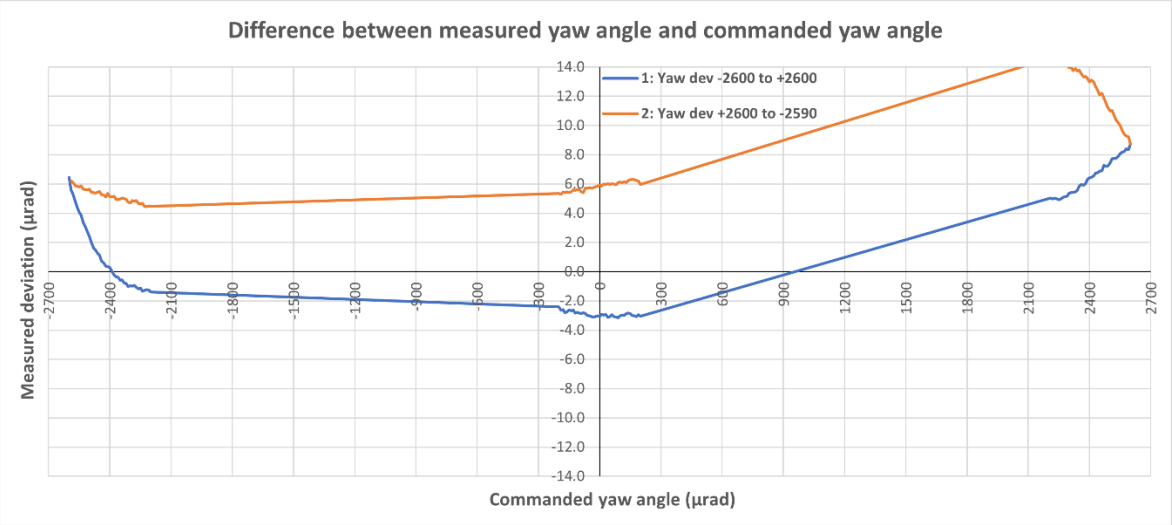

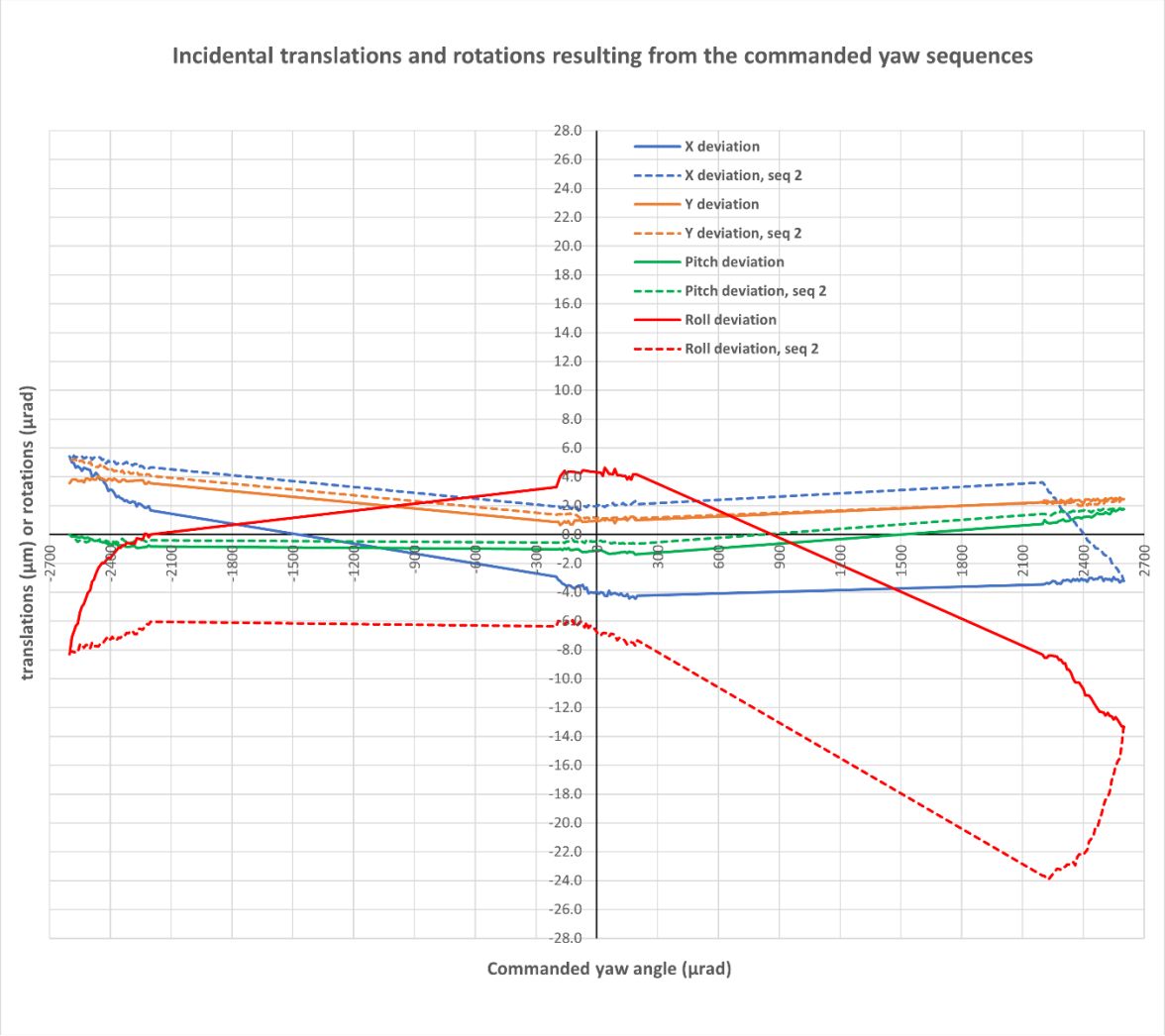

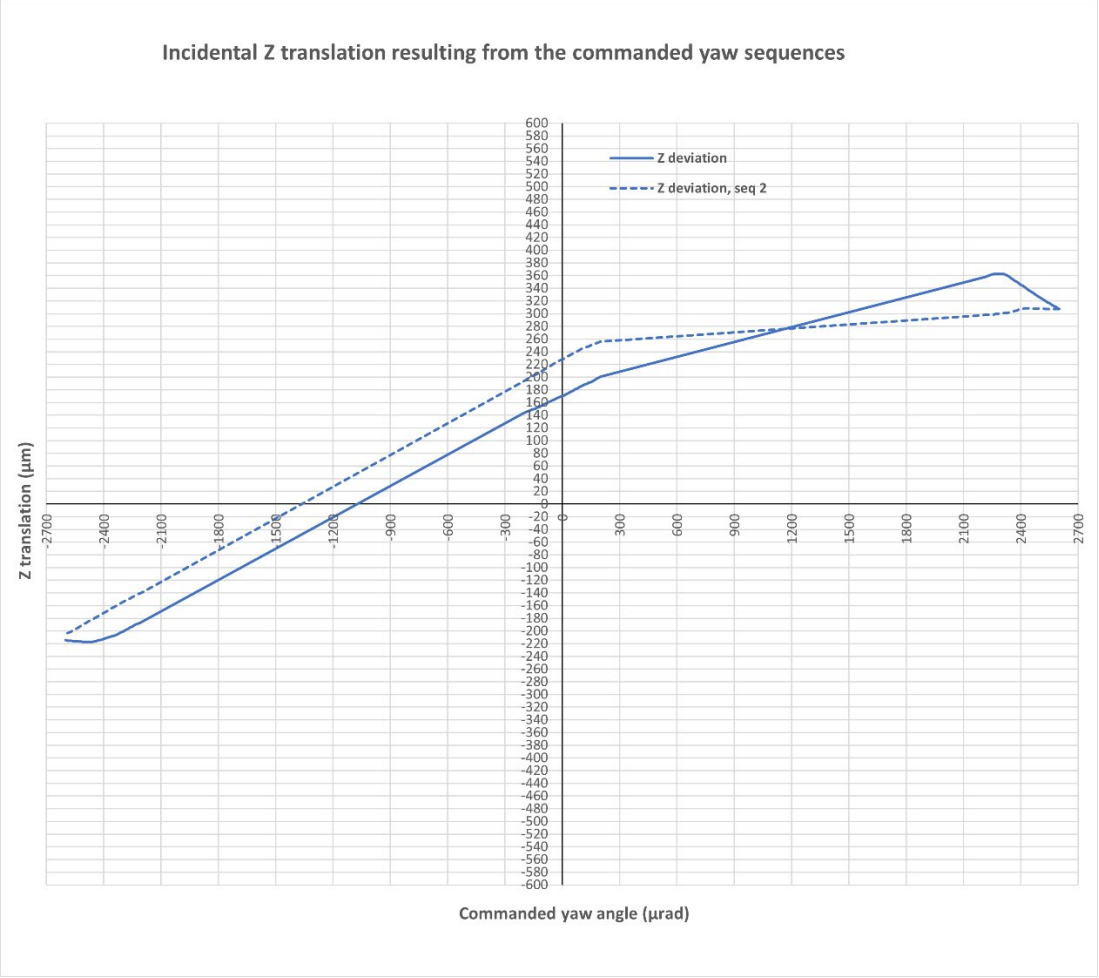
Incidental Z translation resulting from the commanded yaw sequences
Z deviation
Z deviation, seq 2
Z translation (µm)
Commanded yaw angle (µrad)

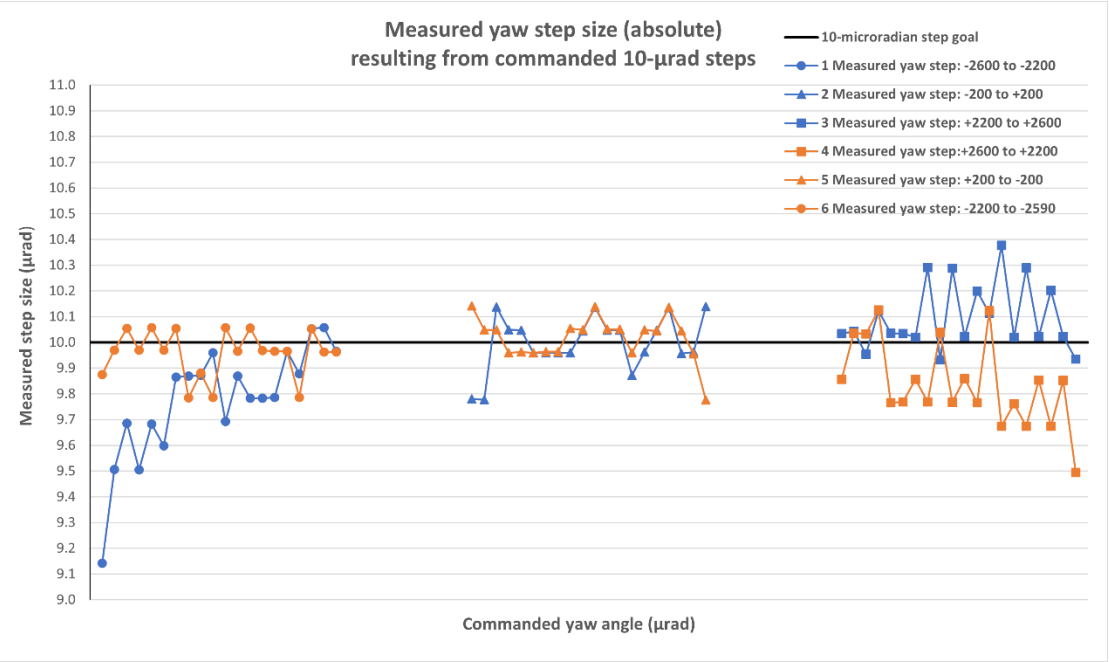
Measured yaw step size (absolute)
resulting from commanded 10-µrad steps
10-microradian step goal
1 Measured yaw step: -2600 to -2200
2 Measured yaw step: -200 to +200
3 Measured yaw step: +2200 to +2600
4 Measured yaw step:+2600 to +2200
5 Measured yaw step: +200 to -200
6 Measured yaw step: -2200 to -2590
Measured step size (µrad)
Commanded yaw angle (µrad)

Scans 9 P & 10 P: Roll moving between –3900 µrad and +3900 µrad:

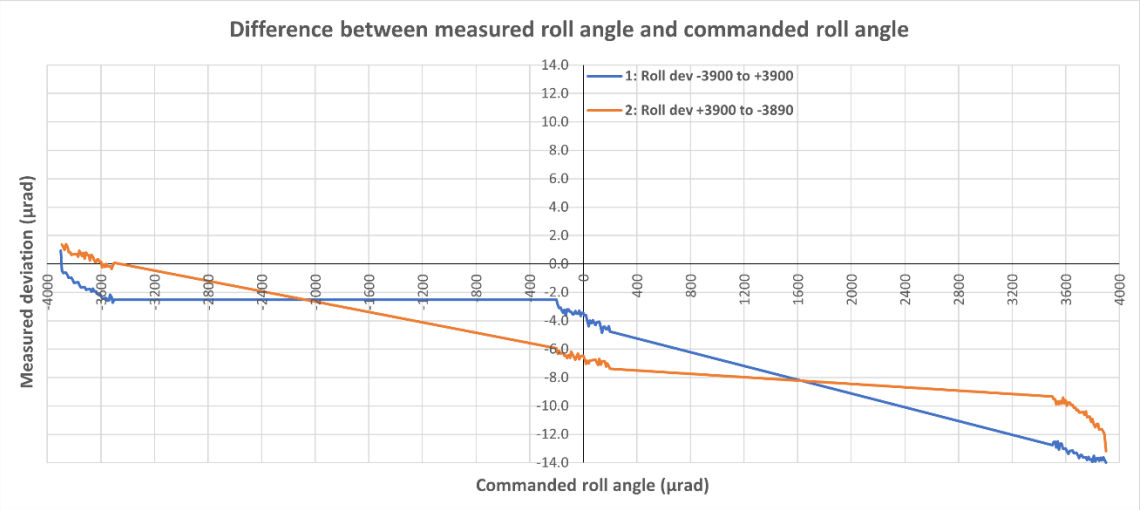

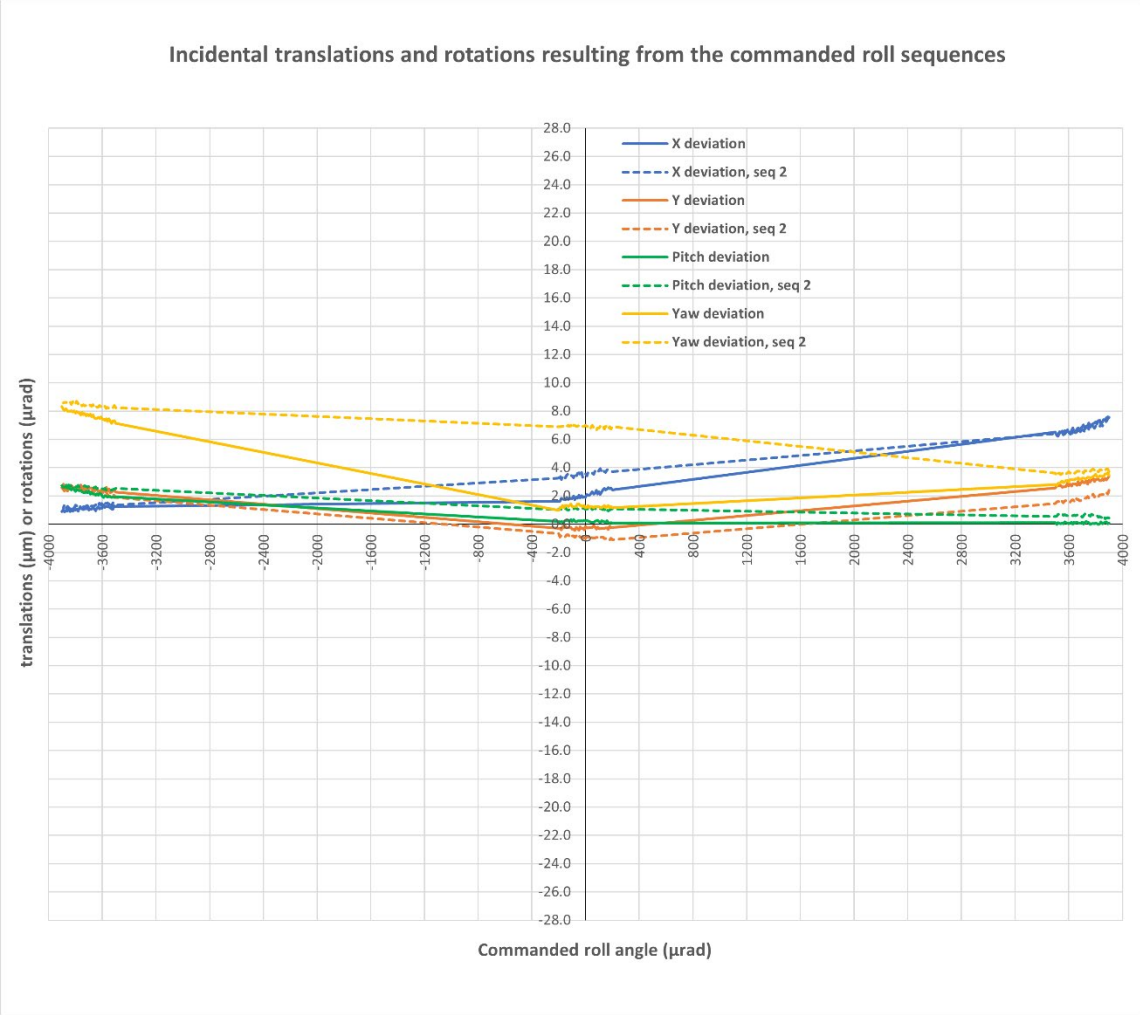

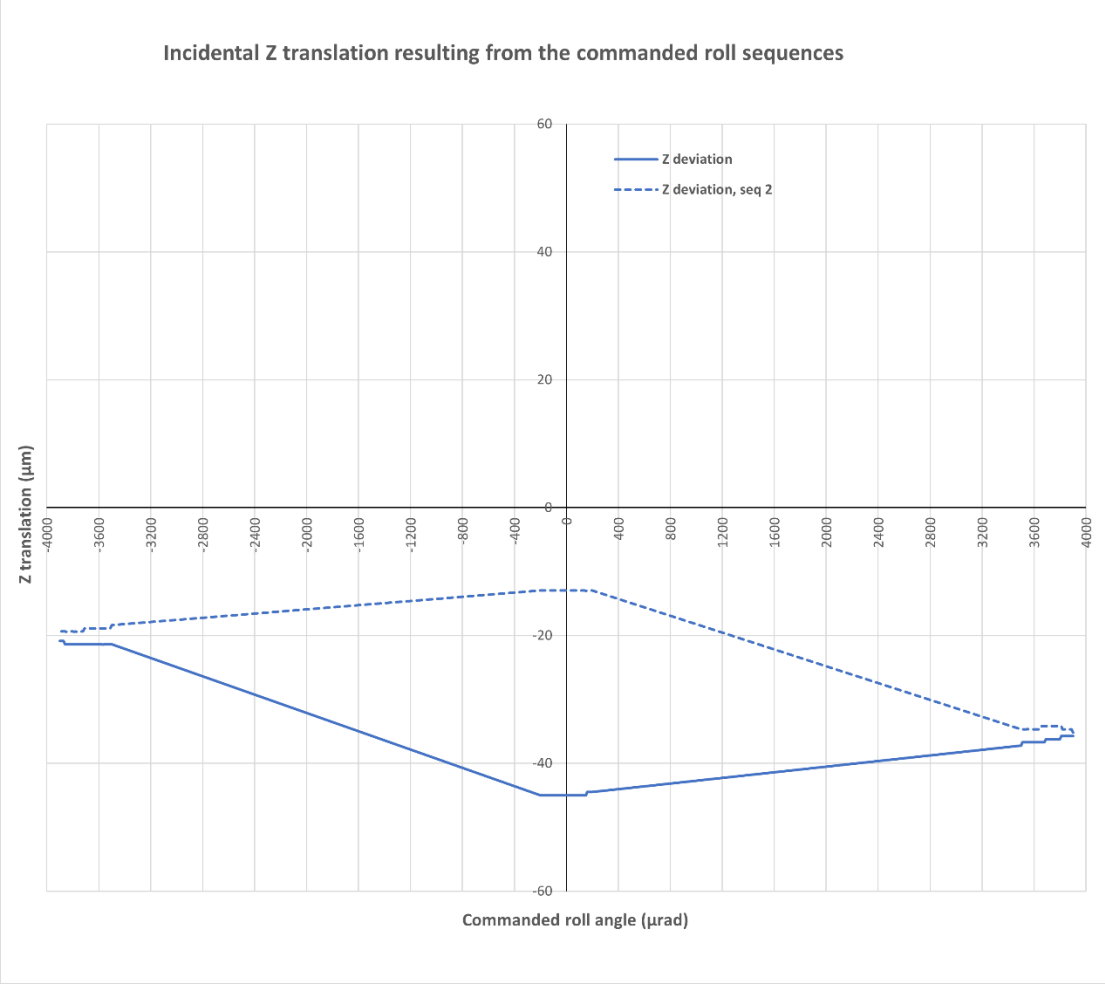
Incidental Z translation resulting from the commanded roll sequences
Z deviation
Z deviation, seq 2
Z translation (µm)
Commanded roll angle (µrad)
60
40
20
0
-20
-40
-60
-4000
-3600
-3200
-2800
-2400
-2000
-1600
-1200
-800
-400
0
400
800
1200
1600
2000
2400
2800
3200
3600
4000

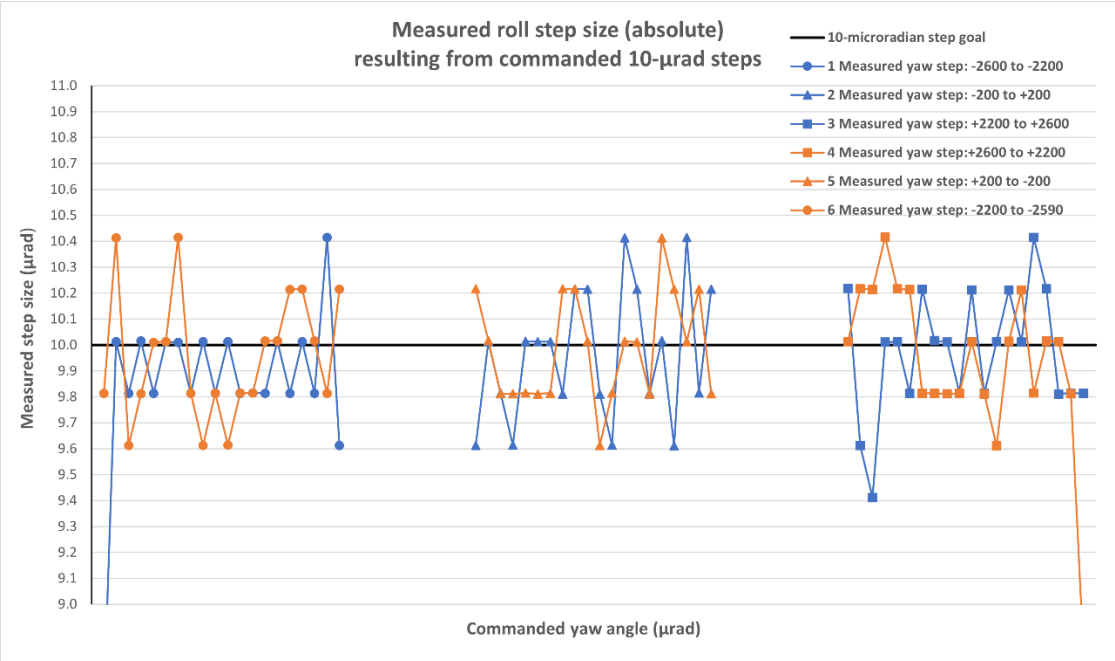
Measured roll step size (absolute)
resulting from commanded 10-µrad steps
10-microradian step goal
1 Measured yaw step: -2600 to -2200
2 Measured yaw step: -200 to +200
3 Measured yaw step: +2200 to +2600
4 Measured yaw step:+2600 to +2200
5 Measured yaw step: +200 to -200
6 Measured yaw step: -2200 to -2590
Measured step size (µrad)
Commanded yaw angle (µrad)
11.0
10.9
10.8
10.7
10.6
10.5
10.4
10.3
10.2
10.1
10.0
9.9
9.8
9.7
9.6
9.5
9.4
9.3
9.2
9.1
9.0